Title
The Development of a Hydrothermal Method for Slurry Feedstock Preparation for Gasification Technology

Author
He, Wei

Publication Date
2011

Peer reviewed|Thesis/dissertation

UNIVERSITY OF CALIFORNIA
RIVERSIDE

"The Development of a Hydrothermal Method for Slurry Feedstock Preparation for Gasification Technologies"

A Dissertation submitted in partial satisfaction
of the requirements for the degree of

Doctor of Philosophy

in

Chemical and Environmental Engineering

by

Wei He

August 2011

Dissertation Committee:
Dr. Joseph M. Norbeck, Chairperson
Dr. Charles E. Wyman
Dr. Mark Matsumoto

The Dissertation of Wei He is approved:

_____

_____

_____

Committee Chairperson

University of California, Riverside

ACKNOWLEDGMENTS

I would like to express my sincere gratitude to my advisor, Professor Joseph M. Norbeck, for the support of my Ph.D study and research, for his patience and inspiration to help me achieve my research goals. Without his help, I cannot have completed my Ph.D in such a smooth and rewarding manner.

I wish to express my sincere thanks to Dr Chan S. Park, my co-advisor, who introduced to me the field of gasification, and Dr Neal Richter, our board advisor, who has given me important guidance toward commencing my Ph.D research.

I owe my sincere gratitude to my reading committee members, Professor Charles Wyman, Professor Mark Mastumoto and my candidacy committee members, Professor David Cocker and Professor Gregory Beran, for their detailed and constructive comments.

I warmly thank Junior Castillo, who offered great help on solving engineering problem during my lab research, and Edward O'Neil, Christophe Cappelli, Evan Kim, Phillip Brendecke, Douglas Duchon and Kevin Castillo, for their assistance on my lab research.

I also wish to thank my colleagues, Xiaoming Lu, Qian Luo, Xin Fan and other graduate students in our lab, for many incisive conversation and discussion we have.

I owe my loving thanks to my Mom and Dad, and my girlfriend, Yang Xie. Their endless encouragement and support gave me strong mental strength to overcome any challenges I have faced.

Riverside, USA, August 2011

Wei He

ABSTRACT OF THE DISSERTATION

The Development of a Hydrothermal Method for Slurry Feedstock Preparation for Gasification Technology

by

Wei He

Doctor of Philosophy, Graduate Program in Chemical and Environmental Engineering
University of California, Riverside, August 2011
Dr Joseph M. Norbeck, Chairperson

Liquid fuels produced via the steam hydrogasification of biomass feedstock followed by downstream gas to liquid processes appears to be a cost effective approach to replace fossil fuels, to decrease the dependence of imported oil and to decrease greenhouse gas emissions. A critical technical obstacle of using biomass feedstock effectively in many gasification processes, including steam hydrogasification, is the need to prepare a high carbon concentrated (i.e., high energy) slurry that can be introduced into a pressurized reactor in a cost effective and energy efficient manner. Conventional dry feeding systems, such as lock-hopper and pressurized pneumatic transport, are complex, unreliable, and operationally expensive. An extra carrier gas is needed in some instances or vibrators to avoid fluctuations in the quantity of feed introduced into the reactor. Slurry feeding is a simpler, reliable, and inexpensive method of transporting and pressurizing the feedstock into gasification reactors and has been demonstrated in

commercial scale application using 100% coal. Biomass slurries have less energy density compared to coal and require high carbon content in order to be efficiently gasified. The hygroscopic and hydrophilic nature of biomass results in a significantly reduced amount of carbon in pumpable slurries. The main goal of this thesis was to develop, design, and implement a Hydro-Thermal Pretreatment (HTP) process that will result in a pumpable biomass slurry with high energy and carbon content for use in a commercial scale, pressurized steam hydrogasification reactor.

The first objective of this thesis was to design, build and evaluate the performance of a laboratory scale HTP process. Four carbonaceous feedstocks (coal-wood-water, wood-water, wood-biosolids and wood-manure) were hydrothermally treated using a procedure developed as part of this thesis. The viscosity, flow and energy content were determined under various experimental conditions including: particle size; initial composition of feedstocks (carbon/water ratio), thermal input (time and temperature of the heating process) and head space gas composition as a consequence of heating. The rheology properties and the settling velocities of the particles for the resultant slurries were evaluated before and after HTP. An empirical model was developed to simulate the rheology properties. The modeling work was necessary to assist with predicting flow behavior of the slurry for commercial applications. The carbon balance for the cumulative gas, liquid and solid phases of the feedstock slurry after HTP was analyzed to determine the carbon recovery in the slurries and found to be greater than 98% recovery. Finally, the heating value of pretreated wood particles was determined to estimate the energy recovery in the slurries which was also found to be in excess of 98%.

The second objective of this thesis focused on obtaining a better understanding of the chemical mechanism of the formation of the biomass slurry as a consequence of the HTP. Four mechanisms and analytical methods were utilized to assist in the explanation: 1. Surface charge alternation, zeta potentials of raw wood particle and pretreated wood particle were analyzed and compared; 2. Particle shrink, Scanning Electron Microscopy (SEM) comparison of wood particles before and after HTP were compared to visualize this effect of HTP; 3. Free bulk water release from biomass microstructure, both SEM observation and liquid-solid distribution of slurry were used to confirm porous site generation and free water release into bulk phase.

The third objective of this thesis focused on the design and scale up of HTP at the lab scale basis, a demonstration scale basis and a commercial scale basis. The lab scale and demonstration scale HTP process was designed and tested in our laboratory. Feedstocks production rates were targeted at 90g/hr and 8kg/hr on a wet basis for lab and demonstration scales. Mass and energy balance of both processes were performed based on experimental data. An ASPEN Plus simulation of a commercial scale HTP process was done using a production rate of 16,700kg/hr on a wet basis. Comparison of economy and energy efficiency was performed between biomass gasification with or without HTP process using the ASPEN Plus results.

Table of Contents

List of Figures

List of Tables

1 Introduction

1.1 Development of Biomass Gasification

1.1.1 Energy from biomass

Biomass represents a broad selection of recent living organic matter, such as forests trees, agricultural products and waste residues, and city and industry green wastes, etc [1-3]. Biomass is produced by photosynthesis of photoautotrophs [4, 5]. In photosynthesis, energy, in the form of solar radiation, is captured and stored by biomass in its chemical bonds synthesized by reaction of Carbon Dioxide (CO_2) with water (H_2O). Carbohydrates ($C_xH_yO_z$), such as sugar, are produced [6-8]. The carbohydrates are used as building blocks for the structural components of biomass and stored energy of biomass [8-10]. When biomass is effectively processed, either in a single step of combustion or in multiple steps processing, such as gasification, the stored energy is extracted in a way that the carbohydrates are oxidized to CO_2 and H_2O [1, 2, 9]. Theoretically, the life cycle of biomass, from its growth toward utilization, has a net CO_2 production of zero [11-13], as is shown in Figure 1.1.

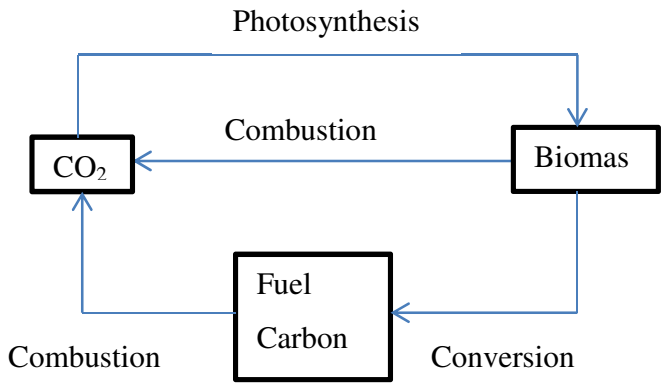

Fig 1.1 CO_2 Cycle in Biomass Growth and Utilization

Fossil energy (such as coal, petroleum and natural gas) also originated as biomass, but after millions of years of storage within the earth [14-16]. In this sense, fossil fuels are considered non-renewable within the time-scale that humans can use. The term "non-renewable" here means: 1) fossil fuels cannot be reproduced within a time scale of human use; 2) conversion of fossil fuels into other forms of chemical product, such as Carbon Dioxide, is irreversible. The non-renewable nature of fossil fuel leads to two major concerns: 1) the inevitable depletion of its reserve [17] and 2) the irreversible release of Greenhouse Gas (GHG) emission, particularly carbon dioxide [18-20]. The urgency in obtaining an alternative and renewable energy supply for global use has evolved in recent years primarily because of the two concerns listed above [21, 22].

First and foremost concern of the utilization of fossil fuels as a primary energy source is that the inevitable depletion and the mismatch between its geological availability and demand patterns. The geographical concentration of finite petroleum supplies challenge the economic viability and energy security in many parts of the world

[23-25]. Petroleum reserves are concentrated in the Middle East, which accounts for 56% of all the known petroleum reserves [26, 27]. Natural gas reserves are concentrated in Middle East and Eurasia areas, accounting for over 74% of global reserves [28]. Coal is relatively widely distributed compared with petroleum and natural gas [29], but would need to be converted to other forms of usable energy to provide resources for the transportation sector. As a result, energy security becomes a world-wide issue and the continuous depletion of reserves only worsens the situation. For example, in year 2007 to 2010, imported petroleum in the US was over 55% of the total energy utilization [30, 31]. China also imported 50% of the oil it consumed [32]. Japan, Germany, and France, which have very limited amount of domestic oil reservation [31, 33, 34], imported almost all their crude oil. The constant increase of oil prices ($12/barrel in 1999 and $60/barrel in 2010, peaked at $145/barrel in July, 2008 [35]) provides a heavy deterrent to economic growth. US imported over 3.58 billion barrels of crude oil in 2008 resulting in a trade deficit of $327.5 billion. China in the same year imported 1.44 billion barrels of crude oil, equal to $131.7 billion [36, 37]. Crude oil imports by China will be equal to the US by 2030 based on projections by the Energy Information Administration (EIA) [38]. Most countries of the world have a high dependency on oil imports, and are vulnerable to shocks in the energy supply and oil trade economics [39]. There is no long term solution for this if no other alternative energy supply is available.

The other concern of fossil fuel usage is greenhouse gas emissions. The scientific consensus is that anthropological fossil fuel combustion, causing release of CO_2, has had a significance impact in current and future global warming (GW) [40-42]. Global

warming, if left uncontrolled, would have a devastating effect on the natural and ecological system [43]. The increase of meteorological occurrences of extreme weather conditions, such as heat waves and hurricanes, are now attributed to global warming. Ocean acidification by CO_2 dissolving in sea water has caused concerns of retreat of coral reefs and damage to other ocean habitats [44, 45]. The melting of glaciers, permafrost and sea ice would result in sea level rising, endangering coastal cities [46, 47]. There are many more indirect threats to the global eco-system associated with global warming [48, 49] which are not discussed here but documented in the literature. The 15th UNFCCC (United Nations Framework Convention on Climate Change) outlined a framework to limit the future increase of global mean temperature to less than 2°C in an attempt to prevent potential disastrous events such as discussed above [50-52]. The accord was later ratified by 140 countries. This goal can never be fulfilled if there is not an immediate stringent policy enacted to limit fossil fuels usage for electricity generation and transportation.

Fuels and chemicals derived from biomass could be an interim solution to the usage of fossil fuels [53, 54]. Biomass was the major source of energy before industrialization and is still an important fuel today for cooking and home heating in many parts of the world. Biomass accounts for approximately 14% of today's world's primary energy production [55], but much of the biomass resources are largely squandered by inefficient use and poor management [56]. Interest in biomass as an alternative and renewable energy source has increased considerably, particularly in the renewable transportation sector [57].

Biofuels could be an intermediate solution to building a fully carbon free renewable transportation sector. Liquid biofuels would be a viable compliment to other renewable fuels, such as solar electricity and hydrogen fuels [58]. New renewable vehicle technologies such as fully electric and fuel cell vehicles are still expensive or at a nascent stage of development. Unless technological breakthroughs happen in battery or fuel cell technology, they are not economically competitive to replace liquid fuels powered vehicles in the short term [59-62].

There are several benefits of using biomass as an energy supply. Firstly, biomass is a carbon sink [12, 53, 63-67]. Carbon is removed from the atmosphere and fixed in the biomass structure during its photosynthesis, and is later released back into the atmosphere during biomass utilization, such as combustion. There is no net carbon emission in the life cycle of biomass when utilized as an energy source [58, 64]. Moreover, biomass is geographically available to the end user and in many circumstances, is otherwise wasted or ignored in human activity [53, 68, 69]. Forestry wastes, agriculture wastes and green city wastes are all examples of underutilized biomass that could be otherwise valuable and renewable energy source if properly processed [70-73]. In this sense, biomass offers an alternative option of energy supply to countries that are heavily dependent on foreign trade for energy and are thus vulnerable to energy shocks. In addition, biomass is an economically competitive energy source to fossil fuels and not subject to depletion in a foreseeable future [73, 74]. Lastly, biomass is the major renewable resource that has high concentrations of carbon [75, 76]. This renders it as an excellent renewable alternative to liquid fossil fuels.

There is a wide range of biofuels that can be produced from biomass, including ethanol, methanol, DME, synthetic gasoline, diesel fuel, and kerosene derivatives for production of aviation fuel [53, 77, 78]. These biofuels produced have ultra-low sulfur levels thanks to the conversion technology advancement [79, 80], and with proper fuel synthesis technology, will meet Federal and California low carbon fuels standards [81-83].

In summary, the benefits of biomass as an energy source are:

1. It is broadly available to regions where fossil energy is scarce and depends heavily on foreign oil supply;
2. It is an inexpensive energy source and would have been wasted otherwise in human activity;
3. It has net carbon footprint of low in its life cycle as compared with conventional fossil fuels;
4. It is the only carbon concentrated renewable source and can be used as an alternative source of liquid transportation fuels;
5. It contains ultra-low sulfur level and could meet the low carbon fuels standards with proper synthesis technologies.

Biofuels technologies

Biofuels can be derived from a wide selection of living or recently living organic materials. Various conversion technologies have been actively investigated in the last century but, unfortunately, the intensity of these investigations usually follows some form of global energy crisis and faded off quickly after the crisis was over [84].

It is generally recognized that the development of biofuels and the associate technologies have been through two phases (generations) [85]. First generation biofuels are derived from edible plants containing sugar, starch and vegetable oils. Bio-alcohols (eg. ethanol) are produced by fermentation of sugar and starch, and biodiesels are produced by trans-esterification of vegetable oils and animal fats [86]. The first generation biofuels compete with land use for food supply [87, 88]. Thus, it is considered less sustainable compared to biofuels derived from lingo-cellulosic biomass. Lingo-cellulosic biomass is nonfood crops comprising of cellulose, hemicellulose and lignin. Lingo-cellulosic biofuels are generally considered as the second generation biofuels [89]. Conversion technologies of lingo-cellulosic biomass to biofuels can be summarized in two categories: biochemical conversion and thermochemical conversion [90].

Biochemical conversion of lingo-cellulosic biomass includes a hydrolysis of lignocellulose to enhance the release of sugars and starches, and followed by an enzymatic fermentation step to produce liquid alcoholic fuels [75, 91, 92]. Ethanol is the major alcoholic fuel product and it can be combusted directly or co-mingled with other liquid fuels (gasoline) for use in spark ignited engines. Little effort is required to modify a gasoline powered engine to burn ethanol fuel or blends, which is one of the main attractions of ethanol fuel [93, 94]. The hemicellulose and cellulose fractions of lingo-cellulosic biomass are subject to hydrolytic reaction to yield sugars (pentose and hexose) in the hydrolysis step [95]. Cellulose is resistant to hydrolysis, so it needs to be enhanced by using special enzymatic catalysts [96]. The yield of sugar released from cellulose is rather low. Thus, considerable research is now focused on investigating cost effective

technologies to release increased levels of sugar from lingo-cellulosic biomass [97]. The lignin in lingo-cellulosic biomass is difficult to convert in biochemical conversion processes, and in most bio-refinery processes is separated, dried and combusted as a downstream process to provide heat and electricity for supply in the bio-refinery plant [98, 99].

Thermochemical conversion technologies for lingo-cellulosic biomass include pyrolysis, gasification and direct liquefaction [100, 101]. There are usually two types of liquid fuels produced: heavy oil residuals and Fischer-Tropsch oils. Pyrolysis and gasification both involve thermochemical conversion of carbonaceous material in a reductive (no oxygen) or lean oxygen environment [102, 103]. The main difference is that pyrolysis takes place at a temperature range of 200ºC to 550ºC depending on the feedstock properties and technological requirements. The process temperature of gasification is normally higher than 800ºC. Products from pyrolysis and gasification both contain gas products (CO, CO_2, H_2, CH_4 and tar) and unburned char, usually in different mass fractions [100, 104]. Liquid biofuels are then generally produced by either Fischer-Tropsch synthesis of the syngas produced in gasification or by refining purified pyrolysis heavy oil residuals [105]. Liquefaction is another type of thermochemical technology recently being commercialized in China with coal as the feedstock [106-108]. In liquefaction, thermolysis of carbonaceous materials occur and liquid fuels form through carbonation or hydrogenation of carbonaceous feedstocks. Solid char and ash are separated from liquefaction products through distillation and the distillates contain hydrocarbons which can be combusted as liquid fuels [109, 110]. Gaseous products are

produced in pyrolysis and hydrogenation, and this is why it was also categorized as gasification technology in many other studies [100, 111].

This thesis will focus on biofuel production through biomass gasification. A literature based review of biomass gasification technologies is presented in the next section.

1.1.2 Introduction to Gasification

Carbonaceous materials can be converted into gaseous products with a useable heating value sufficient for downstream liquid fuels production via chemical conversion technologies [100, 102, 112-114]. These technologies are referred to as gasification. The gaseous products in gasification processes normally include hydrogen, carbon monoxide, methane and other volatile hydrocarbons. In this sense, gasification could be viewed as a retained combustion process, yet is operated under reductive (no oxygen) or sub-stoichiometry oxygen conditions. In gasification, syngas (carbon monoxide and hydrogen) is produced instead of carbon dioxide and water as is in the combustion process [114]. It is important to classify major chemical reactions in gasification, which has already been depicted in great details in other studies [100]. Eq. 1.1 through 1.9 summarizes basic chemical reactions involved in gasification [100, 115].

Combustion reactions:

$$C + 1/2O_2 \rightarrow CO \qquad \Delta H = -111MJ/Kmol \qquad \text{(Eq. 1.1)}$$

$$C + O_2 \rightarrow CO_2 \qquad \Delta H = -394MJ/Kmol \qquad \text{(Eq. 1.2)}$$

$$CO + 1/2O_2 \rightarrow CO_2 \qquad \Delta H = -283MJ/Kmol \qquad \text{(Eq. 1.3)}$$

$$H_2 + 1/2O_2 \rightarrow H_2O \qquad \Delta H = -242MJ/Kmol \qquad \text{(Eq. 1.4)}$$

Boudouard reaction [115]:

$C + CO_2 \leftrightarrow 2CO$ $\Delta H = +172MJ/Kmol$ (Eq. 1.5)

Water gas reaction:

$C + H_2O \leftrightarrow CO + H_2$ $\Delta H = +131MJ/Kmol$ (Eq. 1.6)

Methanation reaction

$C + 2H_2 \leftrightarrow CH_4$ $\Delta H = -75MJ/Kmol$ (Eq. 1.7)

CO shift reaction [115]

$CO + H_2O \leftrightarrow CO_2 + H_2$ $\Delta H = -41MJ/Kmol$ (Eq. 1.8)

Steam methane reforming reaction

$CH_4 + H_2O \leftrightarrow CO + 3H_2$ $\Delta H = +206MJ/Kmol$ (Eq. 1.9)

In the reactions above, a positive entropy value means an endothermic reaction and a negative entropy value means an exothermic reaction. And it is worth noticing that reaction (1.5) through (1.9) are reversible reactions in which chemical components reach equilibrium at given pressure and temperature. Generally, oxidation are complete and irreversible (reaction 1.1 to 1.5) while others (reaction 1.6 to 1.9) are incomplete and reversible.

Gasification technology was developed initially for the industrial utilization of town gas and used for purpose of illumination in the nineteenth century. Coke ovens were used as the gasifier for town gas production. It was operated at ambient pressure of less than 2bar. This resulted in voluminous equipment sizes and low volumetric heating value of the gaseous products [100, 112, 116]. Later, more gasification agents, such as steam and hydrogen, were added and many other gasification technologies were developed

[100]. The following section summarizes several of these technologies related to the gasification.

Partial Oxidation (POX)

Partial Oxidation (POX) is the most widely applied gasification technology to date [100]. POX involves lean combustion of carbonaceous materials with oxygen. Oxygen is supplied either by air or in the form of pure oxygen. Reactions (1.1), (1.2), (1.3) and (1.5) describe the four reactions in which carbon is gasified in POX. Heat produced from exothermic reaction (1.2) and (1.3) provide the necessary heat to maintain the reaction temperature (850°C ~1600°C) in POX gasifier [116]. In practice, the feedstock is more complex than pure carbon. It may contain other chemical compounds such as hydrogen, sulfur, nitrogen and trace metals [68, 100]. The following reactions are summarized with hydrocarbons in the feedstocks:

$$C_nH_m + \frac{2n+m}{4}O_2 \rightarrow nCO + \frac{m}{2}H_2O \quad without\ catalyst \qquad \text{(Eq. 1.10)}$$

$$C_nH_m + \frac{n}{2}O_2 \rightarrow nCO + \frac{m}{2}H_2 \quad with\ catalyst \qquad \text{(Eq. 1.11)}$$

Where

For gas, such as methane, m=4 and n=1

For oil, m/n ≈ 2, hence m=2 and n=1

For coal, m/n ≈ 1, hence m=1 and n=1

Catalysts are used in some circumstances, to enhance the hydrogen production in POX, but such practice would complicate the gasification system, and the decision is made on the production yields and economic considerations [116].

The POX process is one of the simplest gasification technologies to build and implement. It is straightforward to scale to large size [117]. The potential lack of sufficient hydrogen makes variation of the H_2/CO ratio difficult in POX. Thus its application has limits without additional technology. This is especially true if the desired final products are ammonia and methanol in the downstream processes [116, 118, 119].

Steam is added when modification of the H_2/CO ratio is required as required for downstream processing of the syngas products. Reaction (1.6) plays the predominant role in the addition of water. Steam has two functions in gasification [116, 120]: 1) it acts as a moderator in the gasifier to control the reactor temperature and recycle the sensible heat; 2) it provides source of hydrogen in gasification scheme. Thus, the H_2/CO ratio in the product could be modified by adjusting the steam input. When steam is added as a moderator in POX, pure oxygen, instead of air, is usually used as the oxygen source to enhance the exothermic oxidation of carbon. This will provide heat to evaporate the water and maintain the reaction temperature [116]. The use of pure oxygen was only available when cryogenic air separation technology was developed [121]. The absence of nitrogen in the gasifier results in a better efficiency of carbon conversion and consequently reduces the size of gasifier. Air is not abandoned, however, especially in ammonia production, where N_2 is a useful feedstock to maintain a stoichiometry balance between H_2 and N_2 of 3:1 [122]. N_2 could also be compressed and mixed with gaseous products after the gasifier, but has been shown to be inefficient compared to direct air use. Additionally, an oxygen separator is expensive to build and operate [116]. In some extreme cases, it can account for more than 1/3 of the total capital investment of the fully

configured gasification plant [123-125]. To summary, it would be a decision based on the specific application and economic consideration to choose either air or pure oxygen injection in POX gasification processes.

Steam Gasification

Pure steam gasification is also possible. However, the reaction rates are orders of magnitude lower than POX [126, 127]. This results in long feedstock residence time and considerable increase of the equipment volume. The thermal efficiency of steam gasification is low and an external heat source is always needed to compensate for the latent heat required for water evaporation. Local variation in the temperature within the reactor (cold spots) caused by water evaporation in contact with feedstock can result in an unacceptable synthesis gas product quality for downstream applications [128, 129]. The impurity level of such product gas can be so high that there are little or no economic benefits in commercial applications.

Active research has been observed in recent years on a steam gasification using supercritical water technology [130]. Supercritical water gasification is performed in supercritical water regime where process temperature ranges from 374°C to 775°C. The pressure of supercritical waster gasification normally exceeds 22MPa [131]. Flowable feedstocks, such as woody waste, agricultural waste, and organic waste from anaerobic wastewater digester and black liquid from paper pulping process have been investigated in the supercritical water gasification process [132]. Dilute acid is usually added as catalyst to promote gas production and to inhibit liquid and char formation [133]. Hydrogen and carbon dioxide rich gas is produced in this process; other gaseous products

include methane and trace carbon monoxide [130, 134]. For supercritical water gasification to be economical viable in commercial scale, feed concentration in the would need to be increase, where biomass loading in most reported supercritical research is lower than 10wt.%. Other technical issues need to be tackled in supercritical water gasification include improve catalyst reliability under high pressure conditions and equipment corrosion resistance [135].

Hydrogasification

Hydrogen can be used as a gasification agent. Hydrogasification is defined as the gasification process where carbon reacts with hydrogen. Methanation (reaction 1.7) is the predominant reaction in hydrogasification [136]. The reaction rate of hydrogasification (carbon and hydrogen) is considerably slower compared to the carbon-oxygen reaction [137]. Thus, hydrogasification is usually done in the presence of a catalyst, usually Ni-based [138, 139], or is combined with other reaction agents to increase the reaction rate, such as in steam hydrogasification [140]. Additionally, heat produced from the exothermic reaction (1.7) is not enough to maintain the gasification temperature, thus heat has to be supplied externally in most, if not all, applications [116]. Hydrogenation is more recently applied in the direct liquefaction of coal rather than hydrogasification itself [106, 107].

Commercial gasification processes are usually a combination of several kinds of technologies [100]. This is due to the complexity of processing the feedstock, and the operational requirements of the integrated system, such as temperature and pressure considerations of the gasifier, the quality and composition of the syngas, and the

requirements for the downstream fuel production technology. In general, the overall efficiency of the carbon conversion needs to be considered carefully and optimized in gasification. There are two commonly used parameters encountered with gasification efficiency: Cold Gas Efficiency (CGE) and Carbon Conversion (CC) [116].

The definitions of CGE and CC are:

$$Cold\ Gas\ Efficiency\ (\%) = \frac{Heating\ value\ in\ product\ gas\ (MW)}{Heating\ value\ in\ feedstock\ (MW)} \times 100\% \quad \text{(Eq. 1.12)}$$

$$Carbon\ conversion(\%) = [1 - \frac{carbon\ in\ gasification\ residue\ (mol)}{Carbon\ in\ feedstock\ (mol)}] \times 100\% \quad \text{(Eq. 1.13)}$$

It is important to clarify that the heating value used in Eq. 1.11 is based on a Higher Heating Value (HHV) or a Lower Heating Value (LHV). Cold Gas Efficiency is inappropriate in use as criteria for syngas production where a calculation of syngas yield would be a better guide. Carbon Conversion excludes nonfuel gas in the gaseous product, such as carbon dioxide, and could be useless to exhibit gasification efficiency [116].

In summary, carbonaceous materials are gasified following a sequence of pyrolysis, and then followed by an either gas phase reactions or char-gas reactions, as shown in Figure 1.2.

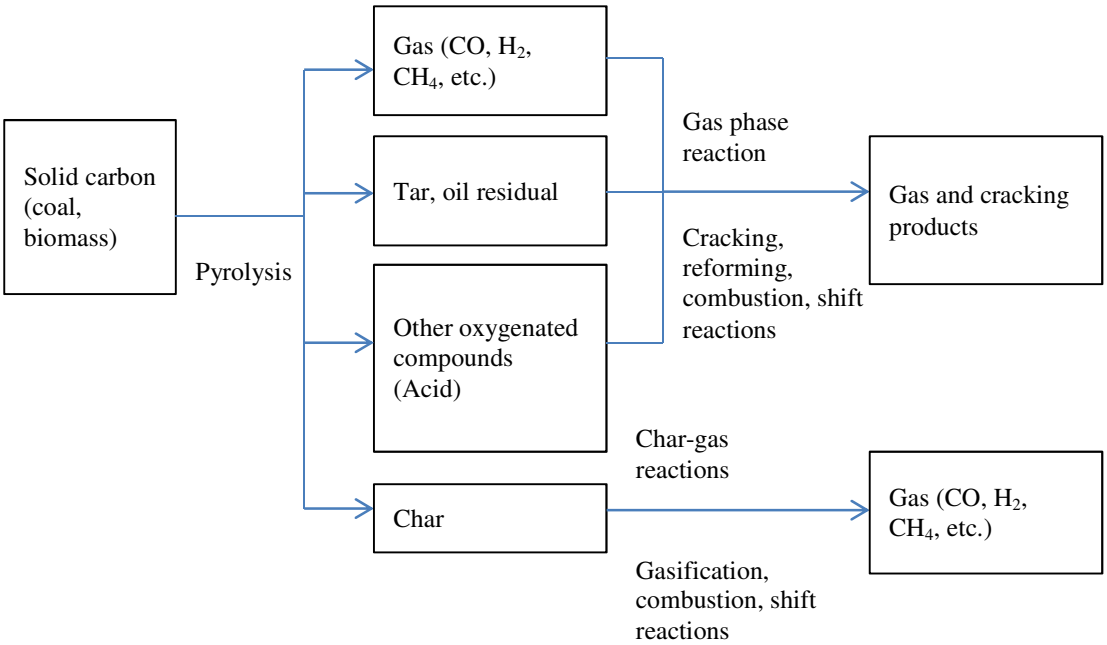

Fig 1.2 Reaction in gasification of coal or biomass (oxidant based processes)

The theoretical rationale of the reaction sequence as shown in Figure 1.2 is based on heat and mass diffusivity in a solid-gas system. Carbonaceous solid materials, such as coal and biomass, contain volatile carbon, fixed carbon and ash fractions. At a temperature range of 300°C to 500°C, pyrolysis happens with decomposition of volatile compounds, resulting in gas, liquid residuals and char production. When the solid particles reach a higher temperature of over 800°C, and sufficient gaseous oxidant is available to be in contact with the carbon left in the solid, further gasification occurs, resulting in further gaseous products production until gasification is complete [104, 141, 142]. If there is not sufficient resident time for the reaction to occur, tar is produced [143]. All of these technical issues must be tackled and could be optimized by advanced

practical design of gasification process. Several types of gasifiers to address these issues have been developed and commercialized so far [101, 114, 144, 145]. Even though there has been no successfully operated commercial scale pure biomass feedstock gasifier up to date, its successful development would be confidently expected in near future. The design specifications of these current commercially available gasifiers are listed in Table 1.1.

Table 1.1 Overall Technical Specifications of Various Commercially Available Gasifiers

Gasifier	Temperature [1]	Feed preference	Oxygen demand	Pressure	Reactor wall	Throughput	Product gas BTU	Ash removal	Commercial brand
Moving Bed	425°C - 650°C	Dry feed, 6-50 mm	Low, air	1-100 bar [2]	Water jacket [3]	Low	Low to median [5]	Dry or slagging	Lurgi, BGL
Fluidized Bed	900°C-1050°C	Dry feed or wet feed, 6-10 mm	Moderate, air or pure oxygen	3-30 bar	Refractory or membrane wall [4]	High	High	Dry or agglomerating	Winkler, HTW, KBR, U-Gas, HRL
Entrained Flow	1250°C-1600°C	Dry feed or wet feed, <100 µm	High, pure oxygen	20-70 bar	Refractory or membrane wall	High	High	Slagging	Koppers-Totzek, Shell, Prenflo, GEE, E-gas, MHI, Siemens

Comments: 1) output gas temperature; 2) only two pilot plants, Ruhr 90 and Ruhr 100, are operated at 90bar and 100bar, respectively; 3) lagging version had refractory lined design on the bottom part; 4) agglomerating version was design with membrane wall; 5) high CO_2 concentration.

The initial commercial coal gasification system was developed by Lurgi [146, 147]. It is a moving bed gasifier that is operated at a temperature of 800°C, and with a pressure of 25-30bar. The feedstock is loaded from the top of the gasifier. Pyrolysis reactions happen in the top portion of the gasifier by utilizing heat of the combusted gas rising from the bottom. Such a design results in low temperature of the output gas (500°C to 600°C) and allows unreacted volatile compounds escaping from the gasifier with the product gas [148]. The slow motion of feedstock moving downwards and the product gas moving upwards in the moving bed reactor requires distributors for the feedstock loader on the top, and gas injecton at the bottom [149]. Such design results in extra mechanical components installed in the reactor which requires frequent maintenance. The top portion of the moving bed gasifier could be considered (and modeled) as a plug flow reactor where pyrolysis occurs, and the bottom portion of the reactor where the complex drying, devolatilization and combustion of carbonaceous materials would occur [150]. Fine particles in the feedstock are not accepted in the moving bed design so low ash softening feedstock is not ideal with this type reactor [116].

Fluidized bed gasifiers were developed because of their good mixing performance with solid-gas systems and its potential for high throughput [151-153]. Gases are introduced at the bottom of the gasifier. The system can be carefully controlled to achieve three types of fluidization of the solid particles: stationary bubbling fluidization, circulating fluidization and transport fluidization [154]. All three of these fluidization regimes have been implemented in commercial designs [100]. The temperature profile throughout the fluidized bed reactor is evenly distributed, allowing for lower

concentrations of the lower volatile compounds in the outlet gas product compared to that of a moving bed reactor. Pressure in the fluidized bed gasifier is determined to maintain the fluidization regime, and is optimized to be conforming to the pressure requirement of downstream processes. Ash slagging does not occur due to the high elevating gas velocity, and the dry ash is disengaged from the gas moves upwards and collected from the bottom of the gasifier. The most promising feature of fluidized bed reactor is that both fine and coarse particles can used [116]. The unreacted fine particles are blasted upwards and circulated back into the gasifier by a cyclone attached at the top of the gasifier. Coarse (larger) particles disengage from gas stream and fall down back into the reactive region of the gasifier. High conversion is achieved with high throughput and low reaction temperature in a fluidized bed gasifier [155]. This characteristic is a critical and promising feature for gasification of biomass because reducing the particle size distribution of biomass is an energy demanding process.

The production of tar free syngas is one of the major advantages of entrained flow reactors [156, 157]. Entrained flow gasifiers operate at high reaction temperatures (1100°C~1600°C) and require high oxygen demand. Thus they are exclusively associated with POX systems. An expensive membrane wall is needed for most entrained flow gasifier because the high temperatures result in the ash slagging issues [113]. Dry feed is preferred and particle size is restricted (normally less than 100μm) because of the short reaction time. Entrained flow reactors have the highest Cold Gas Efficiency (CGE) compared with all the gasifiers discussed above and is considered the most robust gasifier configuration [100, 116].

1.1.3 CE-CERT Steam Hydrogasification

The College of Engineering Center for Environmental Research and Technology (CE-CERT) at the University of California, Riverside (UCR) is developing a multi-step thermal chemical process called steam hydrogasification (referred as the CE-CERT process herein) which has been shown to convert carbonaceous feedstock into syngas with high conversion and potentially a cost effective manner [140, 158, 159]. High carbon conversions have been achieved in a lab scale Steam Hydrogasifcation Reaction (SHR) using coal, woody biomass, agricultural waste and municipal waste. The US National Energy Technology Laboratory (NETL), in an independent evaluation of this technology, reported that the CE-CERT process has the potential to be 12% higher efficiency with 18% lower capital cost than the most up-to-date conventional mainstream gasification technologies [160]. These efficiencies need to be confirmed in a larger pilot application.

A simplified schematic of the CE-CERT process is shown in Figure 1.3.

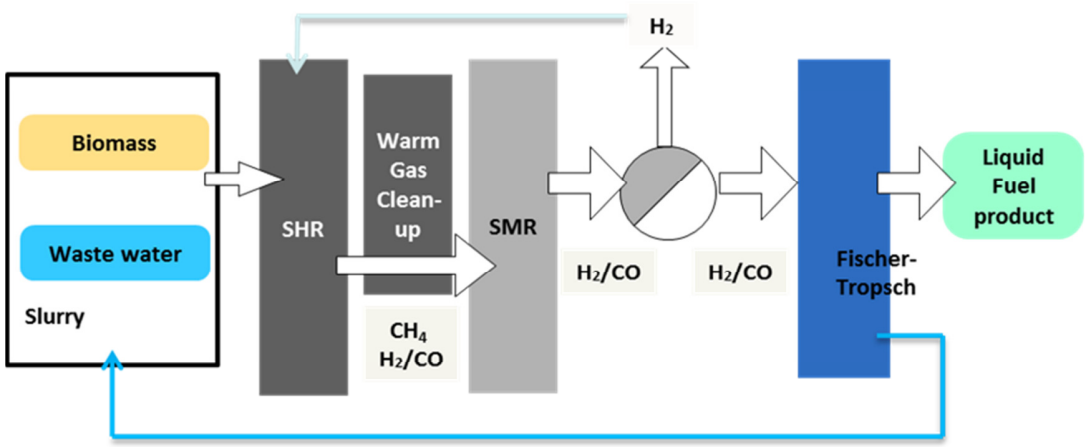

Fig 1.3 Diagram of CE-CERT process

In the SHR, hydrogasification occurs in the presence of steam. The exact chemical pathway when steam is introduced to the reaction scheme can be represented as follows [158]:

$$C + H_2O + 2H_2 \rightarrow CH_4 + H_2O + \text{others } (CO, CO_2, C_{2+}, \text{etc}) \qquad \text{(Eq. 1.14)}$$

After the SHR, the methane rich output gas is then subjected to cleanup of sulfur species (H_2S, COS, etc), tars (organic residual due to incomplete decomposition of large organic molecules) and heavy metals. Warm gas cleanup is implemented to avoid extensive heat lost during gas cooling and reheating. Scrubbed methane along with excess steam is converted to syngas in the Steam Methane Reforming (SMR), through the following reaction:

$$CH_4 + H_2O \leftrightarrow 3H_2 + CO \qquad \text{(Eq. 1.15)}$$

The reformed syngas comprises of H_2 and CO with a ratio dependent on the initial H_2O to C ratio input to the SHR. This ratio is usually optimized for a Fischer-Tropsch Reactor (FTR) by separating and recycling of excess H_2 back into the SHR. An internal self-sustaining source of H_2 could be achieved between the SHR and SMR, which means no external H_2 source is required. This is one of the most unique features in CE-CERT process (see Figure 1.3). The technical advantages of the CE-CERT process are summarized as follows:

1. It utilizes a slurry feed, so wet feedstocks can be used which reduces cost of drying the feedstock and offers the potential of more efficient handling of feedstock;
2. It entails a closed-loop H_2 cycle and is operated without external H_2 supply;

3. It provides a high rate of methane which could be used as a source of clean synthetic natural gas;
4. It operates under reductive conditions; hence no external O_2 supply is required.
5. The gaseous pollutants obtained from the nitrogen and sulfur in the feed are mainly in the form of H_2S and NH_3, which are relatively easy to remove;
6. It operates under relatively lower temperature and lower pressure compared with other gasification processes (e.g. Partial Oxidation) and offers versatility for both small scale and large scale applications;
7. The optimum H_2 to CO ratio for efficient downstream production of fuel products and chemicals can be achieved by controlling the initial H_2O to C ratio input to the SHR.

Like most nascent technologies, some unit operations of the CE-CERT process as outlined in Figure 1.4 need to be improved for optimum performance and commercial viability. These are listed below along with potential mitigation.

1. Like most gasification technologies, the efficient minimization or removal of produced tar and char from the SHR needs to be accomplished. This is being accomplished by improved the overall design of the SHR and further technology for downstream removal of tars;
2. The low reaction rate of hydrogasification in the SHR could result in large, uneconomical gasifiers at the commercial scale, thus catalysts are being investigated to increase the reaction rate in the SHR;

3. Sulfur species and tars are poisonous to downstream catalytic reactions in both the SMR and FT processes. Thus, median or high temperature gas cleanup technologies are being developed;
4. Water consumption is a major concern in most alternative fuel processes. We have found that the CE-CERT process can efficiently utilize the biosolids discharged from wastewater treatment plants or water runoff from animal feedlots. This effluent (and other grey water) can be used as alternative water supply. Moreover, proper wastewater treatment and recycle systems need to be implemented, so that net water consumption in the overall CE-CERT process is minimized;
5. Efficient processing of the feedstock slurries, particularly biomass slurries, is a major potential problem for scale-up of the CE-CERT process. This area is the topic of this thesis.

1.1.4 The Transition from Coal to Biomass Gasification

The transition from coal to biomass gasification requires technical modifications of the gasifier, a change in the physiochemical properties of the biomass, or both. The overall goal is to optimize the Cold Gas Efficiency (CGE) for the biomass system. The operating conditions to yield the optimum CGE in the gasifier depends on the feedstock properties [161], as was discussed in the previous sections. Some worthwhile differences between the feedstock properties of coal and biomass are given in Table 1.2. A discussion as to how these properties affect the operation in the gasification process will be discussed in the following paragraphs.

Table 1.2 Feedstock-wise Comparison of Coal and Biomass

Feedstock	Coal	Biomass
Carbon content	High, ~75 wt.% in low rank coals	Low, less than 50 wt.% in most biomass
Moisture	Low, ~ 10 wt.% and easy to dry	High, Up to 95 wt.%, and hard to dry
Volatile compound	Low	High
H/C ratio	Low, ~ 1:25	High, ~ 1:10
O/C ratio	Low, < 1:3	High, > 1: 1.5
Heating value	high, > 26MJ/kg	Low, < 20 MJ/kg
Grinding resistance	Low, Hardgrove Index >40	High, Hardgrove Index 0~30
Ash properties	High melting point due to high Vanadium and Nickel composition	Low melting point due to high potassium composition
Other chemicals	High Silicon composition results in equipment attrition	High Halogen composition results in fouling issues

Carbon, Hydrogen and Oxygen composition

In general, the chemical composition of biomass has a higher Hydrogen to Carbon ratio compared to coal [162, 163]. Thus, at comparable gasification conditions, higher CH_4 concentration would be expected when biomass is gasified compared to coal. The oxygen to carbon ratio is also higher in biomass which results in a lower heat of combustion for biomass [164]. Consequently, more biomass is required to provide heat to maintain a high reaction temperature. Therefore, biomass gasification, in general, yields lower Cold Gas Efficiency when compared with coal gasification [68]. Moreover, the

ability to modify the syngas composition is limited in biomass gasification, due to the low carbon concentration in biomass feedstocks [165].

Level of Volatile Compounds

Biomass is highly volatile and very susceptible to thermal reactions [166]. Thus, high carbon conversion efficiencies can be obtained at lower gasification temperatures. High levels of tar can result as a consequence of the highly volatile nature of biomass [167]. This could result in lower Cold Gas Efficiency and lower syngas production in the product gas.

Hygroscopicity and Moisture Content

Biomass is highly hydrophilic and hygroscopic. The inherent moisture makes the drying process costly for biomass, and can restrict the use of additional steam as an agent for the modification of the syngas composition [168, 169]. Problems arise in slurry feeds as the high hydropilicity and hygroscopicity nature of biomass results in too much water in the feedstock and results in difficulty obtaining the appropriate water to carbon ratio when biomass feedstocks are mixed to form a slurry [170]. A major focus of this thesis is to develop an economically process to easily alter the hygroscopisity of biomass feedstocks.

Grinding Resistance

The fiber structure of biomass makes biomass hard to be grinded efficiently [171]. The Hardgrove Index of biomass is approximately zero [116]. This is especially true for agricultural wastes [172, 173]. A detailed discussion of the energy cost for biomass grinding is provided in Chapter 5.

Ash Properties

Potassium, calcium and phosphorous are main components in biomass ash [174]. The ash melting point of biomass is low as a consequence [175]. The potassium composition in the ash, however, makes it extremely aggressive towards the production of wall cracks, and can result in leaks or even mechanical fail within the gasifier [116].

Others

Nitrogen is high in some biomass but is inert in gasification. However, its presence lowers the thermal efficiency of the gasification reactions [176]. Halogens, such as chloride, when reacted with ammonia, can cause serious fouling problems in the downstream pipe and equipment [177, 178].

It is proposed that a pretreatment stage for biomass feedstock be developed and implemented prior to the introduction into the gasification reactor. The purpose of the pretreatment is to modify the physiochemical properties of the biomass, so that it can be treated similar to coal when it was fed into a coal based gasifier. In this manner, a minimum of effort and cost would be required in modifying existing gasifies for biomass applications and solves the problematic engineering issues that may arise with gasification biomass feedstocks.

1.2 Introduction to Slurry Rheology and Feedstock Preparation

Commercial scale biofuels production processes, such as gasification, favor a continuous feed system to introduce the feedstock into the gasifier at a high operating pressure [100, 141, 179]. Unfortunately, the handling of biomass feedstock and its subsequent injection into a pressurized reactor poses technical problems, which can be

detrimental in practice [100, 180]. Based on the physical characteristics of the feedstock, there are two types of feeding technologies to introduce material into a pressurized gasifier: dry feed method and wet feed method. Dry feed method is achieved by compression of solid feedstock with a carrier gas, or so-called auxiliary gas, which is normally Nitrogen [181]. Wet feed is achieved by pumping a slurry formed with the carbonaceous feedstock in water, in which water is used as a fluid agent. Commercialized dry feed systems are based on using rotary feeders or lock-hoppers. Both of these feeding methods have technical drawbacks. The pressure elevation with using a rotary feeder is significantly limited due to the seal and attrition problems caused by dry particles [180]. The pressurization achieved by a rotary feeder is normally less than 10bar. Lock-Hopper technology is much more broadly used in commercial applications. It is possible to achieve a pressure increase of over 100bars by using a multiple stage lock-hopper system, such as the feeder system used in the Lurgi Ruhr100 [112]. However, its operation is not continuous, unless a rotary feeder is attached to the end as a transition to continuous feeding [182, 183]. Additionally, maintenance and operation of Lock-Hopper systems can be substantially expensive, due to its complex valve systems that have to provide a gas-tight block in non-optimum environments [183]. In a lock-hopper system, the dry feed is pressurized with auxiliary gas, which then requires cleaning and recycling from the gasifier. The energy loss during the pressurization and depressurization of the auxiliary gas is substantial; while cleaning adds to the operational cost of a lock-hopper system.

Slurry feeding is preferable because it is much simpler, more reliable and economically more efficient than the dry feeding method [184, 185]. The pressure gain by pumping slurry could be as high as 200bar. Previous studies show that, despite the extra energy required for drying the wet feedstock in the gasifier, a slurry feed is 12% more cost efficient when used in a POX coal gasification system [186]. Both dry feed and wet feed systems have been successfully implemented in commercial scale gasification plants and also with specific gasification technologies [187, 188]. Water is utilized within the CE-CERT process as a steam source in the SHR and SMR. Thus, a slurry formed liquid and solid feedstock mixture is obviously preferred [140, 170].

The flow properties of slurries vary according to the physical properties of its solid suspension and fluid agent. Rheological properties of slurries have been characterized to describe its flow behavior under pressure. There are five important parameters to describe the flowability and pumpability of a slurry [189, 190] (see Table 1.3).

Table 1.3 Important parameters in slurry rheology

Rheology parameters	Denotation	Unit	Definition
Shear rate	γ	s^{-1}	Rate of deformation
Shear stress	τ	N/m^2	Force to attain deformation
Viscosity	η	Pa·s	Ratio of shear stress over shear rate
Yield point	τ_y	N/m^2	Shear stress when flow begins
Settling velocity	v_{st}	m/s	Rate of settling

Shear rate describes the flow velocity in a pipeline or through a pump. Shear stress is the corresponding force required to maintain such flow. The ratio of shear stress over shear rate is denoted as viscosity, which also implies the energy required to deform a flow at a certain speed. An elastic limit has to be overcome before flow could happen. The force required to overcome the elastic limit is defined as the yield point. Particle settlement and separation in a slurry is also an important factor. It is defined as the speed that the solid-liquid interface drops when a slurry is undisturbed. It has to be minimized in order to obtain a homogeneous flow, and to avoid solid agglomeration.

Extensive studies have focused on the rheology of coal-water slurries [191-198]. It was found that shear rate value of slurry flow varies during different stages of the gasification processes. Typical shear rate ranges of coal-water slurry during feedstock mixing, pipe flow and injection are 10-1000s^{-1}, 1-1000s^{-1} and 1000-10000s^{-1}, respectively [199]. Effective viscosity for slurry to be transported under such shear rate ranges needs to be less than 1.5Pa·s, and more preferable when it is less than 1.0Pa·s [200, 201]. Other studies addressed rheological properties of sewage sludge and corn stove slurry. It was found there is a non-Newtonian flow behavior of biomass slurries [202, 203]. A shear thinning property was also observed, which means the viscosity value of the slurry decreased with increasing shear rate. However, few studies have been done focusing on the rheological properties of comingled biomass and coal and water. An additional issue is that a low solid content is expected in all biomass slurry applications which causes issues related to the overall efficiencies of these applications.

Several empirical models have been developed to describe and predict flow properties of coal-water slurries. The Power law (or Ostwald model) and Sisko model [189] are two commonly used shear thinning models for characterizing steady state laminar flow. Equations of these two models are:

$$\eta = k \cdot \gamma^{n-1} \qquad \text{(Eq. 1.16): Ostwald Model}$$

$$\eta = \eta_0 + k \cdot (\frac{1}{\gamma})^m \qquad \text{(Eq. 1.17): Sisko Model}$$

Where

η is viscosity, in Pa·s;

γ is shear rate, in s^{-1};

η_0 is viscosity at yield point, in Pa·s;

k, n, m are fitting constant.

The Sisko model is more accurate when yield point is observed, while Ostwald model is more precise within the shear thinning regime.

Rheological properties, specially the fitting constant n and k are important parameters in pipeline design and pump selection of slurry handling process [204, 205]. Both kinetic energy and friction energy are affected by the rheological properties of the slurry. Eq. 1.16 shows modified Bernoulli equation:

$$\frac{P_1}{\rho} + \frac{\overline{u}_1{}^2}{\alpha} + gZ_1 + W = \frac{P_2}{\rho} + \frac{\overline{u}_2{}^2}{\alpha} + gZ_2 + \sum F \qquad \text{(Eq. 1.18)}$$

Where

$\frac{P}{\rho}$ is pressure energy in the pipeline, in J/kg

$\frac{\overline{u_1}^2}{\alpha}$ is kinetic energy of fluid, in J/kg

gZ is the potential energy of fluid, in J/kg

$\sum F$ is the summation of all friction energy loss, in J/kg

P is the fluid pressure at certain point of the pipe

$\overline{u}$ is the mean flow rate of the fluid at certain point of the pipe

ρ is the volume density of the fluid

α is a constant that is affected by flow rheology

Z is the potential height of the fluid at certain point of the pipe

α = 2.0 for turbulent flow of any fluid; α = 1 for Newtonian laminar flow of fluid; and for laminar flow of power law fluid, α is determined by the following function:

$$\alpha = \frac{2(2n+1)(5n+3)}{3(3n+1)^2} \qquad \text{(Eq. 1.19)}$$

Whereas n is the constant in the rheological property of non-Newtonian fluid.

Friction energy $\sum F$ is always determined by fanning friction factor using following equation:

$$F = \frac{2f\overline{u}^2 L_e}{D} \qquad \text{(Eq. 1.20)}$$

Where f is the fanning friction factor, which is also ¼ of Darcy friction factor. Le is equivalent length of pipe and D is the inner diameter of the pipe.

$$f = fn(N_{Re,nf}) \qquad \text{(Eq. 1.21)}$$

This means the fanning friction factor is a function of Reynolds number of the fluid, and the Reynolds number of non-Newtonian flow is further determined by its rheological properties by several empirically derived equations. Details of the calculation

about friction energy as a function of rheological properties are not within the scope of this study, but maybe discussed in the future work to determine pump and pipe design of the Process Demonstration Scale CE-CERT process.

With calculating the kinetic energy and friction energy of slurry flow at certain point in the pipe, energy W that is required by the pump to flow the material could be decided, which is a basis of pump selection.

1.3 Hydrothermal Process

As stated in the earlier discussion, the success of many future biomass gasification processes relies on its adoption from existing coal gasification technologies. Several technical adaptations are necessary. This is primarily the consequence of the different physiochemical properties between biomass and coal. By definition, biomass covers a wide range of materials. It can be subcategorized into woody biomass, grasses, straws, agriculture leftovers, and animal manure, waste biomass (municipal solid or sewage sludge) and refuse derived fuel (RDF) [206]. Its composition varies significantly among each of these categories [207]. Table 1.4 shows the chemical composition of biomass and coal. Generally speaking, biomass contains less carbon than coal and, most important, is low in its volumetric energy density [174, 208, 209]. Additionally, biomass is highly hygroscopic and hydrophilic, which gives rise to the difficulty to prepare suitable biomass slurries [170]. Thus, a pretreatment step is highly recommended for pre-processing of biomass feedstocks.

Table 1.4 Chemical composition of biomass [a] and coal

Biomass sample	C wt.%	H wt.%	O [d] wt.%	N wt.%	S wt.%	HHV [e] MJ/kg
Woody biomass [b]	52.1	6.2	41.2	0.4	0.08	20.63
Grasses [b]	49.2	6.1	43.7	0.9	0.13	19.73
Straws [b]	49.4	6.1	43.2	0.7	0.17	19.77
Agriculture residue [b]	50.2	6.3	41.9	1.4	0.16	20.12
Animal manure [c]	58.9	7.4	23.1	9.2	1.45	n/a
Biosolids [c]	50.9	7.3	33.4	6.1	2.33	n/a
Peat	56.3	5.8	36.2	1.5	0.2	21.51
Coal	78.2	5.2	13.6	1.3	1.7	27.24

a: mean value; b: measured as receive; c: dry base; d: by difference; e: High Heating Value, calculated value.

Since the early 20th century, thermal treatment of wood has been developed to alter wood surface properties in order to increase its resistance to biodegradation, and to improve its dimensional stability [210-214]. Such processes comprise of a thermal conditioning process and a drying process, e.g. the Plato process and the Thermowood process [211]. Hydrothermal process (HTP) was developed afterwards as steam was added externally. However, there is no rigorous definition for HTP. In general, HTP refers to process with only water (or in form of steam) and the thermal energy involved. In some cases, gas is also involved. Steam in HTP could be either from external water or inherent moisture of biomass, depending on its water consumption and the desired solid fraction in the products. HTP is usually operated under mild thermal condition (150–300°C) and with a pressure of equal or less than water vapor pressure. Because there is

no chemicals added in HTP, it is considered to offer environmental and economic benefit. The physiochemical alternations of biomass structures provoked by HTP lead to a variety of applications [214].

Thermal stability of cellulose, hemicellulose and lignin fractions in biomass has been studied [215-218]. Pyrolitic decomposition of hemicellulose and hemicellulose starts at 150°C. At temperatures lower than 300°C, pyrolysis of cellulosic polysaccharides involves depolymerization, resulting in formation of carbonyl, carboxyl and hydroperoxide groups. Water is consumed and carbon monoxide and carbon dioxide are evolved, leaving the charred residue in solid [219, 220]. The degree of depolymerization primarily depends on the thermal severity, including the treatment temperature and operation duration. At temperatures above 300°C, pyrolysis of cellulose leads to liquid product. Generally, cellulose will be decomposed to activated cellulose as the first step of pyrolytic reaction, and then followed by depolymerization and fragmentation pathways. Anhydro-oligosaccarides, levoglucosan and other monomeric anhydrosugars, furans and other related derivatives will be generated from depolymerization of cellulose. Defragmentation of cellulose, on the other hand, results in the formation ofhydroxyacetaldehyde (HAA), acetol (HA), carbonyls, esters and other products [221]. Pyrolysis of lignin happens at higher temperature than that of holocellulose. This is due to the complex, heterogeneous polymers that form lignin [222]. Its depolymerization is limited at the HTP temeperatue range of up to 300°C.

A literature based summarization of existing HTP is listed in Table 1.5.

Table 1.5 literature review of hydrothermal pretreatment technologies

process	Purpose	Conditions	Mechanism	Tech. Carrier
Torrefaction with Pellestisation	Biomass energy densification and increase the biomass grindability, upgrading biomass suitability as co-firing fuel	200°C -300°C, atmospheric inert (argon) gas, dry condition (<10% moisture content), for 1 hr, heating rate <50 °C/min	a) Devolatilisation and carbonization of hemicelluloses; b) volumetric density of biomass increases as raw materials are dehydrated; c) energy densification: Less energy loss through gas phase than mass loss though gas phase; d) Pellestisation further condense volume of biomass	Energy research Centre of the Netherlands (ECN)
Steam explosion (autohydrolysis explosion)	Defibration of lignin and solubilize hemicellulose to improve cellulose accessibility and its enzymatic digestion	160°C -260°C, in saturated steam, 10s-10min, after process, reactor is explosively depressurized to atmospheric pressure and cooled down to room temp.	a) Steam is able to heat cellulosics rapidly without excessive dilution of sugars; b) Hemicellulose was solubilized when heated; c) Lignin was deformed by explosive force and the microstructure of biomass is interrupted.	Masonite plants, Stack II; Rapid Steam Hydrolysis/Continuous Extraction; Iotech process; Siropulper process

Hot compressed water	To solubilize hemicellulose, resulting in particle shrinkage, pore collapse and surface area decrease. Alter biomass hygroscopicity	150°C -250°C, for 1min-2hours, water fraction of 80% to 90%, in saturated steam.	a) Pressurized hot water generate reactive fiber, recover pentosans and produce hydrolysate; b) Organic compounds in biomass are partially solvolyzed into monomeric sugars; c) Particle shrinkage, pore volume collapse and surface area deceases as biomass is thermalized under pressure, hygroscopic property of biomass particles.	
Fast pyrolysis	Thermal decomposition of organic compound in biomass	450°C-500°C in atmospheric pressure.	a) Organic compound in biomass decompose under temperature, into gas, liquid and char.	BTG, Dynamotive
Liquifaction	Solvolysis of biomass compounds to form bio crude oil	350°C, 20Mp of inert gas for 10 min.	a) Organic compound in biomass decompose under temperature, into biocrude	

Plato technology (hydro-thermolysis)	Upgrading wood durability and dimensional stability	1.Hydro-thermolysis stage, 150°C-180°C in an aqueous environment above atmospheric pressure 2.Drying stage 3.Curing stage: 150°C-190°C 4.Conditioning stage	a) This first stage selectively converts two important components of wood (namely hemi cellulose and lignin) for processing in the third stage. Polyposis is transformed into aldehydes and some organic acids are formed. The reactivity of lignin towards alkylation is enhanced. b) The aldehydes formed react with the activated lignin molecules to form non-polar (consequently water repelling) compounds cross-linked into the structure	Plato International BV, The Netherlands
Thermal wood	To swell and shrink wood, improve the biological durability, lighten the wood and improve thermal durability, increase brittleness of wood	1.Drying as first stage; 2.Heating the wood under 185°C -215°C under steam vapor for 2-3 hours; 3.Reconditioning in moisture for 5-15 hours	a) Decrease the moisture content in wood; b) Breaking hemicellulose chain and thus improve the pressability of wood.	Finnish Thermowood Association

LLNL hydrothermal (Taxaco process)	Increase feedstock energy density	250°C-350°C, at pressure sufficient to maintain the water phase	a) Remove oxygen from the solid to boost its energy density; b) Break down the physical cell structure of MSW.	Taxaco Inc.

HTP was broadly studied as a pretreatment step of biochemical conversion of biomass [223, 224]. Many processes have been developed for such applications. For instance, hydrothermolysis is developed in which hot compressed water at 180-230°C Passes through biomass. After hydrothermolysis, sugar is released from cellulose and hemicelluloses, which leads to higher efficiency in enzymatic fermentation [225]. However, because most carbon is solvolyzed into liquid, the solid content in the product is less than 10%, mainly unsolvolyzed lignite. Another HTP process, steam explosion, refers to thermal treatment of biomass with a high pressure steam, followed by an explosive depressurization. In steam explosion, biomass is subjected to high pressure steam at 210°C to 290°C before steam is rapidly vented. Hydrolysis of hemicellulose and defiberation of lignin occur and cellulose accessibility for enzymatic fermentation is improved. However, because of the rapid decompression, more than 10% of total mass is lost in various forms of volatile matter [226-228]. Steam explosion has been applied in the paper pulping industry. Commercial technologies have been developed, such as Masonite Process, Stake II and Iotech process, etc [214, 229]. More recently, HTP is applied to pretreat biomass as a pre-processing step before thermochemical biomass conversion [181, 214, 230]. Energy research Centre of the Netherlands (ECN) has developed a torrefaction process to increase energy density of biomass [231]. In torrefaction, biomass with inherent moisture of less than 10% is heated to 200-300°C in an inert gas (argon) [232, 233]. After the process, volumetric density of biomass increases, and inherent moisture is driven out from biomass. It is reported that torrefied biomass has an energy density of about 20.4MJ/kg. This is primarily due to decrease of

oxygen content in biomass, which is about 30wt.% lower after torrefaction than prior to torrefaction [142, 231, 234-237]. Additionally, it is found that the torrefied wood is prone to grinding, which may reduce its grinding cost [238]. The product of torrefaction is a black carbonized solid. When torrefaction is applied to pretreat biosolids or animal manure, a drying or dewatering step is required. This requires a lot of energy input. More stringent HTP, such as steam pyrolysis [239, 240], was also studied as a pretreatment process for biomass. JGC Corporation in Japan has developed a process to produce high solid content biomass slurry. In the JGC process, biomass and water is subject to 270-380°C under saturated vapor pressure, and then the mixture is dewatered to obtain pumpable slurry with a desired solid content [200]. Carbon recovery is not reported in the JGC process, but a slurry with up to 60wt.% of solid is produced. The slurry has oxygen to carbon ratio as low as 0.38 and its high heating value is around 25MJ/kg [241-243], a number that is comparable to high rank coals. Another cooperative development by Texaco and Lawrence Livermore National Laboratory (LLNL) has demonstrated HTP with a water separation unit for a densification of biosolids (Dissolved Air Floatation Thickener: DAFT from municipal wastewater treatment plant). This process is operated at 300°C in the absence of oxygen. A pumpable biosolids slurry is produced with a low heating value of 13-15MJ/Kg, which is comparable to low rank coal [244, 245]. A similar process, named SlurryCarb^{TM}, was also developed by EnerTech to prepare solid feedstock from biosolids [246]. HTPs with comparison of their operation condition, proposed mechanism and application are reviewed. There is no commercial plant that has applied HTP in biomass gasification, because no commercial scale biomass gasification

is available, and a thorough understanding and systematic design of large scale HTP has never been done to date.

To summarize, HTP has been actively investigated on its ability to boost biomass energy density thru hydrothermal treatment and dewaterization of its inherent moisture. However, no research has yet focused on applying HTP to prepare pumpable high energy content biomass slurry from a variety of biomass combinations. And, a systematic investigation of the pumpability of hydrothermal treated biomass slurry is needed. Furthermore, the mechanism of HTP on biomass slurry formation needs to be investigated so as to predict products and to optimize HTP conditions. These inspired the development of a low temperature CE-CERT HydroThermal Pretreatment (CE-CERT HTP). This process is aimed at continuously providing a high energy and high carbon content slurry feed at low cost.

1.4 Thesis Objectives

Due of the obstacles described above, this thesis is aimed at developing and systematically investigating a CE-CERT HTP to prepare a pumpable biomass or comingled biomass and coal slurry with a high carbon content that could be efficiently gasified using the CE-CERT Steam Hydrogasification technology. The ultimate goal of this thesis is to provide the technical foundation for a commercial scale CE-CERT HTP. The following objectives will be accomplished:

1. Develop and evaluate the performance of a laboratory scale HTP process. Four carbonaceous feedstocks (coal-biomass-water, biomass-water and biomass-biosolids) will be hydrothermally treated using a procedure developed in our

laboratory. The viscosity, flow and energy content will be determined under various experimental conditions including: particle size; initial composition of feedstock (carbon to water ratio), thermal input (time and temperature of the heating process) and head space gas composition as a consequence of heating. The performance of the HTP will be evaluated for the rheological properties of the resultant slurries, and settling velocity of the particles. Moreover, the carbon balance among gas, liquid and solid phase of product after HTP is analyzed to evaluate the carbon recovery in the slurries. Finally, the heating value of pretreated wood particles is analyzed to estimate energy recovery in the slurries.

2. Investigate the potential mechanism of the formation of the biomass slurry as a consequence of the HTP. Four mechanisms and analytical methods will be proposed to assist in the explanation: 1. Surface charge alternation, zeta potentials of raw wood particle and pretreated wood particle will be analyzed and compared; 2. Particle shrink, Scanning Electron Microscopy (SEM) comparison of wood particles before and after HTP will be compared to visualize this effect; 3. Free bulk water release from biomass microstructure, both SEM observation and liquid-solid distribution of slurry is tested to confirm porous site generation and free water release into bulk phase.
3. Provide the initial design and scale up of the HTP on a lab scale basis, a demonstration scale basis and a commercial scale basis. The lab scale and demonstration scale HTP process will be designed and tested in our lab. Feedstock production rates will be 90g/hr and 8kg/hr on a wet basis for lab and

demonstration scales. Mass and energy balance of both processes is performed based on experimental data. Furthermore, an ASPEN Plus simulation of a commercial scale HTP process will be done using a production rate of 16,700kg/hr on a wet basis. Comparison of economy and energy efficiency will be performed between biomass gasification with or without HTP process using the ASPEN Plus results.

2. Rheological Properties of Slurry Products

Rheology is defined as "the study of deformations and flow of matter". It deals with the phenomenological observation that flowable matter deforms when an external force is applied and such force, if not in balance with internal force, causes deformation [247], as is shown in Figure 2.1.

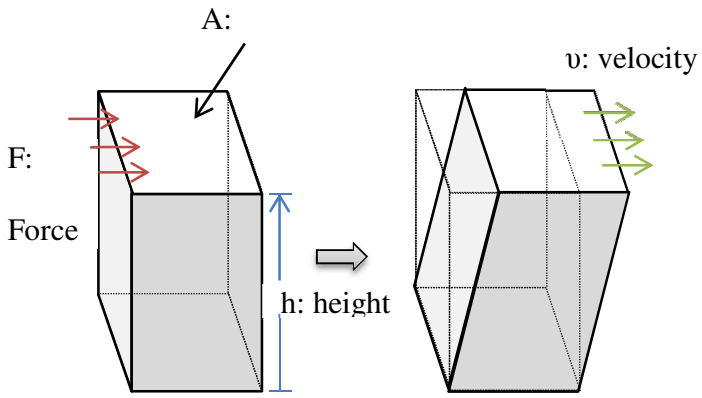

Fig 2.1 Deformation of Flowable Matters due to Applied Force

Rheology, in practice, relates to much broader subjects than just physical response to deformation. Several special features of rheology should to be emphasized:

1. Rheology investigates the property of matter determining its flow behavior rather than its flow and deformation. In other words, it is the internal response of materials to an external force;

2. Rheological properties are non-linear dependencies between forces and deformations or rates of deformations. They are affected by possible impacts, such as time, temperature and magnetic field applied;
3. Rheological properties are measured by the structural change of materials under the influence of an applied force.

The rheology study of slurries is also about its physical properties of resistance to deformation caused by an external force. Several rheological properties that are important in determining the flowability and pumpability of slurries include shear force, shear rate, viscosity and yield stress [248]. The relationship of these parameters is shown in Figure 2.2.

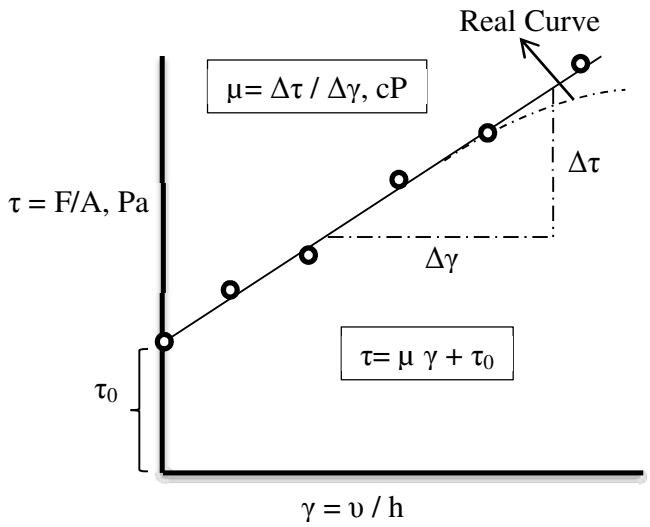

μ: viscosity, τ: shear stress, τ_0: yield stress, F: force applied, A: cross sectional area, γ: shear rate, υ: velocity of moving, h: distance between moving plates.

Fig 2.2 Important Parameter in Rheology Theory and Their Relationship

As can be seen in Figure 2.2, the relationship between shear force and shear rate usually follow a linear relationship, which renders a constant viscosity value at that shear rate value. But, in practice, such a linear relationship does not exist. The viscosity value deviates from its theoretical curve within a certain shear rate range. Such deviation is defined as the non-linear dependency of shear force on shear rate. Previous studies have revealed both coal and biomass (agricultural waste) slurries showed a tendency of decreasing viscosity with an increase in shear rate. The variation in rheological properties was measured for comingled coal and biomass slurries, and the effect of HTP on the rheological properties was investigated. The viscosity determines the pumpability of slurry. This was discussed in the previous chapter. In the chapter that follows, results of experiments will be presented that show the change of viscosity of slurries after HTP.

2.1 Experimental procedure

The following feedstocks were analyzed for their rheological properties:

1. Coal water mixture;
2. Biomass and water mixture;
3. Comingled coal, biomass and water mixture;
4. Comingled biomass and biosolids mixture.

The rheological properties of the biomass and water mixture were determined before and after HTP. A portion of the biomass water slurry after pretreatment was then mixed with coal to form a comingled coal, biomass and water slurry. Several comingled biomass and biosolids slurries were prepared by pretreating biomass and biosolids

mixtures under different conditions. The rheological properties of these slurries were determined in a rheometer. The experiment procedure is shown in Figure 2.3.

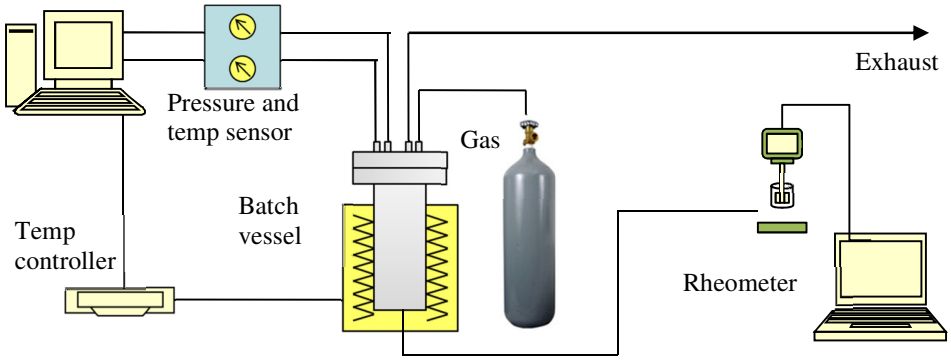

Fig 2.3 Experiment Procedure of Slurry Rheology Tests

Preparation of coal particles

Sub-bituminous coal from southern Utah was used as the coal sample in this study. Lumps of the coal were initially crushed in a laboratory mill (model number: Thomas–Willey model 4, Arthur H. Thomas Company) to reduce the particle size. The particle size of the coal after the initial crush was around 1mm. The mill grind crushed coal particles were pulverized in a grinder (model number: Braun KSM-2W) to obtain fine particles with the particle size smaller than 500 µm. The pulverized particles were sieved into three particle size ranges: 0-150 µm, 150 -250 µm and 250-500 µm. The sieved coal particles were dried in a vacuum oven at 105°C for 3 hours for vaporization of its moisture content.

Preparation of wood particles

Pine wood sawdust was used as a representative for biomass in this study. The sawdust wood particles were first crushed in a laboratory mill (model number: Thomas–Willey model 4, Arthur H. Thomas Company) to reduce the size of the particles. The particle size of wood obtained after the initial crush was around 1mm. Then, following the mill grind, the crushed wood particles were pulverized in a grinder (model number: Braun KSM-2W) to obtain fine particles with a particle size smaller than 500 µm. Then the pulverized particles were sieved into three particle size ranges: 0-150 µm, 150 -250 µm and 250-500 µm. After being sieved, the wood particles were dried in a vacuum oven at 105°C for 3 hours for vaporization of its moisture content.

Preparation of biosolids

Biosolids was obtained from the City of Riverside Wastewater Treatment Facility. They were stored in sealed jar before tests in order to avoid moisture evaporation.

Preparation of coal water mixture

Coal particles were mixed with water to form numerous coal water slurries. The solid loading of these coal water slurries ranged from 40 wt.% to 65 wt.% in increments of 5%.

Preparation of biomass and water mixture

Wood particles were mixed with water to form numerous biomass water slurries. The solid loading of the biomass water slurries ranged from 5 wt.% to 12.5 wt.% in increments of 2.5 wt.%.

Preparation of biomass and water slurry

A portion of the prepared wood particles with the particle size range of 0 μm-150 μm was hydrothermally treated to obtain biomass water slurry. The wood particles were mixed with water, before the pretreatment process, in weight ratios of 1:5, 3:7 and 2:5. The wood and water mixtures were then hydrothermally treated at 240 °C in a hydrogen gas environment pressurized at 100psi for 30min. The solid loading in the slurry products were 20 wt. %, 30 wt.%, and 40 wt.%, respectively.

Preparation of comingled coal, biomass and water slurry

The biomass water slurry obtained from HTP with a solid loading of 20wt.% was mixed with coal with a particle size of 0μm-150μm to form several comingled coal, biomass and water slurries. The weight percentage of coal in the slurries ranged from 0wt.% to 35wt.% in increments of 5wt.%.

Preparation of comingled biomass and biosolids slurry

Wood particles with particle size of 0μm-150μm were mixed with the biosolids in wood to biosolid weight ratios of 1:3, 1:2, 1:1.5 and 1:1.4. The solid loading in these mixtures were 28.75wt.%, 36.67wt.%, 43wt.% and 44.58wt.%, respectively.

All slurry mixtures, after preparation, were stored in glass beakers overnight to allow for complete mixing of solid and liquid. The mixtures were gently stirred immediately before the rheological tests were performed in order to avoid particle settlement. Harsh stirring was avoided to prevent generating small air bubbles in slurries which would impact the rheological test results.

Determination of solid content in comingled feedstocks

Feedstocks were weighted before being comingled. The solid loading in the mixture was calculated by the following equation:

$$wt.\% = \frac{W_s}{W_s + W_l} \times 100\% \qquad \text{(Eq. 2.1)}$$

Where

W_s is the weight of solid fraction;

W_l is the weight of liquid fraction.

The approximate analysis of the solids in the coal, wood and biosolids samples was obtained by Huffman Laboratory Approximate analysis. Table 2.1 shows the results of Huffman Approximate Aanalysis. Notice that the biosolids had a very large percentage of moisture compared to the coal and wood samples. The coal and wood samples accounted for the major source of carbon solid material, as expected.

Table 2.1 Huffman Approximate Analysis of Feedstocks

Fraction (%)	Coal	Pine wood	Biosolids
Moisture	4.0	10.7	92.9
Volatile matter	36.2	74.5	4.9
Fixed carbon	52.2	13.6	0.6
Ash	7.6	0.4	1.6
Total	100	100	100

Rheology test procedure

The rheological properties of the various slurries described above were measured by using an Anton Paar Reolab QC rotational rheometer. This is a coaxial-cylinder type rheometer with a center rotor rotating at a predetermined speed or torque. A six-blade vane spinner with 1 inch outside diameter was used as the center rotor. A picture of the rotor and configuration is shown in Figure 2.4. The vane spinner type center rotor was used for the rheology tests because the vane-cup configuration causes much less error when large particles are present in the test material. There is less impact on the slurry structure compared to cone plate or other rheometer configurations. Consequently, this configuration provides more consistent and reproducible results.

Fig 2.4 Vane-cup System with Six Blade Vane Spinner

The handling of slurries and selection of slurry pumps for industry applications are based on rheological data that are obtained from slurry rheology tests. The crucial parameters for pump selection are the shear stress at certain shear rates, the viscosity of

the slurry, the yield point, and the settlement rate of the slurry. Other physical properties such as attrition and the friction of particles inside the slurry may also need to be considered for selection of the pump. The shear rate and shear stress curve of coal-water and biomass-water slurry coordinates can be characterized by the Generalized Bingham Plastic model as given in Eq. 2.2, where τ is shear stress applied to the system when the shear rate of γ is maintained. τ_y is the yield stress of the starting slurry. K and n are empirical parameters determined by fitting the equation with experimental data. The correlation between shear rate and shear stress corresponds to a power law with a constant coefficient of K. Thus, the viscosity of the slurry is defined as the slope of change in shear rate with a change in shear stress as given by Eq. 2.3. A change in viscosity can be obtained by either shear thinning or shear thickening. The viscosity decreases with increasing shear rate in a shear thinning flow. The viscosity increases with increasing shear rate in a shear thickening flow.

$$\tau = \tau_y + K\gamma^n \qquad \text{(Eq. 2.2)}$$

$$\mu = \frac{\Delta\tau}{\Delta\gamma} \qquad \text{(Eq. 2.3)}$$

One concern is settling of the particles over the time of the experiment and the consistency of the test results. A pretreated biomass water slurry with 20 wt.% solid loading was continuously tested 3 times in a reciprocative manner to evaluate the consistency of data collected during the rheology tests. The results are shown in Figure 2.5. The biomass slurry was first sheared with a shear rate increase of $3s^{-1}$; followed by a reciprocal step, at which the shear rate decreased with a rate of $3s^{-1}$. The sample was

sheared again, with an increase shear rate of $3s^{-1}$, when shear rate reached zero. The apparent viscosity to shear rate profile of the 3 consecutive test runs is shown in Figure 2.5. The direction of the arrows shown in the figure indicates the relative direction of the shear rate. The results exhibited good consistent apparent viscosity values with shear rates of over $60s^{-1}$. However, an error of ±10% was observed at shear rates below $27s^{-1}$, which is probably the result of the settlement of particles at low shear rate.

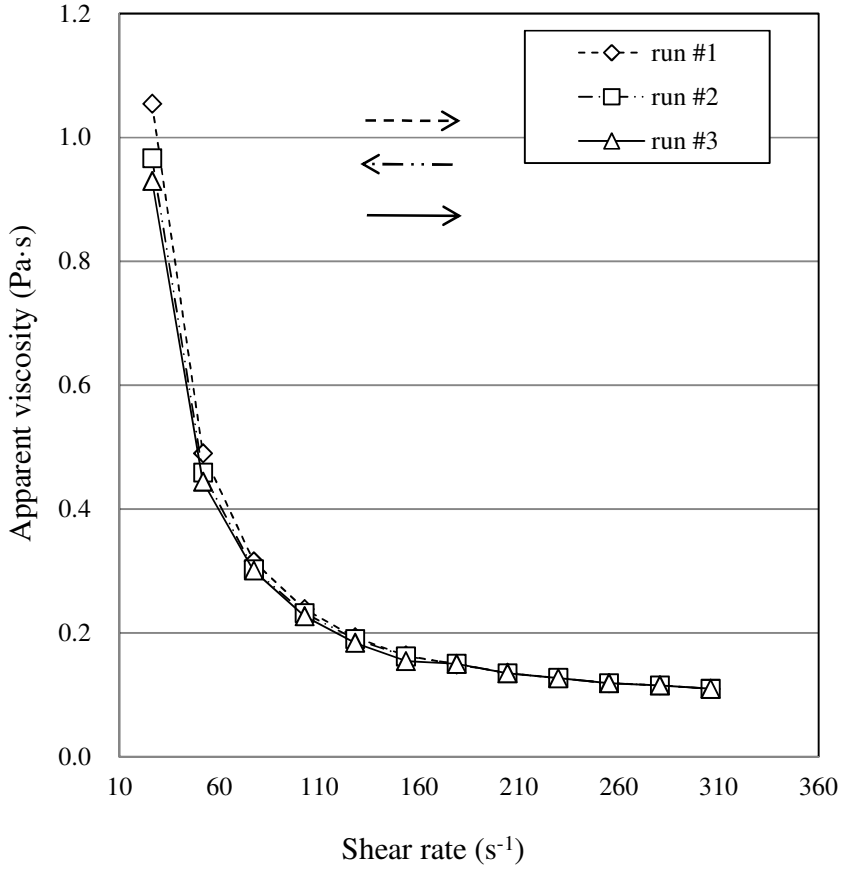

Fig 2.5 Data Consistency of Rheology Test of 20wt.% Pretreated Biomass Water Slurry

2.2 Results and Discussion

2.2.1 Rheological Properties of Coal-Biomass-Slurry

Rheological properties of coal water and biomass water slurries

The effect of an increase in shear rate on slurry viscosity was evaluated for different particle sizes and solid loading for both coal-water and biomass-water slurries. The relationship between shear rate and viscosity was obtained for different particle sizes for coal-water and biomass-water slurries. The results are shown in Figure 2.6 and Figure 2.7, respectively. The solid loading in the coal-water and biomass-water slurries was fixed at 60 wt.% and 10 wt.%, respectively.

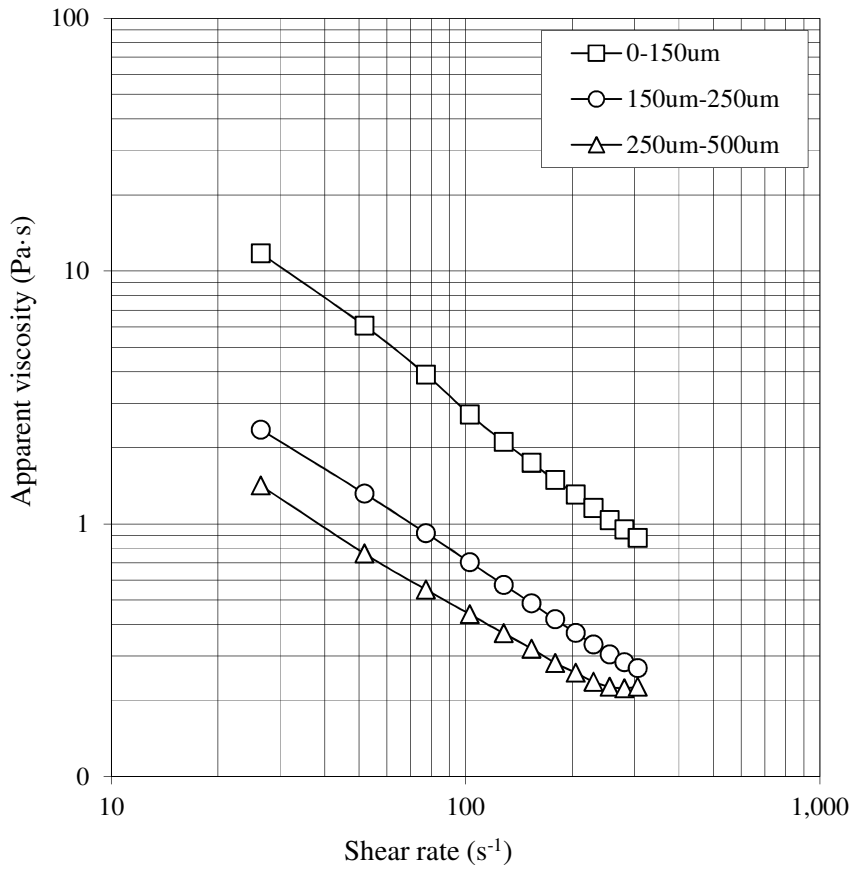

Fig 2.6 Effect of particle size in coal-water slurries (solid loading 60%)

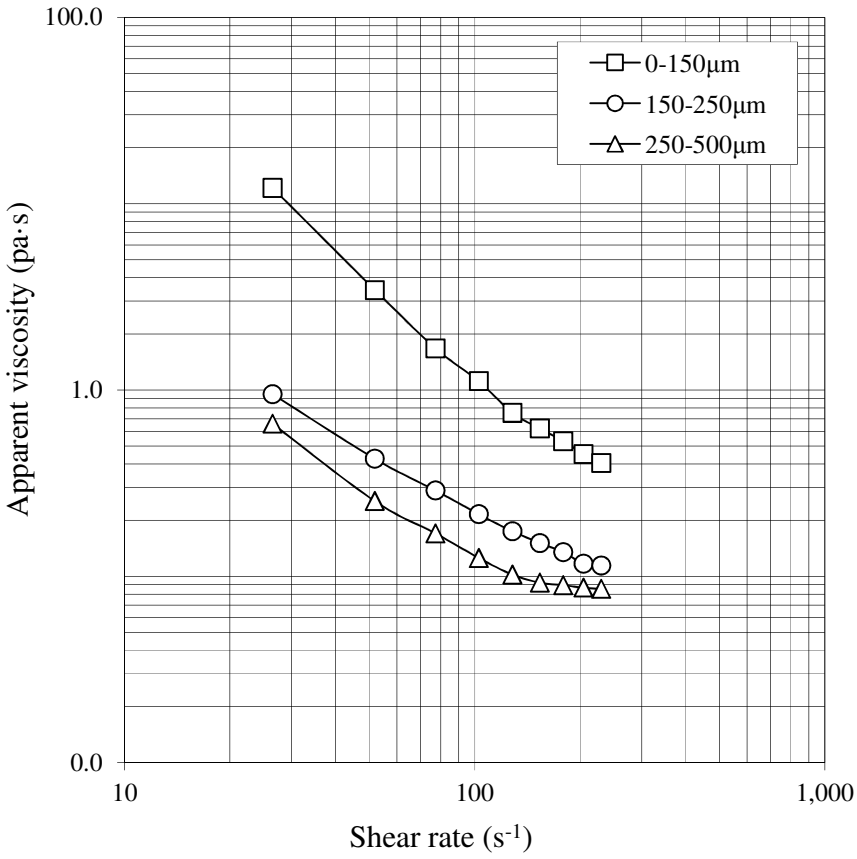

Fig 2.7 Effect of particle size in wood-water slurries (solid loading 10%)

Non-Newtonian shear thinning was observed for both coal-water and biomass-water slurries. The viscosity of the coal-water slurries, shown in Figure 2.6, decreased rapidly with increased shear rate of up to $200s^{-1}$ but then reduced at a slower rate beyond $200s^{-1}$. Also, larger particle sizes had lower slurry viscosity. A similar trend was observed in biomass-water slurries as seen in Figure 2.7. The viscosity of biomass-water slurries decreased rapidly with increased shear rates of up to $100s^{-1}$ but decreased at a slower rate beyond $100s^{-1}$. The viscosity decreased with increasing particle size; similar to that

observed for the coal-water slurries. A comparison of these two figures shows that much higher shear thinning properties were observed for biomass-water slurries. This may be a consequence that water is highly hydrogen bonded with biomass particles, thus higher shear stress was needed for the biomass-water slurries to maintain a same shear rate compared to coal-water slurries.

The maximum solid loading in coal-water and biomass-water slurries varied for different particle sizes. The mixture was not uniform as slurry and particles bound together to form larger particles when the maximum solid loading was exceeded. Table 2.2 shows the maximum solid loading for coal-water and biomass-water slurries.

Table 2.2 Maximum Solid Loading in Biomass-Water and Coal-Water Slurries

	Maximum biomass loading in slurry (wt.%)	Maximum coal loading in slurry (wt.%)
0-150 μm	13	65
150 μm-250 μm	13.5	66.5
250 μm-500 μm	15	68

Experimental results for different solid loading on coal-water and biomass-water slurries are shown in Figure 2.8 and Figure 2.9, respectively.

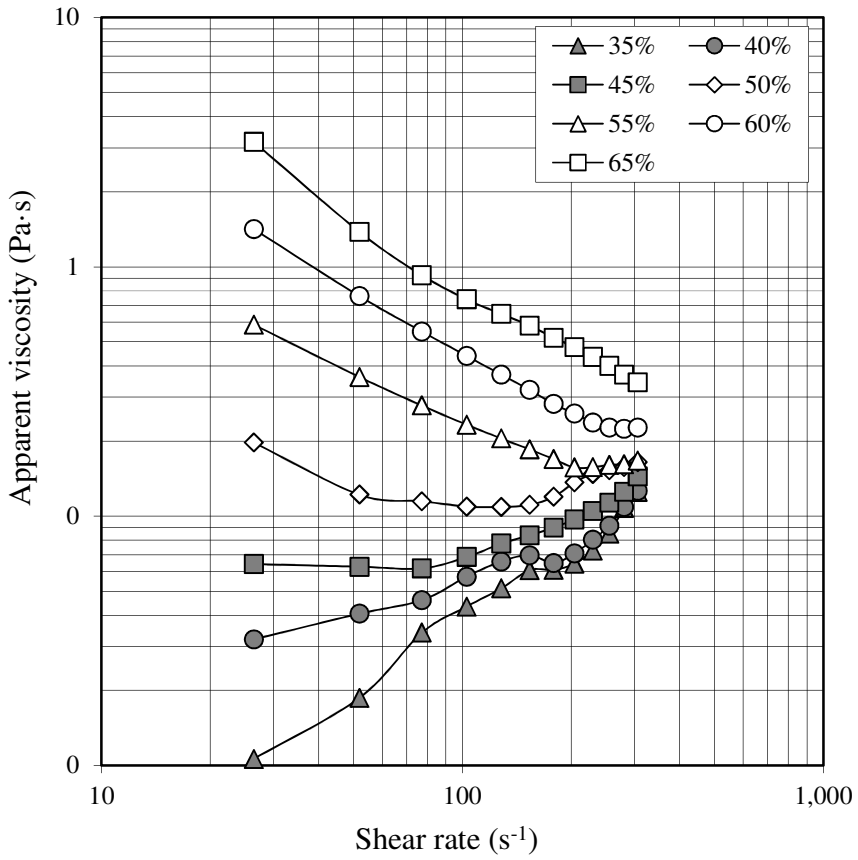

Fig 2.8 Effect of solid loading in coal-water slurries (particle size 250μm-500μm)

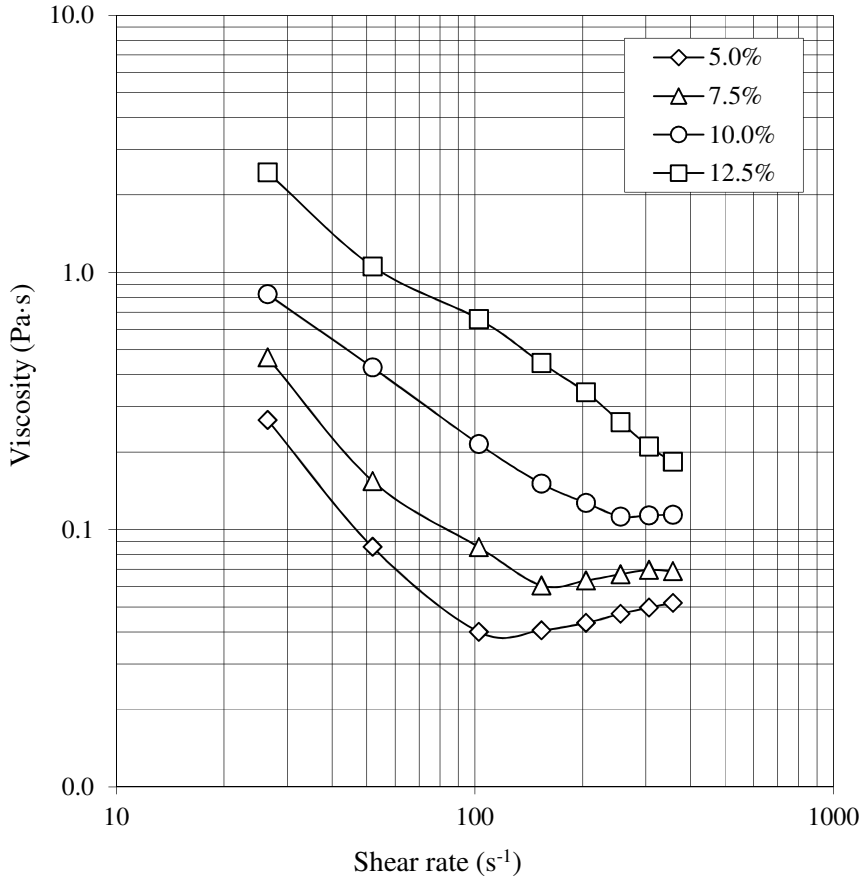

Fig 2.9 Effect of solid loading in wood-water slurries (particle size: 0μm-150μm)

It can be seen from Figure 2.8 that the coal-water slurries changed from a shear thinning property to a shear thickening property as the coal-loading decreased from 50wt.% to 45wt.%. The shear thickening property of coal-water slurry was rarely observed by other studies. Majumder reported that the reason for the thickening was due to the emulsion-solids exhibiting dilatants flow behavior with low solid loading range. It is also seen that the viscosity of coal-water slurries increased with increasing solid loading. There was not much difference between slurries with solid loading of less than 55wt.%

for shear rates over $150s^{-1}$. Similar to the coal-water slurries, the viscosity of biomass-water slurries also increased with increasing solid loading. However, at a shear rate over $100s^{-1}$, Newtonian fluid properties were observed at a solid loading less than 7.5wt.% and the viscosity increased slightly with increasing shear rate. This is shown in Figure 2.9.

The effect of shear rate on viscosity in pretreated biomass-water slurry was also evaluated. Figure 2.10 shows the shear rate to viscosity profile of pretreated biomass slurries with solid loading of 20wt.%, 30wt.% and 40wt%. Unlike the biomass-water slurry before pretreatment, the viscosity profile of pretreated biomass-water slurry dropped rapidly as shear rate increased from $10s^{-1}$ to $200s^{-1}$, then decreased slightly beyond $200s^{-1}$. The viscosity increased with increasing solid loading which is consistent with the biomass-water slurry before pretreatment.

The important result is that with pretreatment there is an increase in the solid loading of a biomass-water slurry to 40wt.% as compared to 12.5wt.% before pretreatment. It is believed that the treatment in the presence of hydrogen under 230°C and 100psi help break down the cellulose and semi-cellulose structure of the biomass which resulted in breaking the hydrogen bond between the biomass and water. This will be further discussed in following chapters.

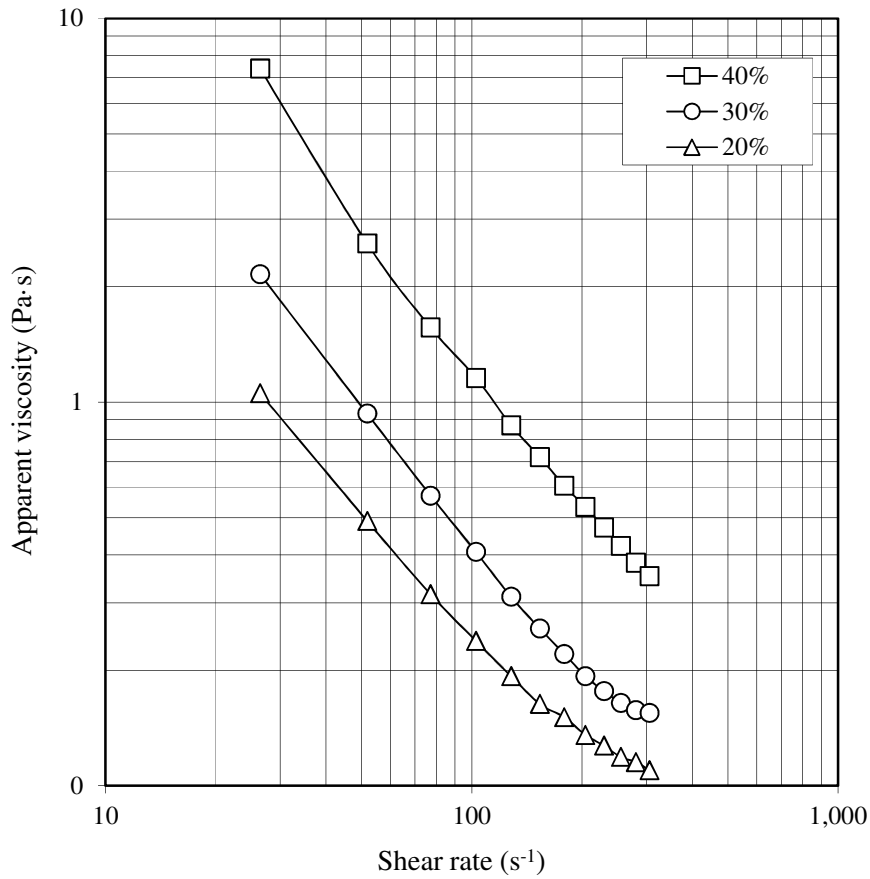

Fig 2.10 Shear rate vs. viscosity of pretreated wood slurry

Figure 2.11 shows the comparison of the viscosity of the various slurries with increasing solid loading. It is obvious that the pretreatment process greatly helped increase the solid content in biomass-water slurry at a similar viscosity. The coal-water slurry had the highest solid content at the same viscosity; followed by the co-mingled biomass and coal slurry. The pretreated biomass-water slurry has significantly higher solid content compared to the biomass-water mixture without pretreatment. The 20 wt.%

of pretreated biomass commingled with 35 wt.% of coal produces a biomass and coal slurry with solid loading of 55 wt.% at the same viscosity.

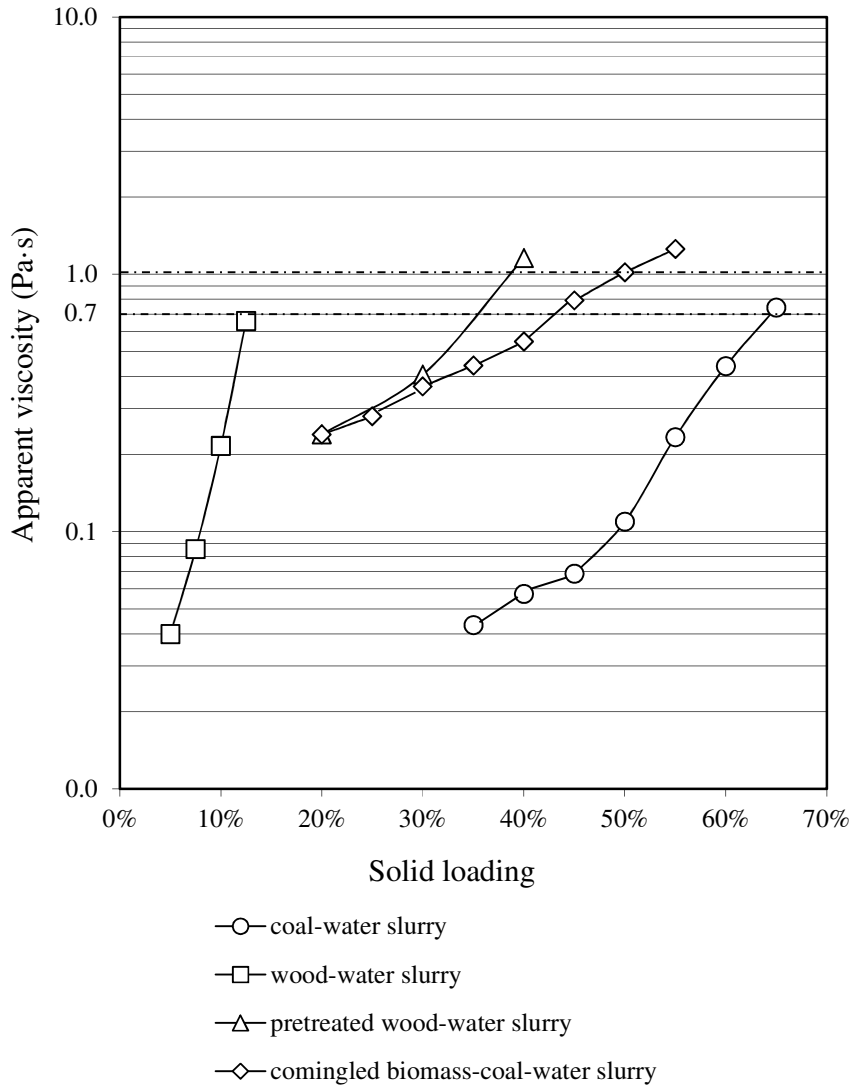

Fig 2.11 Comparison of viscosity of slurries as increasing solid loading (shear rate 102s^{-1})

Earlier in this thesis we suggested that the maximum viscosity of a pumpable slurry is 1.0Pa·s [200, 201], thereby. We have set a target of a viscosity of less than

0.7Pa·s for safely pumping of slurries to our reactor. The pretreatment process outlined herein successfully increased the solid loading in the biomass-water slurry while maintaining the target viscosity. We co-mingled the pretreated biomass-water slurry with coal to increase its solid loading and carbon content. The results of viscosity with increased solid loading of coal-water, biomass-water, pretreated biomass-water and co-mingled biomass and coal slurries are shown in Figure 2.11. It is shown that at 0.7Pa·s viscosity, coal-water slurry had the highest solid loading of up to 65wt.%, and biomass-water slurry before pretreatment had the lowest solid loading of less than 12.5wt.%. After pretreatment, the solid loading in biomass-water slurry of 0.7Pa·s increased to nearly 35wt.% and when commingled with coal, the solid loading increased to nearly 45wt.%. Closer investigation of the water to carbon ratio of these slurries further suggested that the co-mingled biomass and coal slurry provided a water to carbon ratio of 2:1. The optimized water to carbon ratio is 3:1 when using our gasification process. Thus, with pretreatment, the rheological properties of the co-mingled biomass and coal slurry are improved for use as a feedstock for effective steam hydrogasification. Table 2.3 shows the results of mass based on the water to carbon ratio of different slurries at a viscosity of 0.7Pa·s.

Table 2.3 Mass based water to carbon ratio of slurries (under 0.7Pa·s)

	coal-water slurry	biomass-water slurry	pretreated biomass-water slurry	co-mingled biomass and coal slurry
Ratio	0.78	13.82	3.67	2.01

The viscosity plot of different water to carbon ratio in co-mingled biomass and coal slurry is shown in Figure 2.12. Under optimized water to carbon feed ratio of 3:1 which is preferred in our gasification process, the slurry viscosity is less than 0.45Pa·s and provides good pumpability.

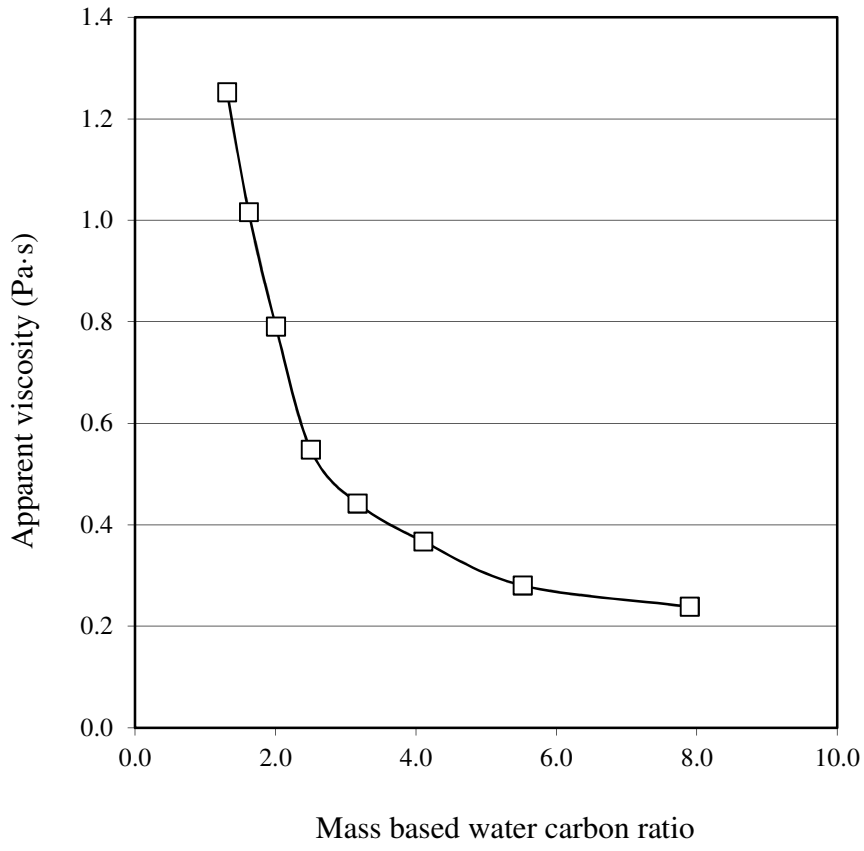

Fig 2.12 Viscosity of Co-Mingled Biomass and Coal Slurries with Different Water to Carbon Ratios

2.2.2 Rheological properties of biomass biosolids slurry

Rheological properties of biosolids slurries

The effect of an increase in shear rate on the apparent viscosity was evaluated with biosolids with and without pretreatment and at different pretreatment temperatures. The results are shown in Figure 2.13. The pretreatment temperature was set at 180°C, 210°C and 240°C, respectively.

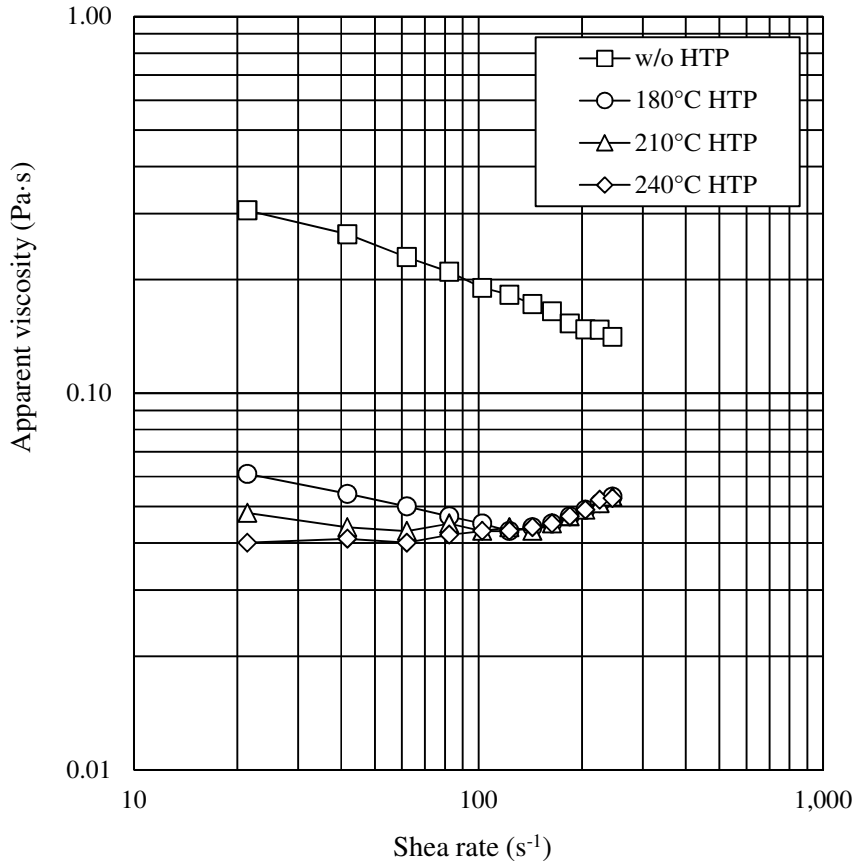

Fig 2.13 Apparent Viscosity to Shear Rate Profile of Biosolids With or Without Pretreatment

Figure 2.13 shows a comparison of the shear rate to viscosity profiles of biosolids with and without HTP at different pretreatment temperatures. It can be observed that without HTP the biosolids slurry exhibited non-Newtonian shear thinning property. The viscosity of biosolids decreased with an increase of shear rate up to $200s^{-1}$, but then reduced at a slower rate beyond $200s^{-1}$. HTP significantly reduced the apparent viscosity of biosolids in all ranges of shear rate. It was found that the biosolids exhibited a homogenous appearance before being pretreated, however, after being pretreated, the biosolids separated into a solid suspension and a liquid fraction when settled. The volume fraction of the solid suspension in the pretreated biosolids decreased with an increase in the pretreatment temperature. The biosolids exhibited Newtonian flow behavior when being hydrothermally pretreated at 240°C and its viscosity value stayed constant at a low shear rate range of less than $100s^{-1}$. This is due to that the large portion of liquid was freed into the bulk phase after HTP. Same apparent viscosity values were observed at higher shear rate of over $200s^{-1}$ when the biosolids were thermally treated at 180°C, 210°C and 240°C. The volume fraction of the solid suspension in the biosolids was less than 20% after HTP.

Experiments were attempted to mix wood particles with both fine and coarse particle size with biosolids. These mixtures failed to form a flowable suspension when the wood loading exceeded 1wt.%. HTP was required for biomass and biosolids mixtures to form a flowable slurry. It was also found that after being pretreated at temperatures of 180°C and 210°C flowable slurries were only occurred with a wood solid loading of less than 10wt.%. When the pretreatment temperature was set at 240°C, a flowable slurry was

produced with a wood loading of up to 41.7wt.%. Rheology tests were performed with biomass-biosolids slurries pretreated at 240°C. The influence of the initial solid content and biomass particle size on the rheological properties of biomass and biosolids slurries was investigated. The results are shown in Figure 2.14 and Figure 2.15, respectively.

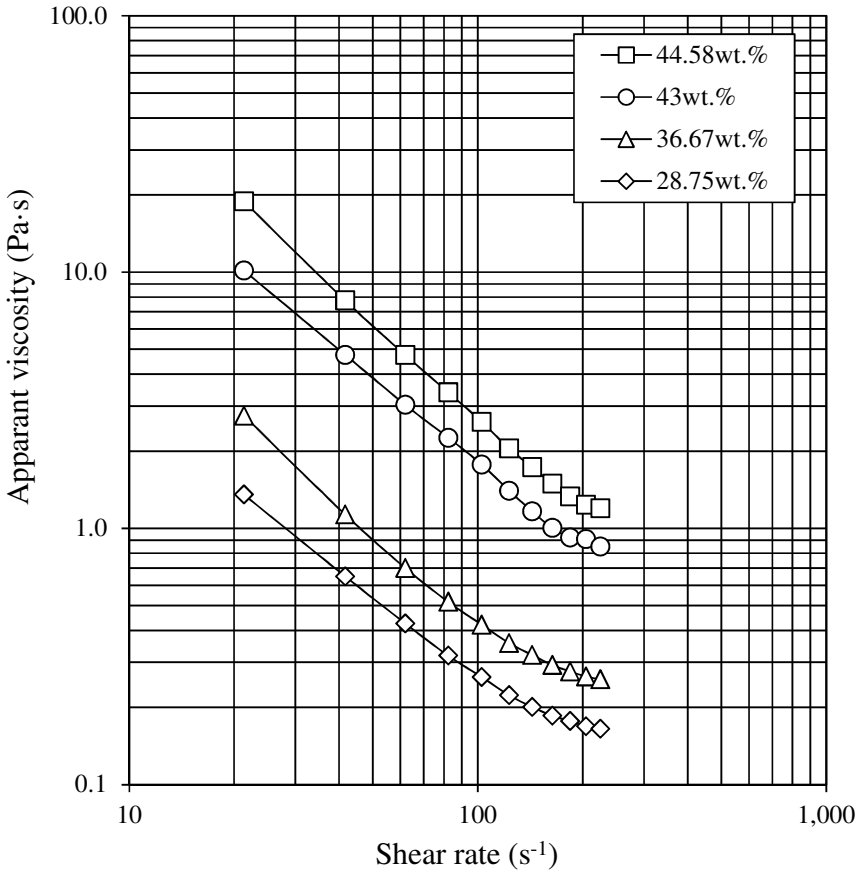

Fig 2.14 Apparent Viscosity to Shear Rate Profile of Pretreated Biomass and Biosolids Slurry: Effect of Initial Solid Loading

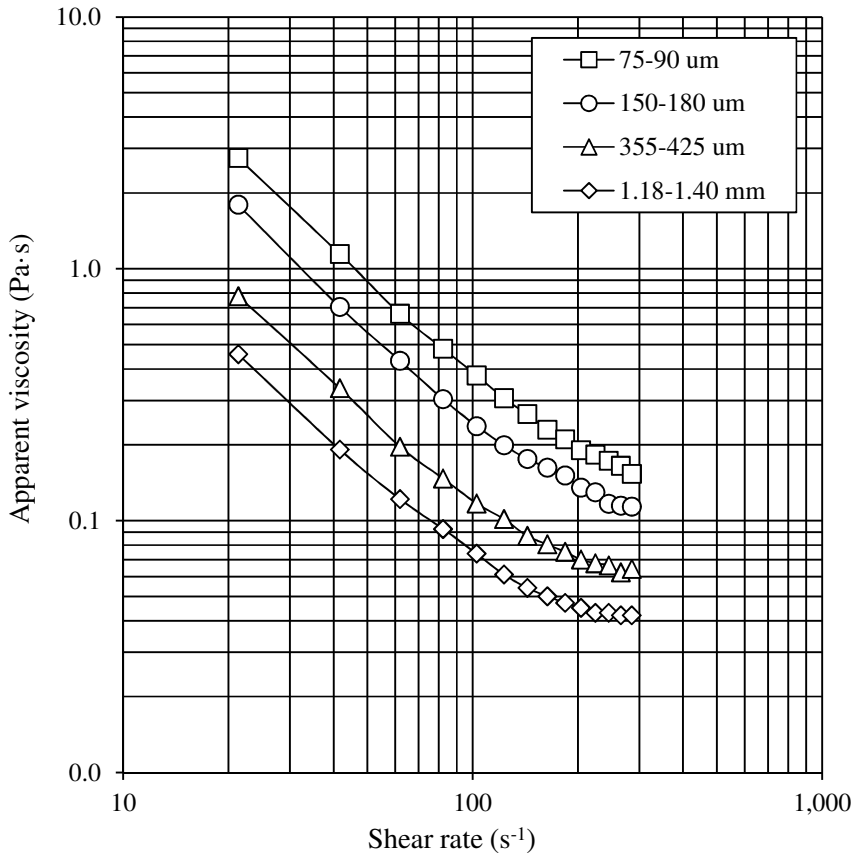

Fig 2.15 Apparent Viscosity to Shear Rate Profile of Pretreated Wood and Biosolids Slurry: Effect of Initial Biomass Particle Size

It was found that biomass and biosolids slurries after HTP exhibited shear thining properties. The viscosity value rapidly decreased with increased shear rate up to $200s^{-1}$ but then reduced at a slower rate beyond $200s^{-1}$. The viscosity value increased with an increase of initial solid loading in the slurries, as shown in Figure 2.14, and decreased with an increase of initial biomass particle size in the slurries, as shown in Figure 2.15. This is due to the fact that less free liquid in the bulk phase was available when more

solids were added. The important result is that at a shear rate of 102s^{-1}, a slurry with a solid loading of 43wt.% and a viscosity value of less than 0.7pa·s was produced. The rheological properties of pretreated biomass-biosolids slurry were similar to that of pretreated biomass water slurry. The comparison of viscosity of slurries as increasing solid loading is shown in Figure 2.16.

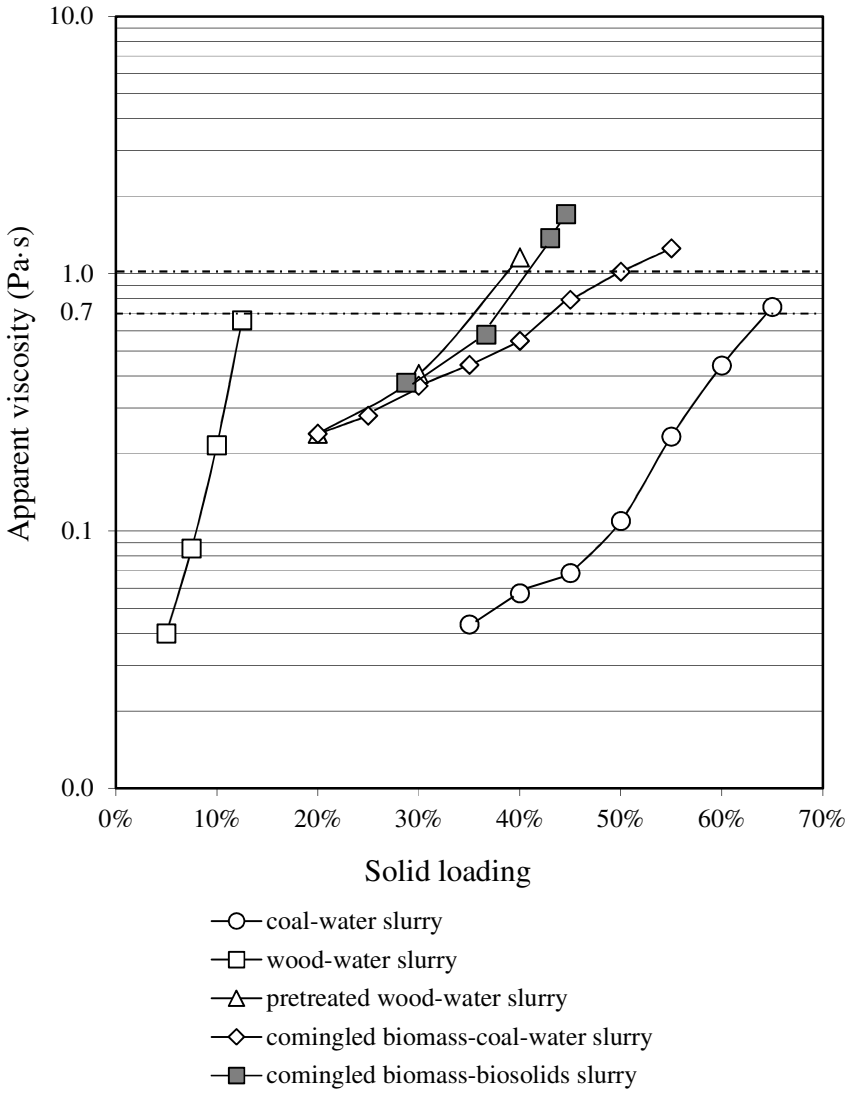

Fig 2.16 Comparison of viscosity of slurries as increasing solid loading (shear rate 102 s^{-1})

It can be concluded that replacing water with biosolids increased the solid content in slurry products at a same viscosity value. This is due to the contribution of solid fraction in biosolids. At the threshold of pumpable slurry visocisty value of 0.7pa·s, the solid loading of biomass biosolids slurry was 38wt.%, compared with 34wt.% of solid in biomass water slurry at the same viscosity value.

3. Carbon Redistribution in Products

It was shown in the previous chapter that after being hydrothermally pretreated the solid loading of wood and water slurries can be increased up to 35wt.% and its viscosity value was maintained at less than 0.7pa·s. It was also found that some material loss and carbon redistribution in the gas, liquid and solid products occurred due to hydrolysis and pyrolysis reactions involved in the HTP. The minimization of carbon loss through gas phase and the maximization of carbon conservation in the slurry are essentially important in increasing the overall carbon conversion in downstream gasification. In other studies, it was reported that elevated fixed carbon content in the feedstock has a positive impact on increasing steam reactivity and suppression of tar formation in gasification processes. Other studies have investigated the material recovery in wood or biosolids using different hydrothermal treatment technologies. It was reported that a total mass loss of 10wt.% have happened in a hydrothermal pretreatment of agricultural wastes by using steam explosion. Another study concluded that the solid recovery after pretreatment of wood by using Torrefaction was from 73% to 90%, depending on the wood species and pretreatment conditions, such as temperature. However, the initial moisture content of wood in this study was less than 11 wt.%, and the pretreatment temperature was set at 270-350ºC. In a similar study, torrified wood product was reported to have a carbon to oxygen ratio of 0.38, which meant more oxygen was lost during the HTP than carbon. Another study on HTP of biosolids showed an increase of solid content to 25wt.% by vaporizing moisture from biosolids. There is yet a lack of studies on examining the carbon redistribution in the resultant products of the

comingled biomass after hydrothermal pretreatment, especially when the biomass is comingled with high moisture content, such as biosolids.

An analysis of the carbon redistribution in the gas, liquid and solid phase after HTP for comingled biomass and biosolids feedstock was done and the results are reported here. The impact of process conditions on the redistribution of carbon composition in the gaseous, liquid and solid products, as well as the carbon recovery in the slurry, was examined

3.1 Experimental Procedure

The samples were quenched to ambient temperature after HTP. The exhaust gas was collected in a Tedler bag. The gas sample was then analyzed of its carbon components by using a Gas Chromatography (GC). The slurry product was then separated of its liquid and solid fraction by vacuum filtration. Polytetrafluoroethylene (PTFE) filters were used in the vacuum filtration in order to avoid absorption of organic compounds. The pressure difference was set at 1 atm in the vacuum filtration process.

Preparation of gaseous, liquid and solid products

The biomass feedstock was prepared using pine wood sawdust. The pine wood was initially crushed in a laboratory mill (model number: Thomas–Willey model 4, Arthur H. Thomas Company) for purpose of particle size reduction. The particle size of wood obtained after the initial crush was approximately 1mm. Following the mill grind, crushed wood particles were pulverized in a grinder (model number: Braun KSM-2W) to obtain fine particles with an average particle size smaller than 500 µm. The pulverized particles were sieved into three particle size ranges 75µm-90µm, 150µm-180µm and

355μm-425μm. The wood particles were dried in a vacuum oven at 105°C for 3 hours to remove the moisture content. Dissolved Air Floatation Thickener (DAFT: discharged from the Wastewater Treatment Plant, Riverside, CA) was used as a representative of biosolids.

A batch type vessel made of Inconel was used as a hydrothermal reactor in the HTP process. The reactor is heated by an electrical heater. The heating rate was measured to be 20°C/min. The initial headspace gas was controlled by pressuring 100psi hydrogen. The reactor was sealed and heated up to the operation temperature and kept at that temperature for 30min. The reactor was convectively quenched to ambient temperature after the HTP by forcing compressed air through. A cooling rate of 42.5°C/min was achieved by using this specific equipment setup. When the temperature in the reactor reached ambient temperature, the exhaust gas was collected in a Tedler bag and the remaining slurry was collected and sealed in glass jars. The pressure in the reactor reached 1420psi when the temperature approached 240°C.

Operation conditions of HTP

A series of experiments were performed to investigate the impact of experimental conditions on the carbon redistribution in gaseous, liquid and solid products. The impact of the initial mass ratio of biomass to biosolids on the carbon redistribution was investigated. In these tests, the prepared wood particles in the particle size of 75μm-90μm were mixed with biosolids to a weight ratio of 1:3, 1:2 and 1:1.5, and were hydrothermally treated at 240°C. The initial carbon to water ratio in such comingled mixtures were 1:5, 1:3.5 and 1:2, respectively. The impact of the initial wood particle

sizes on the carbon redistribution was also investigated. In these tests, the prepared wood particles with particle sizes of 75μm-90μm, 355μm-425μm and 1.18mm-1.4mm were mixed with biosolids in a weight ratio of 1:1.5, and were hydrothermally treated at 240°C. Moreover, the comingled wood and biosolids mixture with an initial wood particle size of 150μm-180μm, and an initial wood to biosolids weight ratio of 1:1.5 was hydrothermally pretreated at temperatures of 180˚C, 210˚C and 240˚C to investigate the impact of pretreatment temperature on the carbon redistribution in the gaseous, liquid and solid products after HTP.

Analysis of Carbon in the Resultant Products

The gaseous product gas after the HTP was sampled in a Tedler bag and analyzed for its carbon composition and relative concentration. A Hewlett Packard 5890 series II Gas Chromatography (GC) equipped with Flame Ionization Detector (FID) was used to measure the hydrocarbon (CxHy) concentration. Another Hewlett Packard 5890 series II Gas Chromatography (GC) equipped with a Thermal Conductivity Detector (TCD) was used to measure the carbon oxide (CO and CO_2) concentrations in the gas phase. The slurry products after the HTP were separated of their liquid and solid fraction. The liquid fraction was tested for its organic and inorganic carbon concentrations by using a Shimadzu TOC-5050 Total Organic Carbon (TOC) analyzer. The solid fraction was dried of its inherent moisture at ambient temperature, and then it was analyzed in a Thermogravimetric Analyzer (TGA) to decide the volatile compound, fixed carbon and ash compositions. The experimental setup implemented in this study is shown in Figure 3.1.

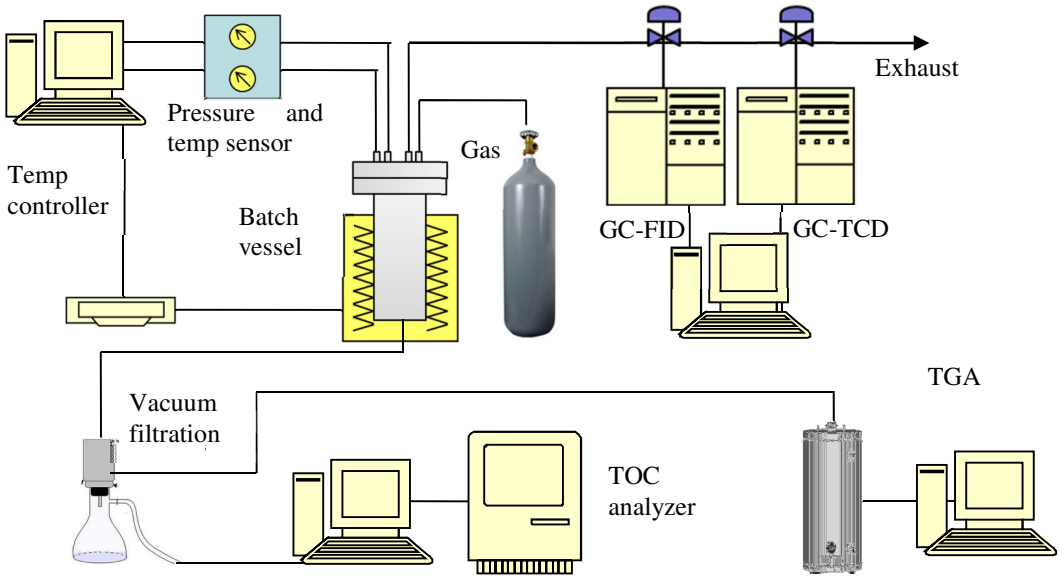

Fig 3.1 Experimental Procedure of Carbon Analysis of HTP Products

3.2 Results and Discussion

3.2.1 Carbon in the gas phase

QPLOT GC column manufactured by Restek™ was used to separate hydrocarbons in the gas mixture and Flame Ionized Detector (FID) was used to measure the hydrocarbon compositions. The QPLOT column was made with divinylbenzene as the stationary phase, which retains light hydrocarbons at above ambient temperature. Other hydrocarbons with higher boiling point are then released with increased column temperature. Therefore, in the chromatograms, response peaks were clearly distributed in five groups. Sequence of the peaks roughly followed the boiling point of corresponding hydrocarbon species, which was in accordance to the number of carbons in its molecule.

Hydrocarbons with carbon number of less than 6 were detected in the gas phase by such GC configuration. It is believed that hydrocarbons with carbon number of equal to or over 6 condensed into liquid phase when the reactor was quenched to ambient temperature.

Carbon oxides were detected in the gaseous products. Alltech 8100/2 capillary column coupled with Thermal Conductivity Detector (TCD) was used to detect the carbon oxides concentrations in this study.

Figure 3.2 and Figure 3.3 show the GC-FID and GC-TCD chromatogram of wood and biosolids HTP process. The HTP was performed with biosolids to biomass mass ratio of 3:1, pretreatment of temperature of 240°C, and biomass particle size of 150μm-180μm.

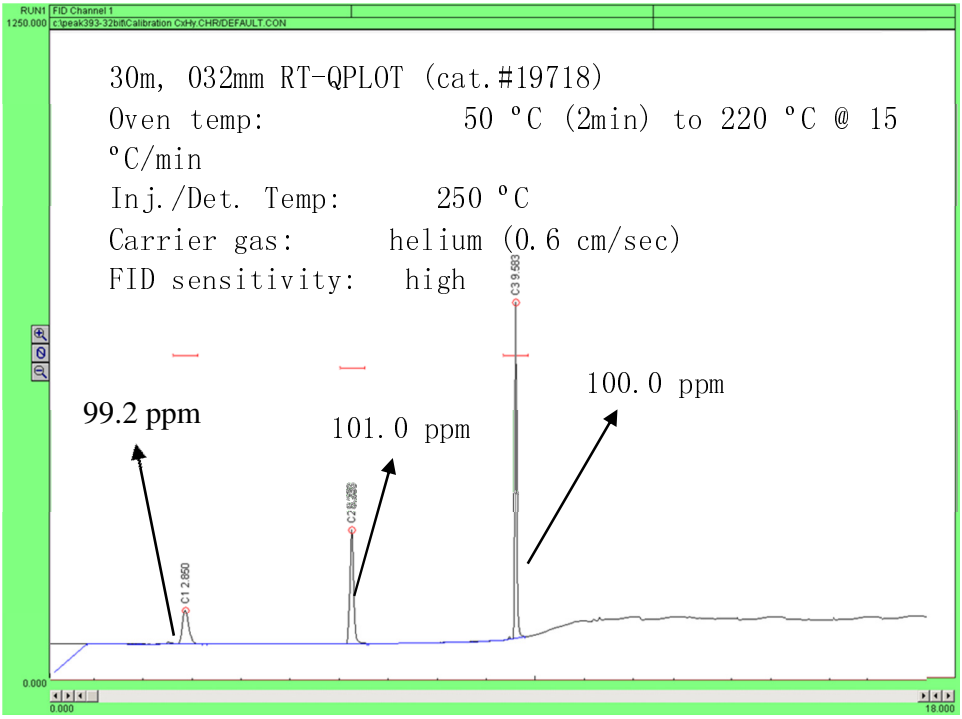

Fig 3.2 Sample GC-FID results: calibration with sample gas (99.2ppm Methane, 101.0ppm Ethane and 100.0 ppm Propane, balanced with Nitrogen)

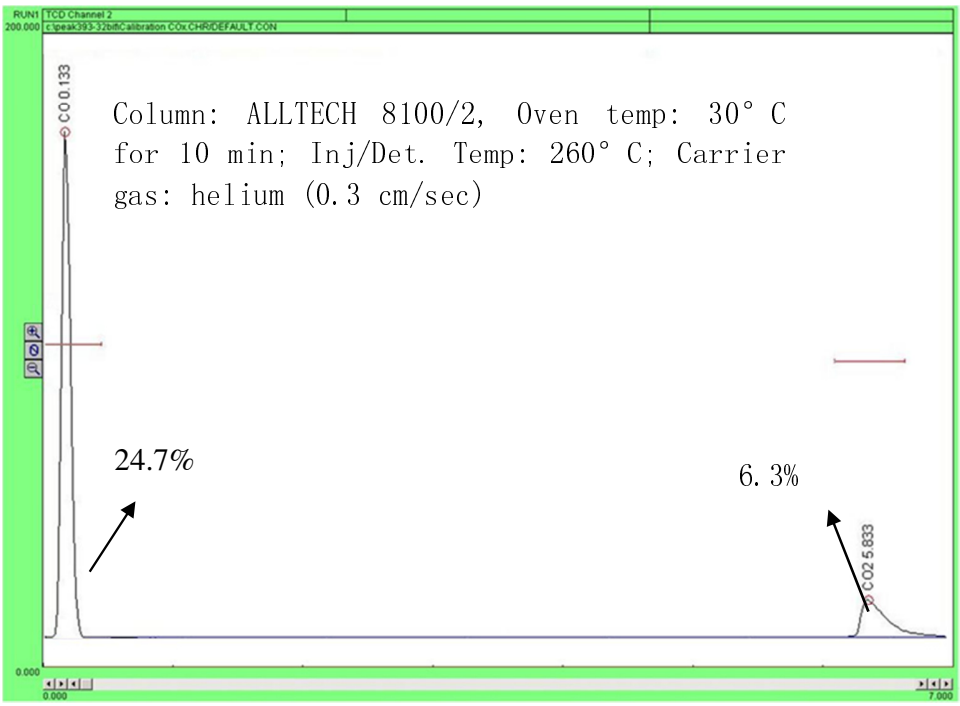

Fig 3.3 Sample GC-TCD results: calibration with sample gas (24.7% CO and 6.3% CO_2, balanced with Nitrogen)

Explicit intervals between groups of peak signals can be distinguished from the GC-FID results. The carbon species in the gas were then categorized into five groups with respect to their carbon numbers. And the concentration of carbon in all species was then obtained by calculation of its carbon number timed with the concentration of the corresponding carbon species:

$$[C]_{cn} = n[C_n] \qquad \text{(Eq. 3.1)}$$

Where

$[C]_{cn}$ is the carbon concentration in hydrocarbons with carbon number of n;

$[C_n]$ is the concentration of the hydrocarbons with carbon number of n.

The amount of carbon in each carbon species was then calculated by following equation:

$$m_{cn} = \frac{[C]_{cn} \times P \times V_g}{RT} \times 12 \qquad \text{(Eq. 3.2)}$$

Where

m_{cn} is the amount (grams) of carbon in hydrocarbon with carbon number of n;

P is the pressure of reactor after HTP, in Pa;

V_g is the head space gas volume after HTP, in m^3;

R is the Avogadro's constant, equals 8.314 $J \cdot K^{-1} \cdot mol^{-1}$;

T is the temperature of gas samples, in K;

12 is the atomic mass of carbon, in g/mol.

The Carbon Percentage (CP) was defined in this study to represent the percentage of carbon presented in the gas phase after HTP over the total carbon initially input in the feedstock. Its definition was defined by the equation below:

$$CP = \frac{m_{cn}}{m_c} \times 100\% \qquad \text{(Eq. 3.3)}$$

Whereas m_c is the total amount of carbon input in the feedstock, which is calculated by combination of Huffman test results of feedstock and the total weight of feedstock loading.

The results of carbon percentage in the gas phase after HTP with different pretreatment temperature was shown in Figure 3.4.

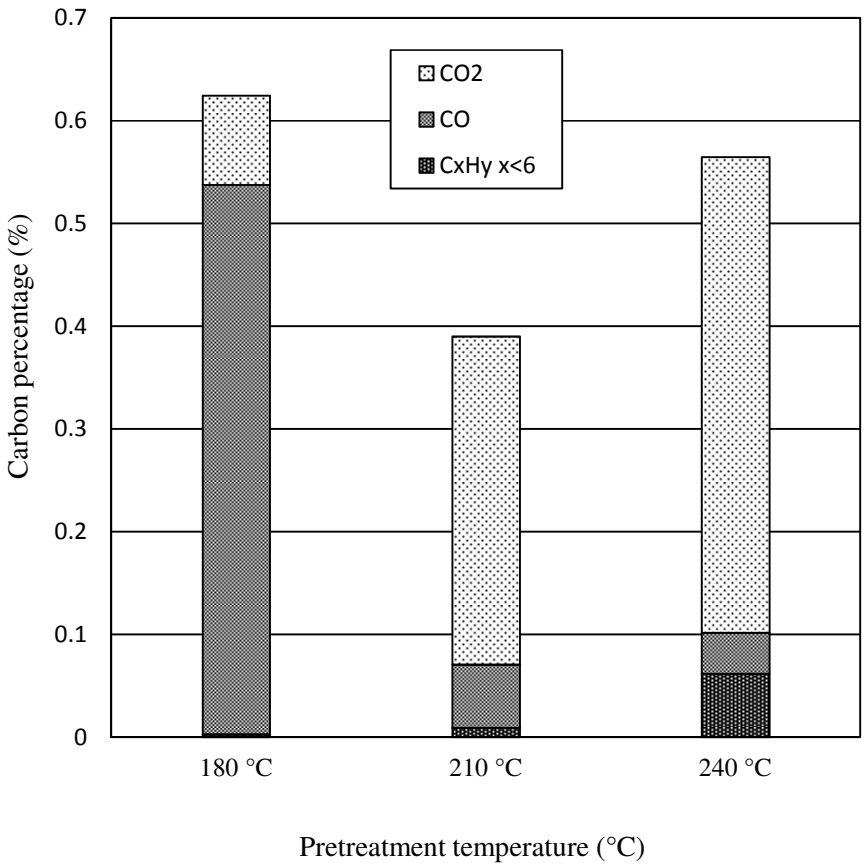

Fig 3.4 carbon percentage in the gas phase: effect of pretreatment temperature

It was found that pretreatment temperature had a major effect on the carbon composition. A noticeable increase of C_xH_y concentrations was observed when pretreatment temperature reached 240°C. The total carbon percentage in the gas phase in the form of C_xH_y was less than 0.07%. The major carbon species in the gas after HTP was CO when pretreatment was performed at 180°C. The CO concentration decreased while the CO_2 concentration increased and became the major product as the pretreatment temperature increased. The total carbon percentage in the gas phase was less than 0.7%

after the HTP. It is believed that low temperature catalytic Water Gas Shift (WGS) reaction occurred when temperature exceeded 210°C, through a reaction shown below, which led to the conversion of CO to CO_2.

$$CO + H_2O \leftrightarrow CO_2 + H_2$$

Iron and copper present in the biosolids were believed to be possible source of WGS catalysts. Such assumption needs to be verified and is not within the scope of this study.

The carbon percentage in the gas phase was also evaluated by varying the initial biosolids to wood mass ratios. These experiments were carried out with an initial wood particle size of 150μm-180μm, and the pretreatment temperature was set at 240°C. The results are shown in Figure 3.5. It was observed that with an increase of wood wastes to biosolids ratios in the feedstocks, more CO and CO_2 were found in the gas phase, and CxHy concentrations in the gas phase had an unnoticeable change. It was believed that with an increase of wood wastes in the feedstocks, more carbon was available for chemical conversions. Data presented in Figure 3.5 showed that with an initial biosolids to wood wastes ratio of 1.5:1, less than 1.2% of carbon was present in the gas phase.

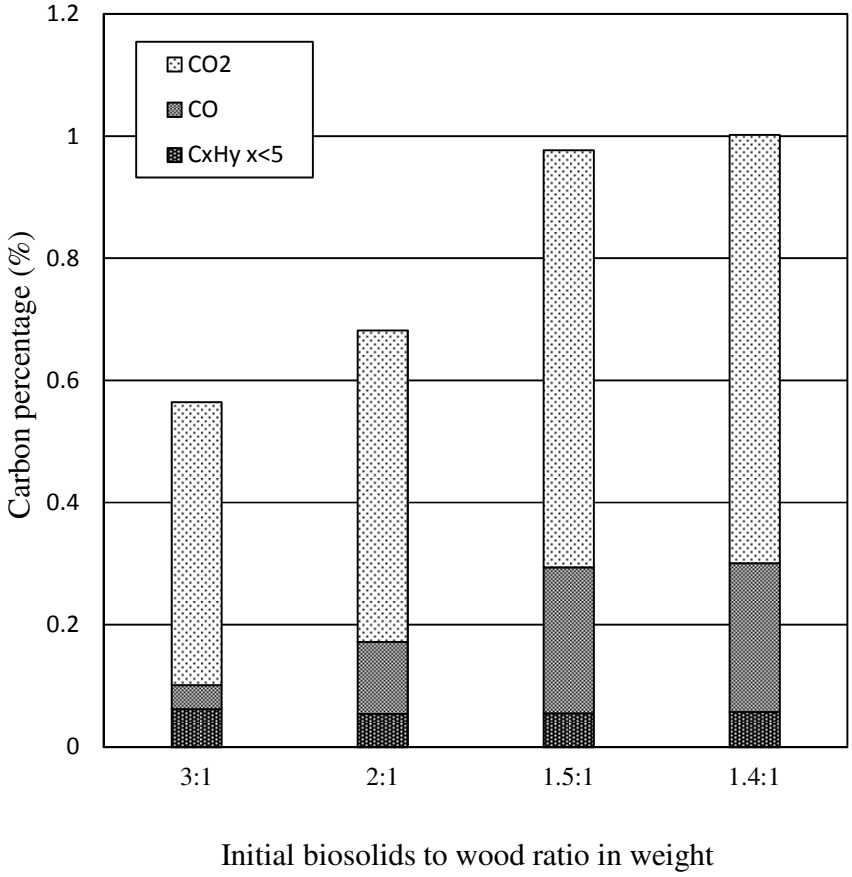

Fig 3.5 Carbon percentage in the gas phase: effect of initial biosolids to wood ratio in weight

The effect of initial wood particle size on carbon percentages in the gas phase after HTP was also evaluated. It was found that the initial particle size of the wood has insignificant effect on the carbon percentages in the gas phase after HTP, as shown in Figure 3.6.

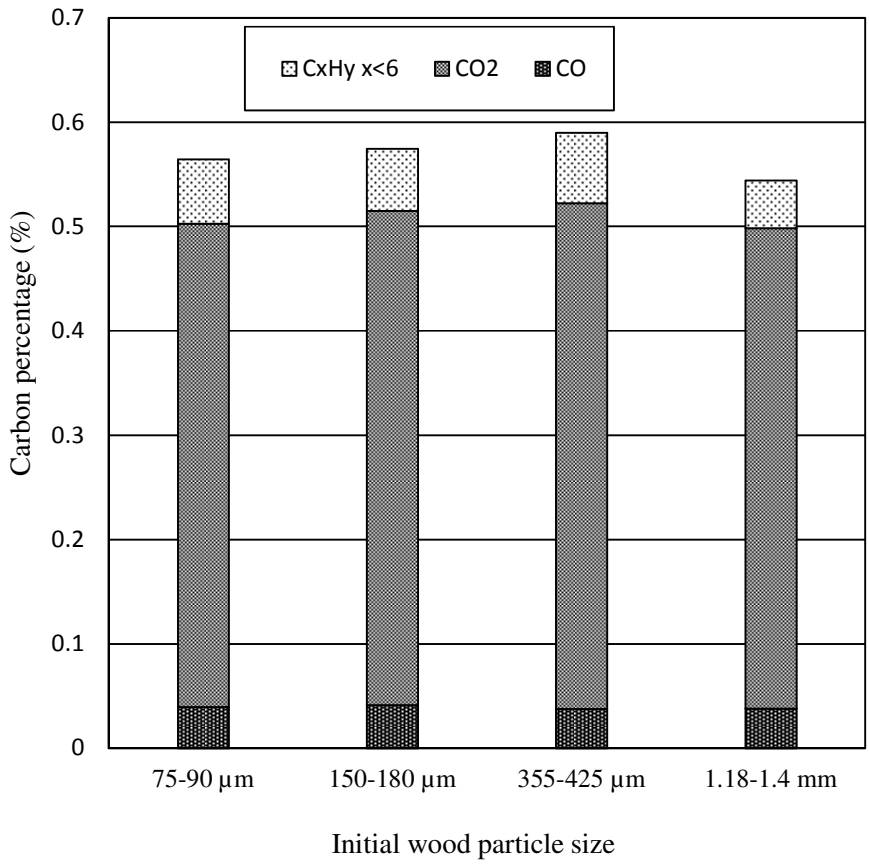

Fig 3.6 carbon percentage in the gas phase: effect of initial wood particle size

3.2.2 Carbon in the Liquid Phase

The liquid in the pretreated slurries include two parts: free bulk liquid and the inherent moisture. Liquid in the bulk phase is defined as the liquid that could be separated from the slurries by a mechanic force, such as vacuum filtration. The inherent moisture is the liquid that was trapped in the microstructure of the solid, and it could be measured by TGA. It was assumed in this study that the carbon composition was identical in the two liquid forms. The organic and inorganic carbon fractions in the free bulk liquid were

measured by using TOC analyzer. And carbon percentage in the liquid phase included carbon in both liquid forms.

The Carbon Percentage is used to represent the amount of carbon in the liquid phase after HTP, and it defined as follows.

$$CP = \frac{m_{cl}}{m_c} \times 100\%$$

Where

m_c is the total amount of carbon input in the feedstock;

m_{cl} is the amount of carbon in the liquid phase, either in form of organic carbon or inorganic species, m_{cl} was further defined by the following equation:

$$m_{cl} = [c]_{cl} \times V_l$$

Where

$[C]_{cl}$ is the concentration of carbon read from TOC/TC analyzer, in mg/L;

V_l is the volume of liquid product, in L.

The effect of pretreatment on carbon percentage in the liquid phase of the biosolids after HTP was determined. The result is shown in Figure 3.7. It was found that the total organic carbon concentration in the liquid phase increased from 20mg/L to over 200mg/L. The concentration of the inorganic species showed no significant change.

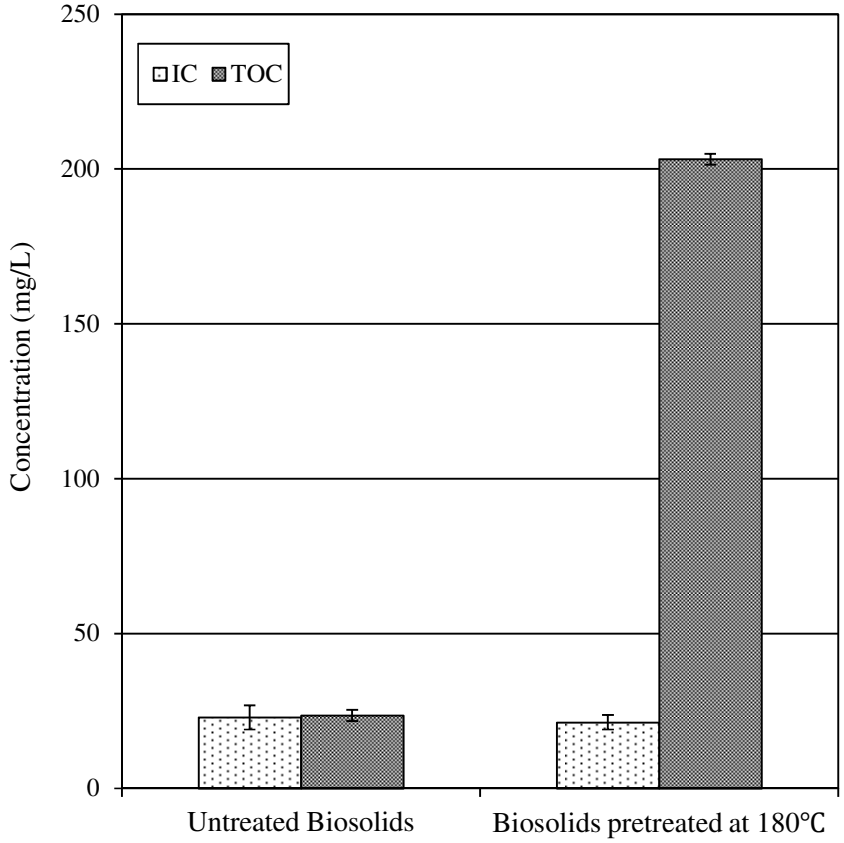

Fig 3.7 TC/TOC results of liquid in biosolids before and after HTP

The effect of temperature on carbon percentages in the liquid phase after HTP was evaluated. The results are shown in Figure 3.8.

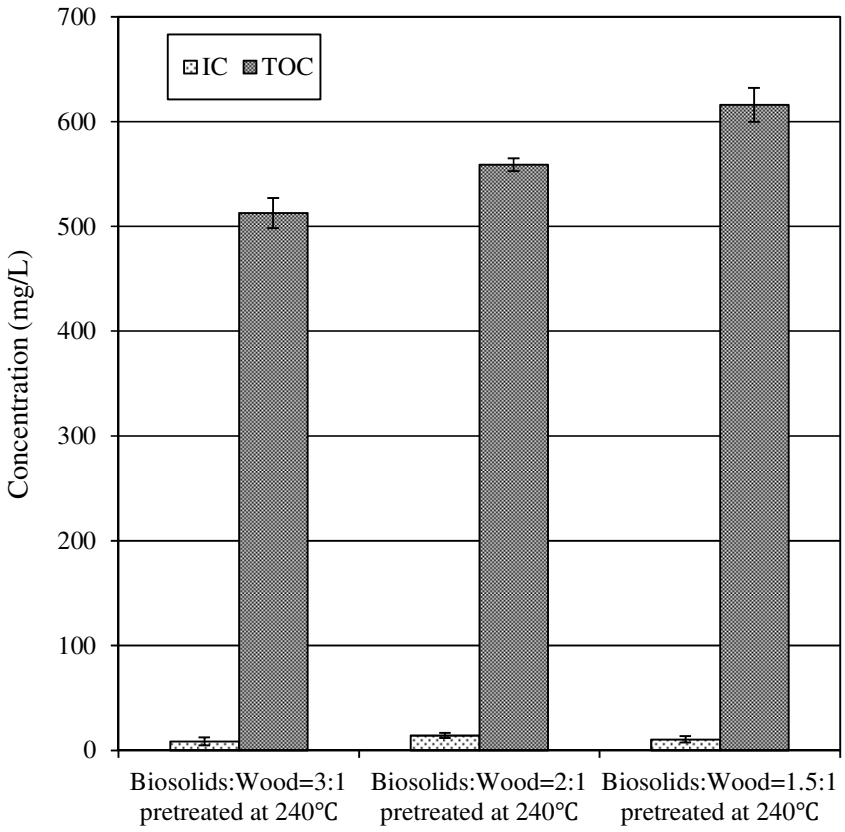

Fig 3.8 TC/TOC Results of Comingled Wood and Biosolids Slurry: Effect of Initial Biosolids to Wood Ratio

It was observed that less than 0.2% of carbon was in the liquid before HTP, which was the carbon dissolved in the biosolids. The inorganic species in the liquid phase was consumed when HTP was applied. And, it was believed this is the result of the decomposition of metal carbonates at elevated temperature and pressure. However, no experimental confirmation has been performed at this stage of study to confirm this opinion. It was also observed that with an increase of pretreatment temperature, more

carbon was found in the liquid phase. Over 95% of carbon presented in the liquid phase was in the form of organic carbon. And the total carbon percentage presented in the liquid phase after HTP was less than 3% of the total carbon initial loaded in the feedstocks.

The effect of the initial biosolid to wood ratios on the carbon percentage in the liquid phase after HTP was also determined. These results are shown in Figure 3.9. Even though higher organic and inorganic related carbon concentrations were detected in the liquid phase as a consequence of a higher initial wood loading, the carbon percentage in the liquid phase decreased with an increase of the initial wood to biosolids ratio.

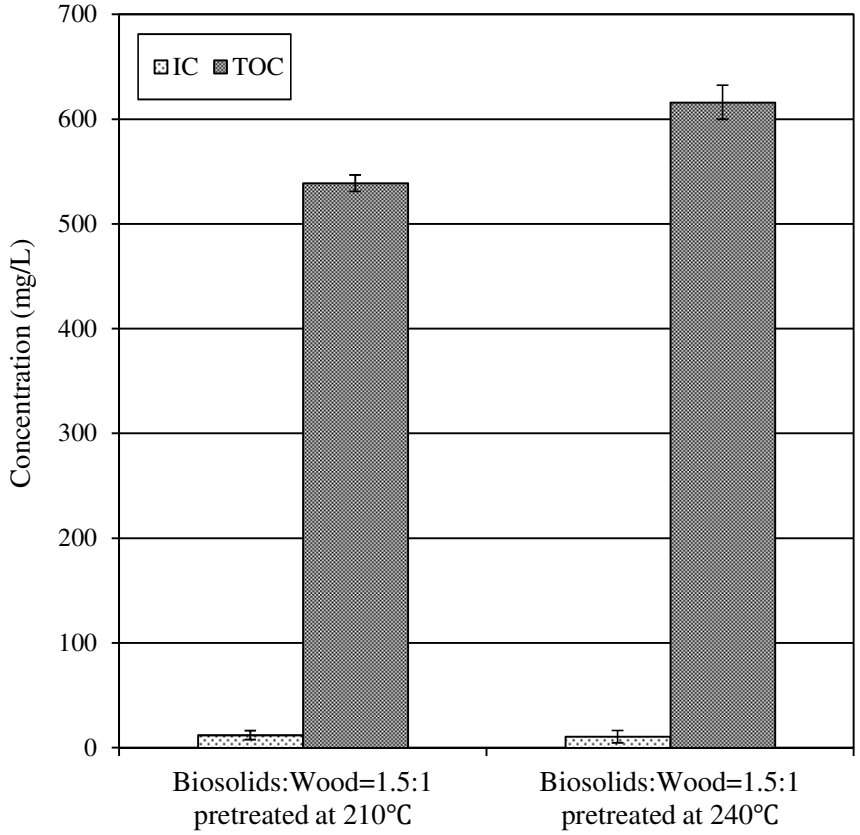

Fig 3.9 TC/TOC Results of Comingled Wood and Biosolids Slurry: Effect of HTP Temperature

The effect of the initial wood particle size on carbon percentages in the liquid phase after HTP was also evaluated. It was found that the initial wood particle size has an insignificant effect on the carbon percentages in the liquid phase after HTP.

3.2.3 Carbon in the Solid Phase

Carbon in the solid phase of the resultant slurries after HTP was evaluated by measuring the thermogravimetric kinetics of the solid fractions. Weight loss of the solid

fraction with an elevated temperature was first carried out with N_2 as a carried gas for the analysis of volatile compounds. When the temperature inside the Thermogravimetry Analyzer (TGA) exceeded 750˚C, N_2 was replaced with O_2, after which the fixed carbon fraction was analyzed. It was found that the temperature has a major effect on changing the carbon compositions in the solid phase after HTP. The effect of pretreatment temperature on carbon compositions in the solid phase after HTP was evaluated and the results are shown in Figure 3.10. Two clear weight losing stages were observed in the TGA curves, as shown in Figure 3.10. These two peaks represent the volatile carbon and fixed carbon in the feedstock. Differential Thermogravimetry Analysis (DTG) was also performed. The results are shown in Figure 3.11. It was concluded that the fixed carbon increased when HTP was applied, and also increased with an increase in the pretreatment temperature. The fixed carbon in the solid increased to 40% in the solid fractions when HTP was performed at a temperature of 240˚C.

The effects of the initial wood to biosolids ratio and initial wood particle size on the solid phase after HTP were also evaluated. It was observed that insignificant changes were found when the initial wood to biosolids ratios and initial wood particle sizes changed.

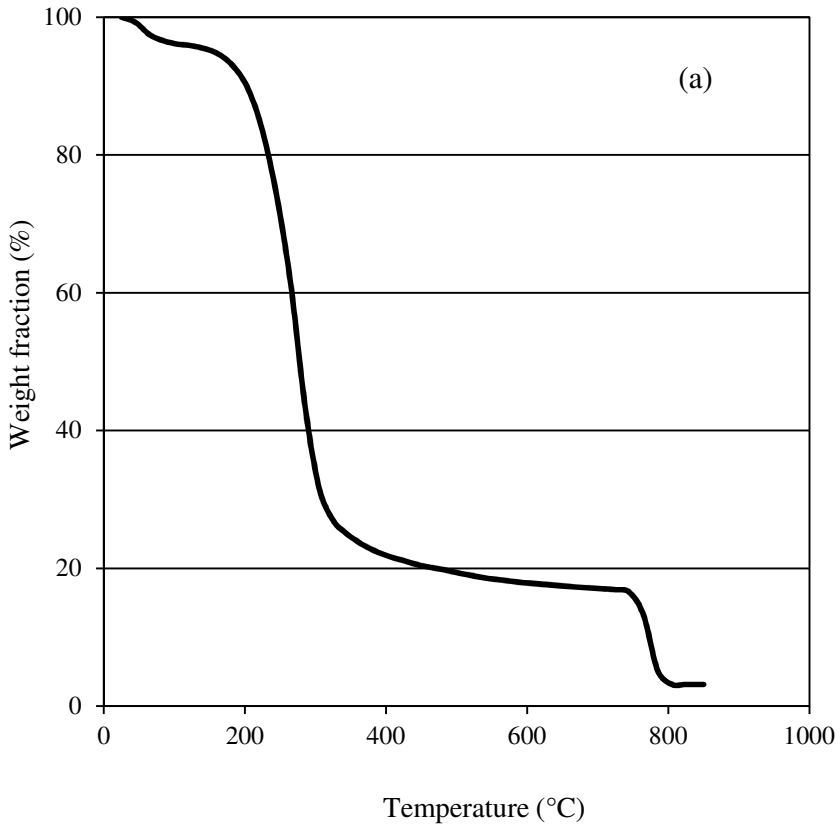
(a)
Weight fraction (%)
100
80
60
40
20
0
0
200
400
600
800
1000
Temperature (°C)

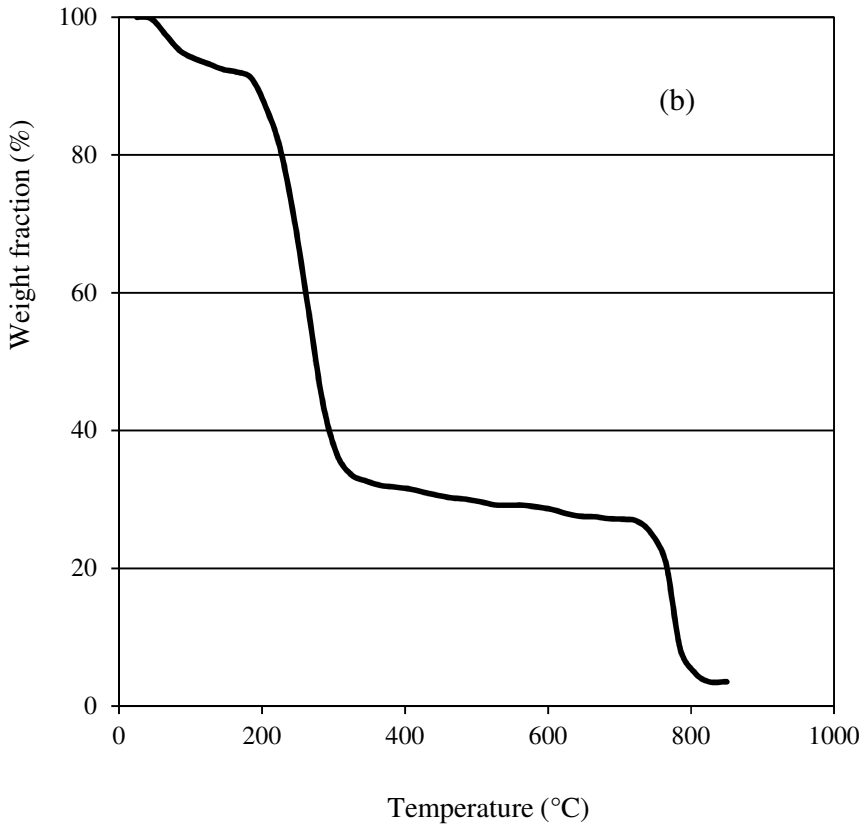
(b)
Weight fraction (%)
100
80
60
40
20
0
0
200
400
600
800
1000
Temperature (°C)

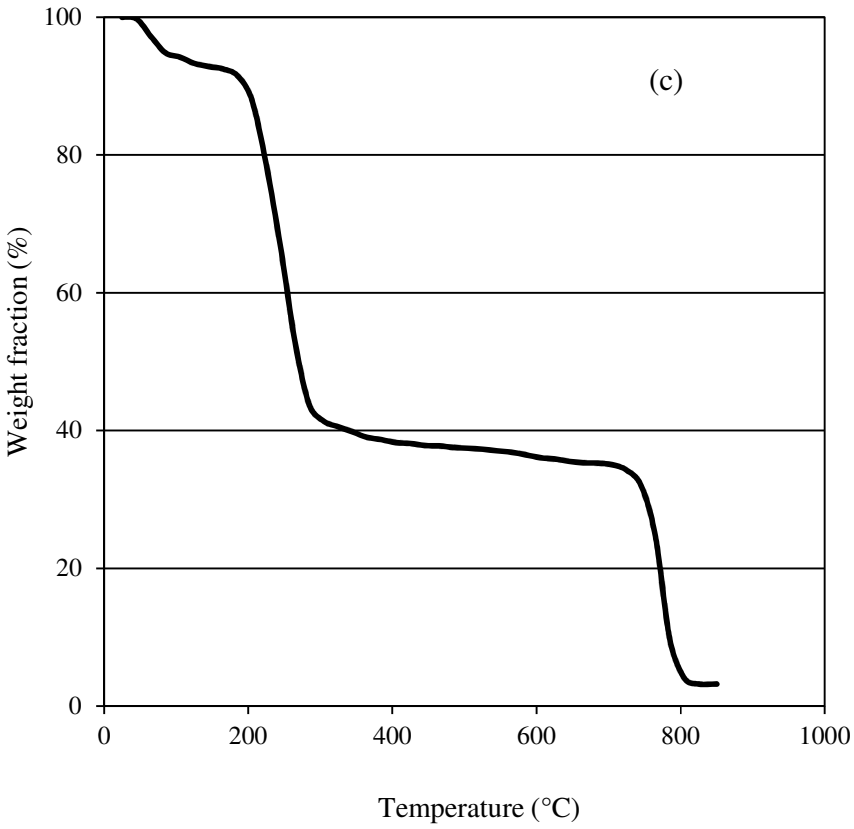
(c)
Weight fraction (%)
100
80
60
40
20
0
0
200
400
600
800
1000
Temperature (°C)

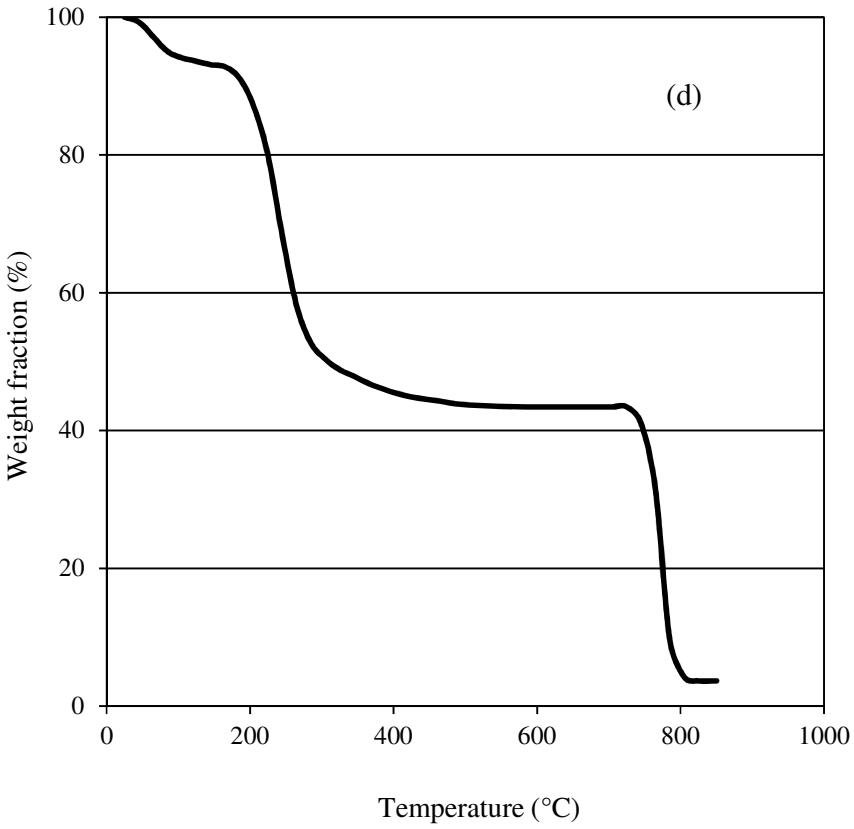

Fig 3.10 (a) TGA result of wood before HTP; (b) TGA result of solid in comingled wood-biosolids slurry after HTP at temperature of 180°C; (c) TGA result of solid in comingled wood-biosolids slurry after HTP at temperature of 210°C; (d) TGA result of solid in comingled wood-biosolids slurry after HTP at temperature of 240°C.

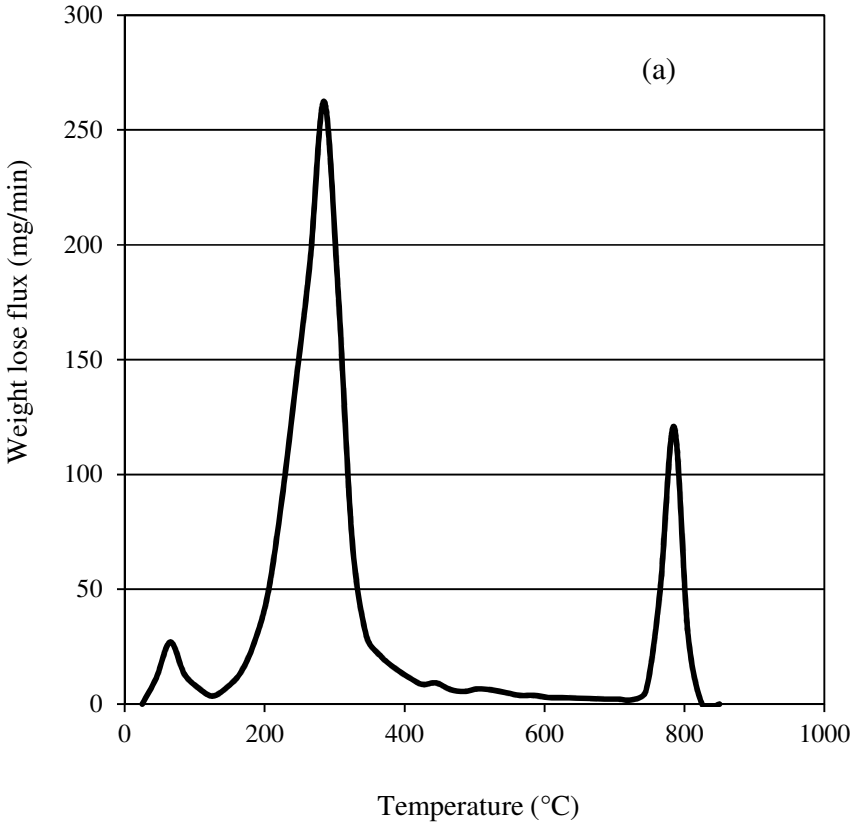
(a)
Weight lose flux (mg/min)
300
250
200
150
100
50
0
0
200
400
600
800
1000
Temperature (°C)

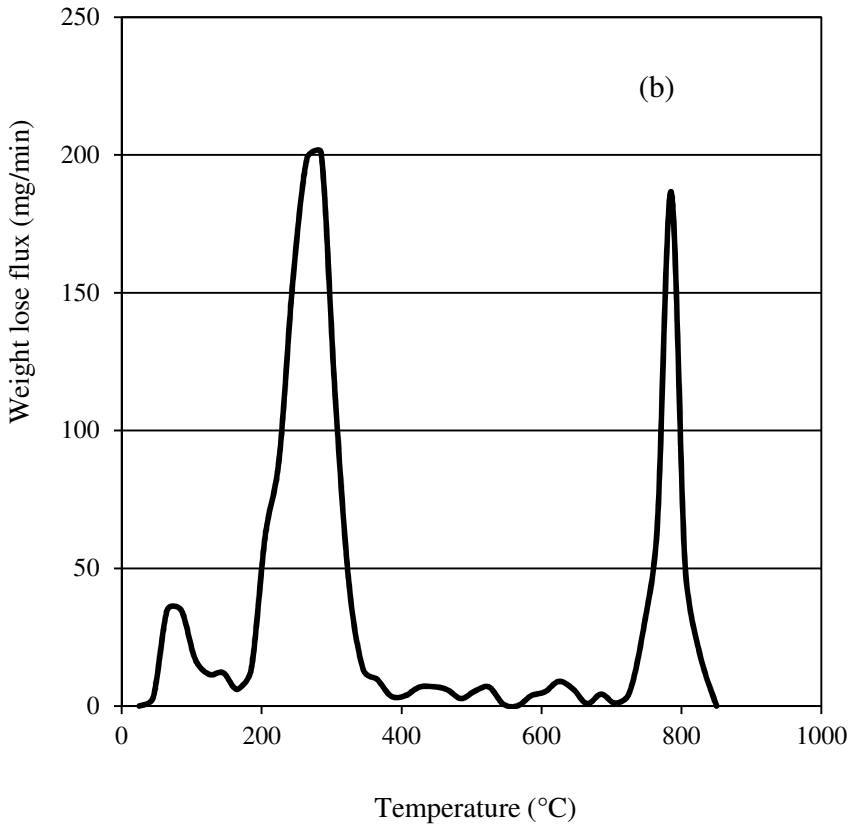
(b)
Weight lose flux (mg/min)
250
200
150
100
50
0
0
200
400
600
800
1000
Temperature (°C)

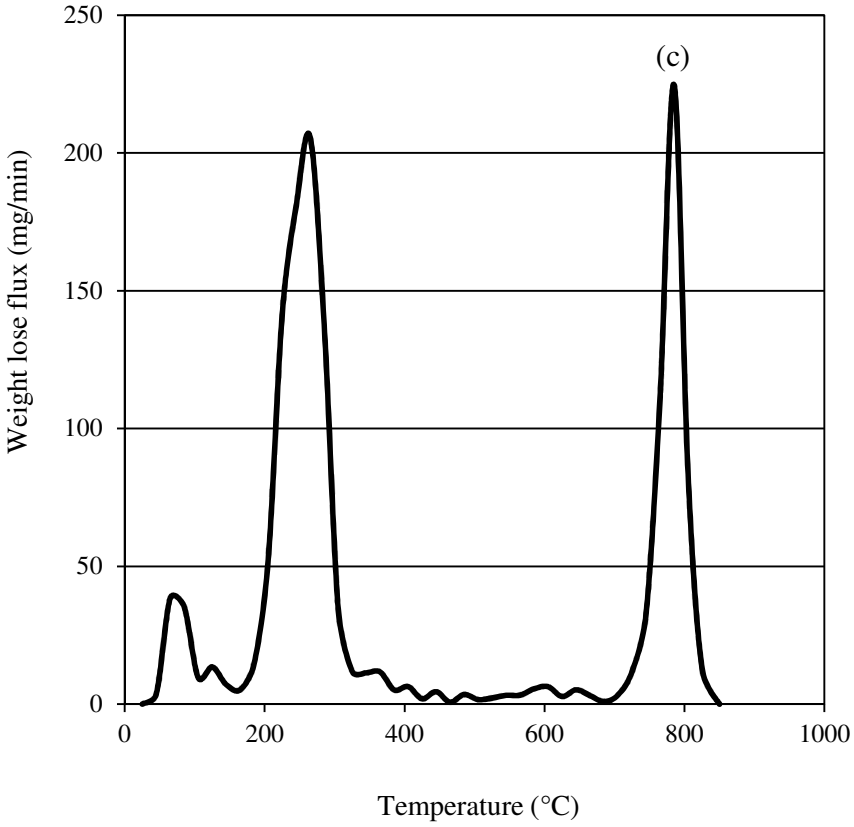
(c)
Weight lose flux (mg/min)
250
200
150
100
50
0
0
200
400
600
800
1000
Temperature (°C)

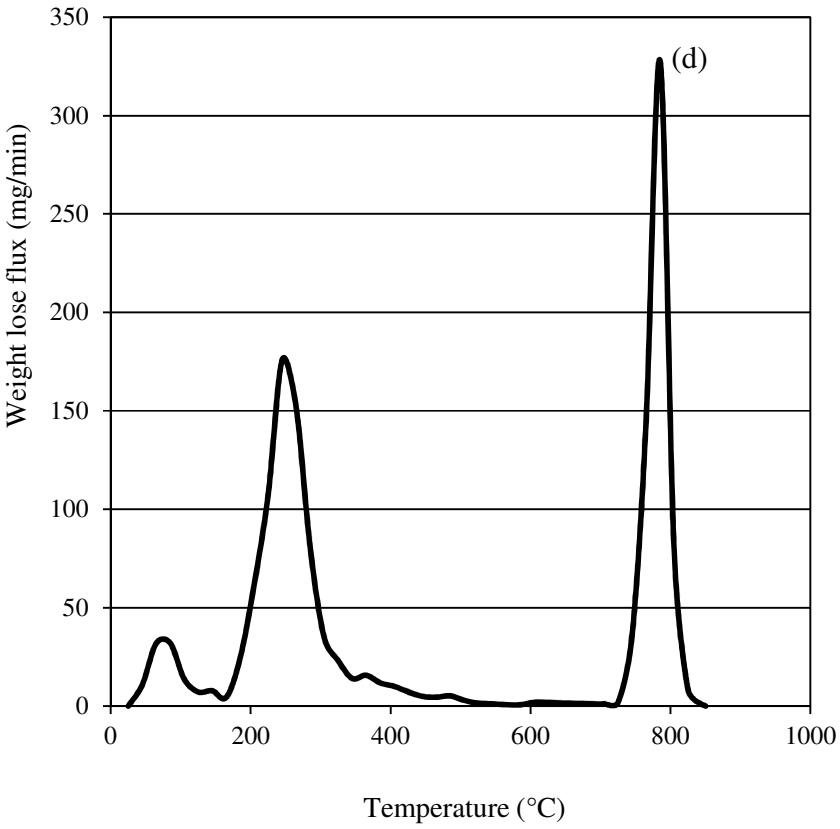

Fig 3.11 (a) DTG result of wood before HTP; (b) DTG result of solid in comingled wood-biosolids slurry after HTP at temperature of 180°C; (c) DTG result of solid in comingled wood-biosolids slurry after HTP at temperature of 210°C; (d) DTG result of solid in comingled wood-biosolids slurry after HTP at temperature of 240°C.

4. Slurry Formation by Hydrothermal Pretreatment

The results from the previous chapters show that pumpable biomass slurry was produced after HTP. Up to 97wt.% of the carbon was still in the solid phase after HTP, while about 20wt.% the carbon in the solid phase transformed from the volatile fraction into the fixed fraction. Other phenomenological changes after HTP were also observed: 1) The appearance of the biomass particles switched from bright yellow (the color of pine wood) to dark brown or black; 2) Particles became frangible and fissured under force; 3) Much more free water became available in the bulk phase. Such observations were also reported in other studies on hydrothermal pretreatment of biomass. Unfortunately, none of the previous studies presented a systematic overview of the mechanism as to how HTP enhanced the slurry formation. In a study of biomass torrefaction, it was reported the wood particles tended to shrink in all directions and the fiber linking between particles disappeared. The change in the particle size of wood particles in Torrefaction was observed by optical microscopy. Fast pyrolysis processes, such as steam explosion, apply fast depressurization as the last step of the pyrolysis. The forced air flow occurring during the fast depressurization, breaks apart the wood cell wall, and consequently, reduces the wood particle size by several folders. Hydrolysis and solvolysis of polysaccharides resulted in breakage of fiber connection in biomass microstructure. The pressure exerted on the biomass cells and fibers would enhance the disruption of its microstructure. It has been observed that the particle size of wood significantly decreased when being hydrothermally treated. This would indicate that the microstructure of the particle would

have changed due to HTP. The slurry product when pretreatment is applied exhibited better dispersion compared to the biomass water slurry without pretreatment. There is no previous evidence of such phenomena in the literature and will be investigated further in this thesis.

4.1 Particle Size Reduction and Redistribution

Experimental procedure

Analysis of the particle size was as a courtesy of Malvern Instruments to demonstrate the utility of their instruments. Four samples were evaluated. Table 4.1 summarizes the samples provided.

Table 4.1 Samples prepared for particle size measurement

Sample number	Initial particle size	Pretreatment temperature
1	180 µm to 225 µm	N/A
2		180°C
3		210°C
4		240°C

The measurement of particle size was carried out by using a Mastersizer 2000 system. A Hydro 2000SM sample dispersion unit was used for the measurement of wet dispersions. The diameter of the sphere that yields an equivalent light scattering pattern to the particle being measured using laser diffraction is the basis of the procedure. This corresponds, to a good approximation, to the sphere of equivalent average cross-sectional area. The distribution of particle sizes within the sample can be estimated once the

particle size has been calculated for the entire sample. Laser diffraction systems are configured to ensure that an equal volume of particles of different sizes yield an equivalent scattering response. A volume distribution, showing the volume percentage of particles that have given size, is therefore reported. This corresponds to a mass distribution in the case where the particle density is the same for all sizes, as shown in Figure 4.1.

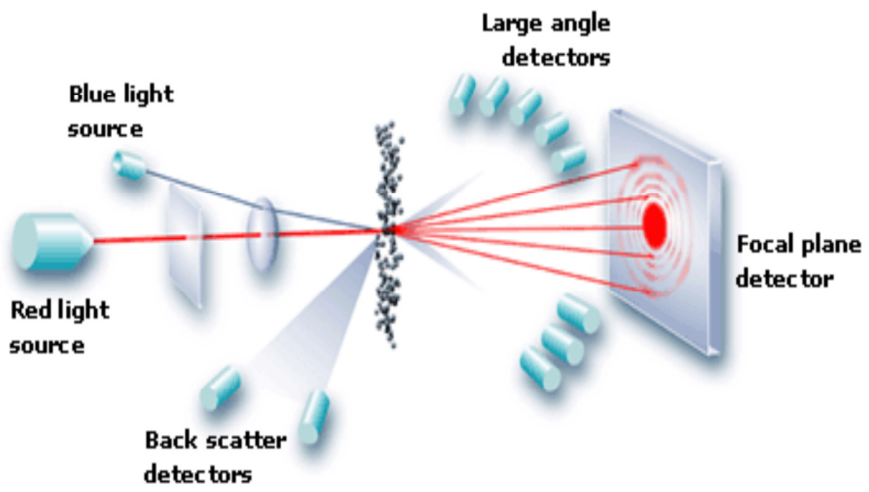

Fig 4.1 Laser diffraction particle size measurement system

Approximately 2 g of solid sample was dispersed in deionized (DI) water in a volume of 150 ml. The mixture was then constantly stirred to achieve even dispersion before being pumped into the laser diffraction measurement chamber where the particle size measurement was carried out. No surfactant was used in these experiments. Extra dispersion was achieved in this experiment by applying sonication. Sonication was applied for about 2min to each sample. Laser diffraction results were then compared

between the samples before and after sonication, to understand re-agglomeration tendency of the particles.

The optical properties of the material were required for size determination accuracy, especially for material less than 40λ in size (~25μm for a He-Ne laser at 632.8nm). In this study, the Refractive Index (RI) number was chosen in accordance with ISO 13320. The dispersants RI number was set to be 1.33 for deionized water, and 1.53 for wood powders. The absorption coefficients were 0.1 for raw wood particles (yellow in color), and 1 for pretreated wood particles (dark brown to black in color), respectively.

Results and discussion

Re-agglomeration of particles was measured for the raw wood particle without pretreatment. It was found that the particle size decreased when sonication was turned on. Raw wood particles tended to re-agglomerate after sonication was turned off, as was shown in Figure 4.2.

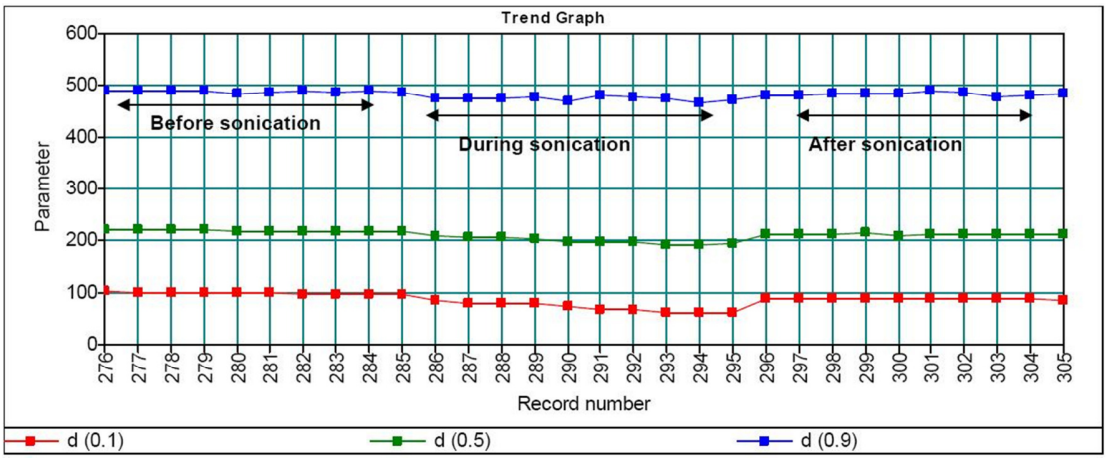

d(0.1): equivalent diameter where 10% mass of the particle has a smaller diameter
d(0.5): equivalent diameter where 50% mass of the particle has a smaller diameter
d(0.9): equivalent diameter where 90% mass of the particle has a smaller diameter

Fig 4.2 Particle size of raw wood particles as a function of sonication

Re-agglomeration was not observed in pretreated biomass slurry after sonication, which means particles in pretreated biomass slurry tend to separate when stirred. The particle size distribution of pretreated biomass slurry was analyzed and compared with the particle size distribution of untreated biomass slurry. The results are shown in Figure 4.3. It is observed, based on these results, that pretreatment decreased the mean average diameter of the solid particles in the slurry, and flattened its particle size distribution range. The mean average diameter of the particles decreased with an increase of pretreatment temperature. These results are shown in Figure 4.4. The mean average particle size decreased from 216μm to 76μm when the biomass slurry was pretreated at 240°C. Comparatively, sonication decreased the particle size of pretreated wood particles

and the distribution stayed unchanged after the sonication was turned off. This is shown in Figure 4.3.

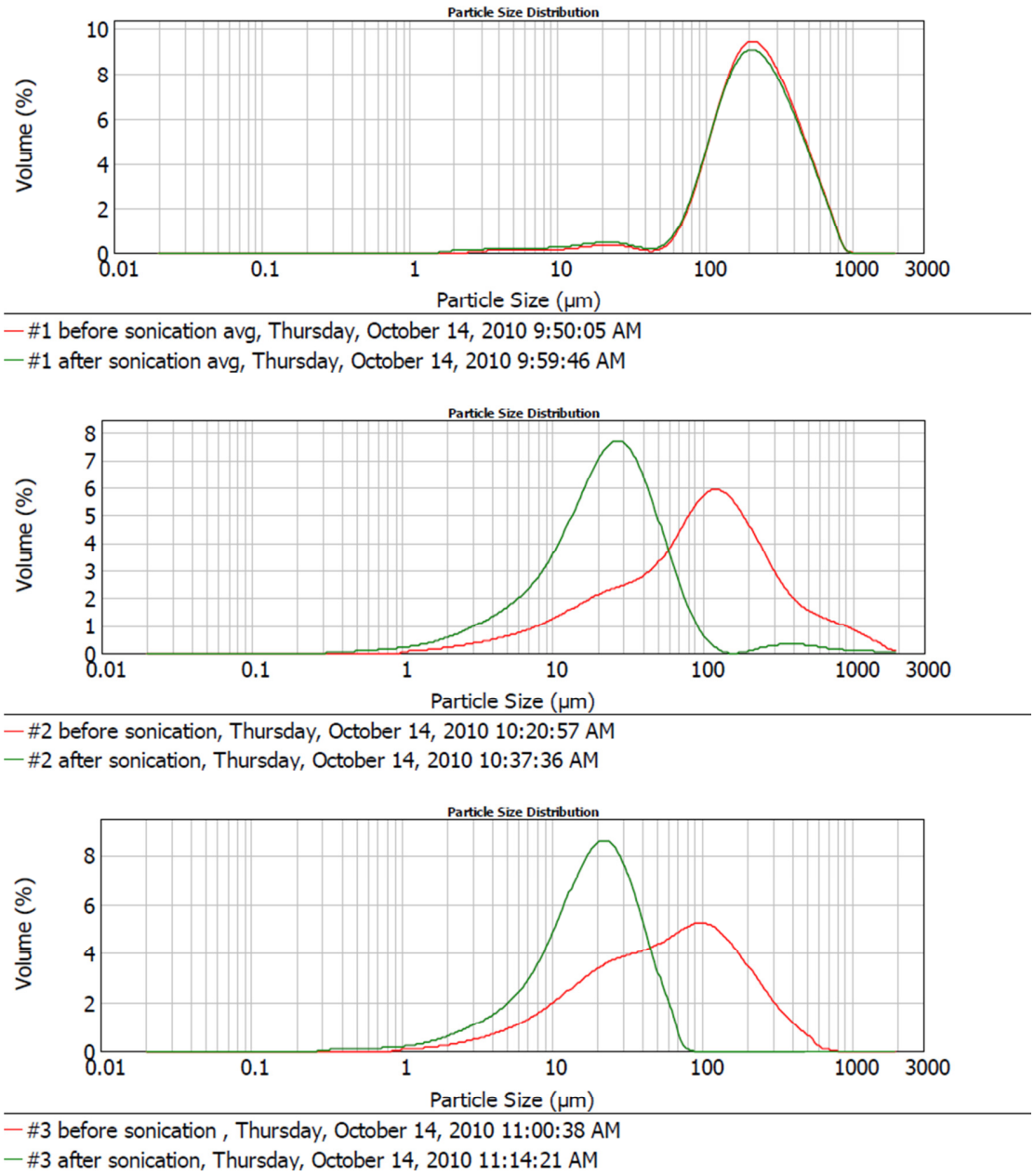

Figure 4.3 Particle size distribution of wood particles before and after sonication: #1, without pretreatment, #2 with pretreatment at 180°C, #3 with pretreatment at 240°C

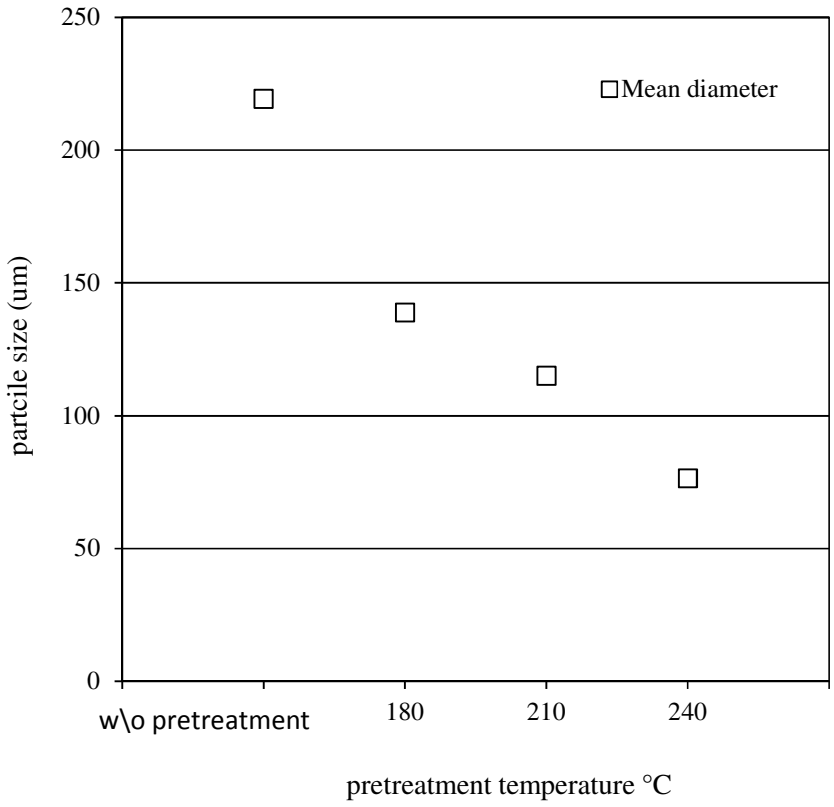

Fig 4.4 Effect of HTP temperature on mean solid particle size

4.2 Biomass Cell Structure

As discussed in previous chapters, hydrolysis and solvolysis of polysaccharides resulted in breakage of fiber connection in biomass microstructure. The pressure exerted on the biomass cells and fibers would enhance the disruption of its microstructure. It has been observed that after HTP the particle size of wood significantly decreased. So it was expected that the microstructure of the particle would have changed due to HTP.

Scanning Electron Microscopy (SEM) was utilized to take images of the solid fraction before and after HTP to visualize such changes.

Experiment procedure

The slurry was dispersed in a glass beaker after HTP. Then several target particles were selected and transferred into an aluminum plate by using a syringe. The alumina plate was then dried overnight before it was coated in a Cressington 108 auto sputter coater and tested in a XL30 FEG SEM.

Results and discussion

The SEM images of pretreated biosolids particles are shown in Figure 4.5. Image (a) was taken at a magnification of 420X and a Working Distance (WD) of 11.2. Image (b) was taken at a magnification of 3362X and WD of 11.2. It is readily observed that the cell structure of microbes in biosolids has opened up, with the releasing internal moisture fraction trapped in its self into the bulk phase. The debris of broken cells is much smaller than the original size, and the pact volume of the solid fraction in the slurry decreased.

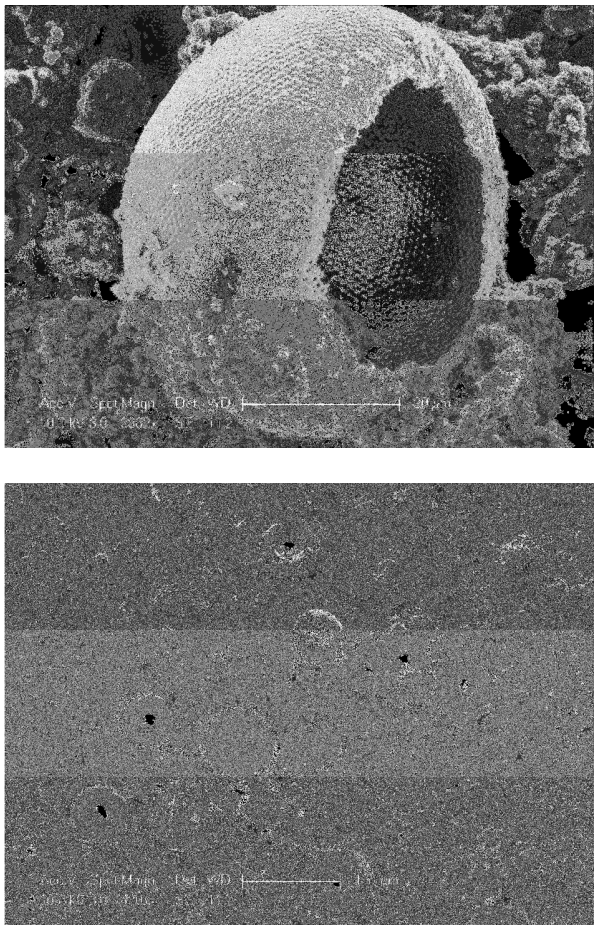

Fig 4.5 SEM image of pretreated biosolids particles

Untreated wood cells were imaged and the photo is shown in Figure 4.6. It is observed that without pretreatment, wood cells retained its original structure, except the cutting edge which was shredded when being grinded. Fragments of the wood piece in this photo would have been caused by force exerted on wood during the extraction of its solid fraction.

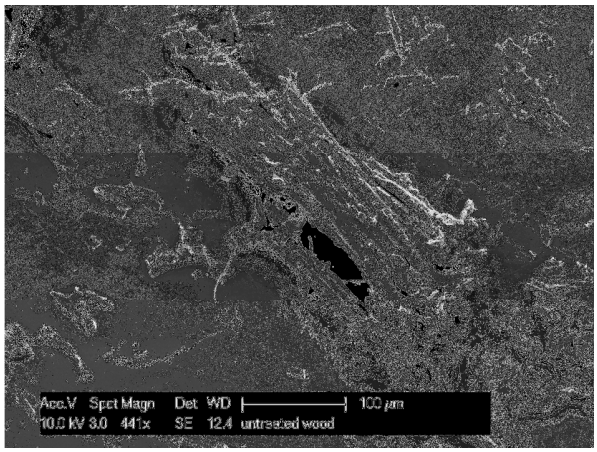

Fig 4.6.SEM image of untreated wood particles

Pretreated wood particle images are shown in Figure 4.7, where (a), (b) and (c) show the wood particles pretreated at temperature of 180°C, 210°C and 240°C, respectively. As pretreatment was applied and the pretreatment temperature increased, the wood cells were destroyed and clear cracks and trenches can be seen on the surface of the wood particles. Many more fragments of wood debris were observed with increased pretreatment temperature. The wood particles that were treated at 240°C have an obvious smaller particle size than the ones without pretreatment, which is in accordance to our experimental results of particle size.

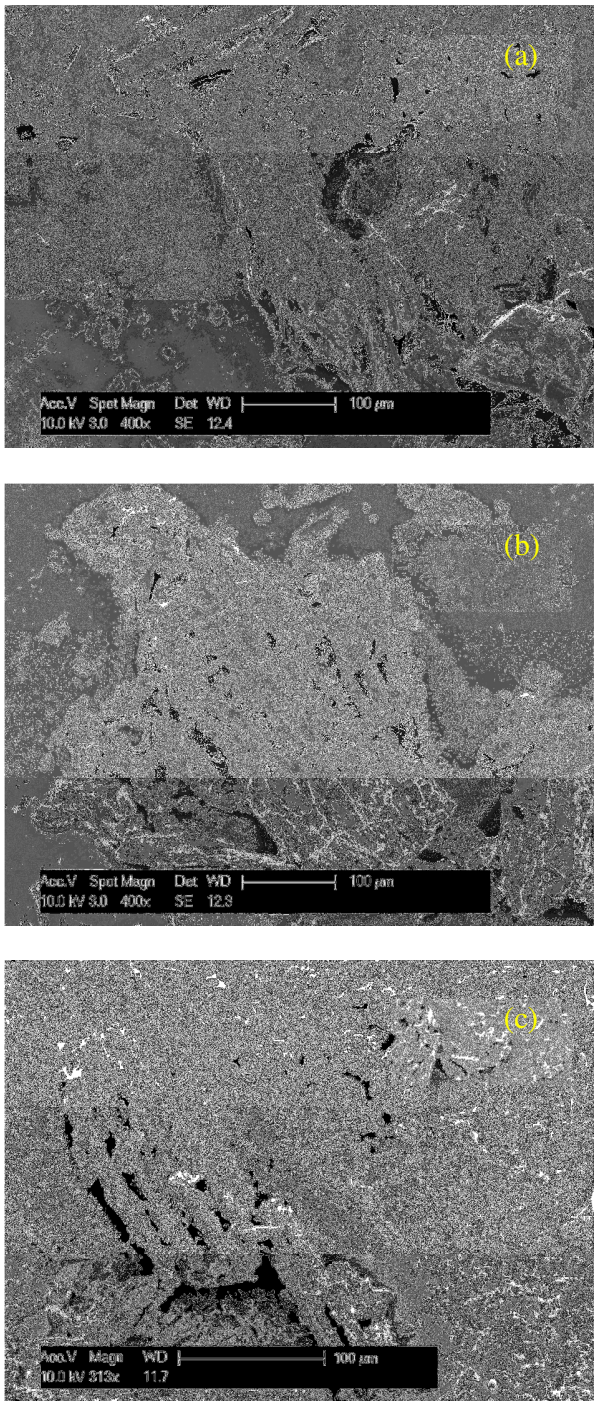

Fig 4.7 SEM image of pretreated wood particles at (a) 180°C, (b) 210°C and (c) 240°C

By increasing the magnification in the SEM to 1600X and 3200X, we have a closer observation of the microstructure of wood particles. This is shown in Figure 4.8.

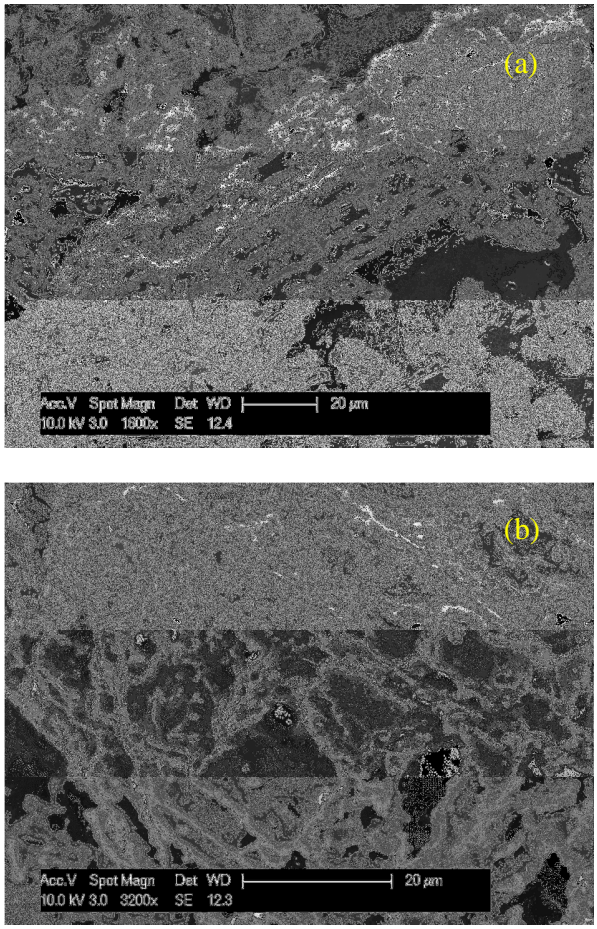

Fig 4.8. SEM image of pretreated wood particles at 240°C (a) with magnification of 1600X; (b) with magnification of 3200X

It can be seen from Figure 4.8 that numerous small cavities were observed on the surface of the wood particles. These cavities open the multiple bridges for internal moisture to be released from inside the wood cells. Small balls attached on the wood

surface were also reported in other HTP of biomass, and is attributed to the decomposed hemicellulose fraction.

4.3 Surface Electrokinetics of Wood Particles.

Surface electrokinetics measurements were used to investigate the surface charge and repulsion force of particles in the comingled wood and biosolids slurries.

The repulsion force between particles in the slurry separate the particles from each other, and reduce their tendency of coagulation and flocculation, which helped with dispersion of the solids in the slurry. Figure 4.9 shows slurry phase separation caused by coagulation and flocculation.

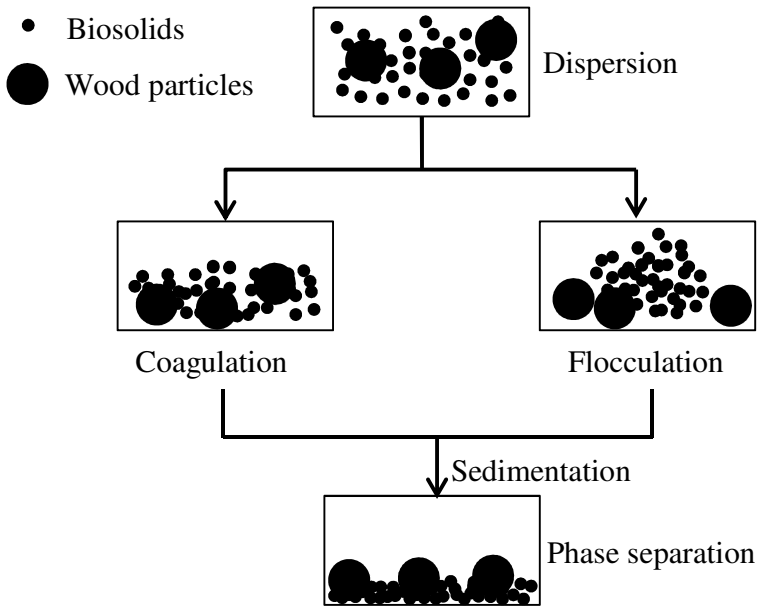

Fig 4.9 Phase Separation in Slurry Caused by Coagulation and Flocculation

Measurement of particle surface electrokinetics can be performed by analyzing either electrophoresis or streaming potential. Electrophoresis analysis was applied in this study, in which the dispersion was measured by applying an electric field across the dispersion. The particles within the dispersion will then migrate with a velocity proportional to the magnitude of the zeta potential. Surface electrokinetics is a physical property of particles, and particle size and density would not have any impact on it. However, it is important to mention out that with particles larger than 300nm, the density and size of the particles are required for calculation of the zeta potential.

The repulsion force, also named as electrical double layer repulsive force, between particles is caused by its surface charge. It is balanced by van der Waals attractive force of particles in a dispersed system. It is a function of distance from the particle surface. So it pushes away neighboring particles, and makes the slurry stable from settling, as is shown in Figure 4.10.

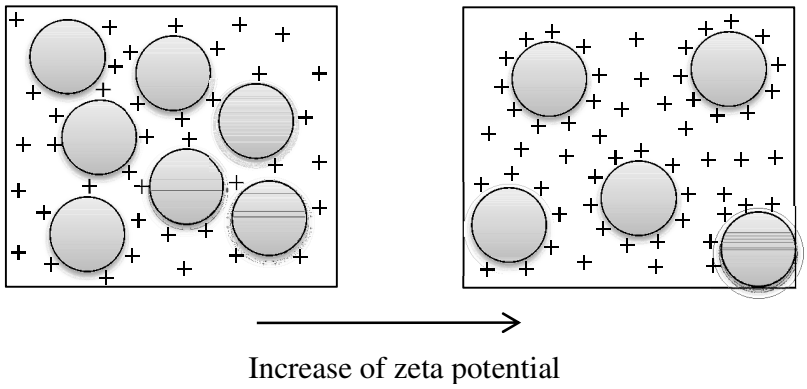

Fig 4.10 Enhanced dispersion of slurry with increase of zeta potential

The rheological properties of slurries are affected by the zeta potential of the slurry. Higher absolute zeta potential means better dispersion of solid particles in the slurry system, and results in lower viscosity of the slurry. A previous study has found that viscosity correlated well with zeta potential in an aluminum hydroxide suspension. Increased particle size attenuated the impact of zeta potential on wood and biosolids mixtures due to the fact that enhanced coagulation is caused by increased gravity force exerted on the particles.

Experiment procedure

Particles of the slurry were dispersed in a beaker. Stirring was avoided to maintain the original particle size in the slurry. The pH of the dispersed slurry was controlled by adding neutralizer solution, and the effect of the pH on the zeta potential was determined. The pH of the slurries were then all set at 5 to measure the zeta potential of the slurry pretreated at different temperatures.

The Zeta potential of the slurries was determined by measuring its electrophoretic velocity. Electrophoretic velocity is proportional to electrophoretic mobility, which could be measured by electrophoretic light scattering in the ZetaPALS. Zeta potential value of the particles was then calculated by ZetaPALS from the velocity of particles moving in the electric field and the strength of the electric field.

Results and discussion

The effect of pH of the slurry on their zeta potential values was measured by varying the pH of biomass and biosolids slurry being hydrothermally treated at 180°C. The results were plotted in Figure 4.11.

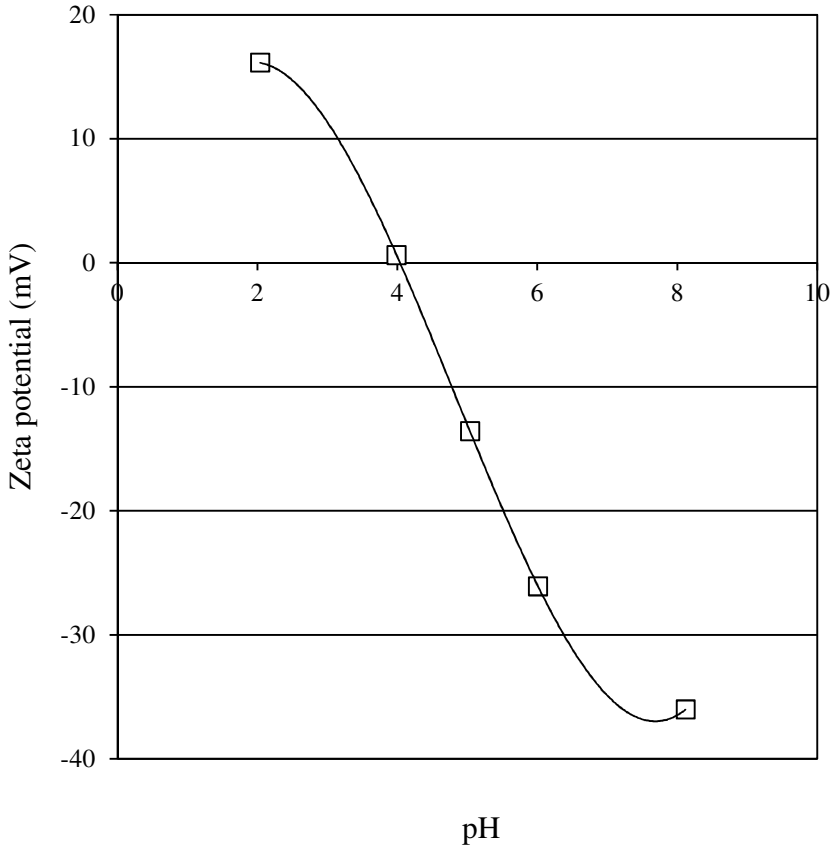

Fig 4.11 Effect of pH on Zeta Potential of Pretreated Biomass and Biosolids Slurry (Pretreatment Temperature: 180°C)

From this graph, it was found that a pretreated wood and biosolids slurry has an isoelectric point (i.e.p.) of 4.1. The zeta potential decreased rapidly with increase of the pH value. This indicates that the slurry would be much more stable with higher pH.

The effect of pretreatment and pretreatment temperature on zeta potential was determined with biosolids, wood and water slurry, and wood and biosolids slurry. The Results are shown in Figure 4.12 and Figure 4.13, respectively.

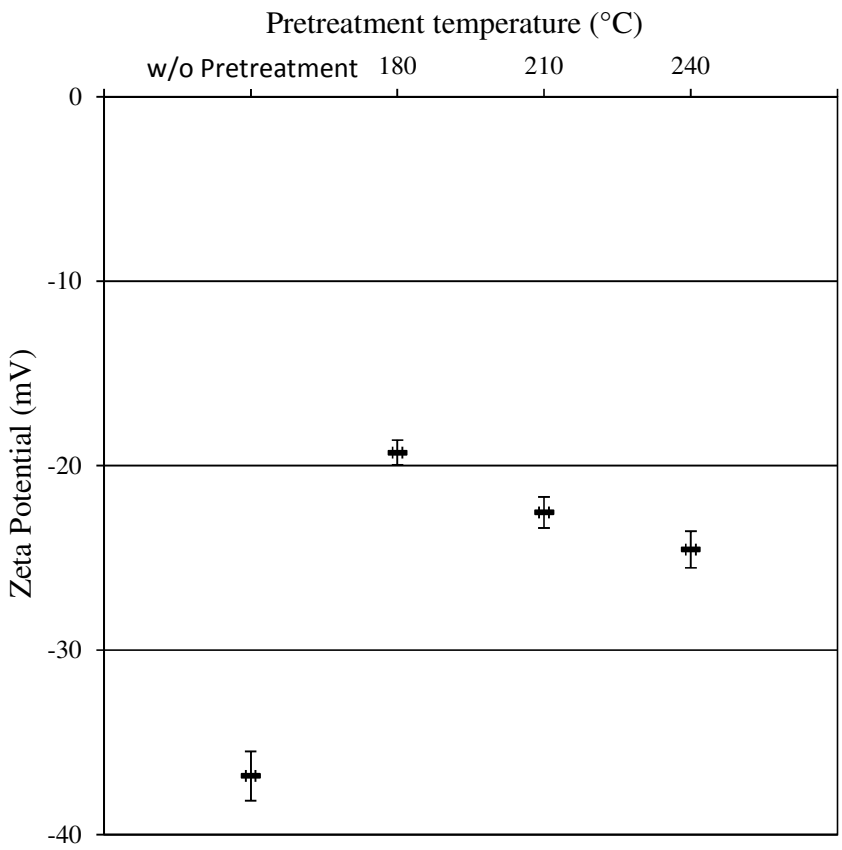

Fig 4.12 Zeta potential analysis of biosolids particles with HTP

The absolute value of the zeta potential in bioslids decreased with pretreatment. These results are in accordance with the settlement evaluation of the slurries, where before pretreatment, biosolids did not settle during the testing period. However, it separated and settled after HTP. The zeta potential results also showed that with increase pretreatment temperature the absolute value of zeta potential increased.

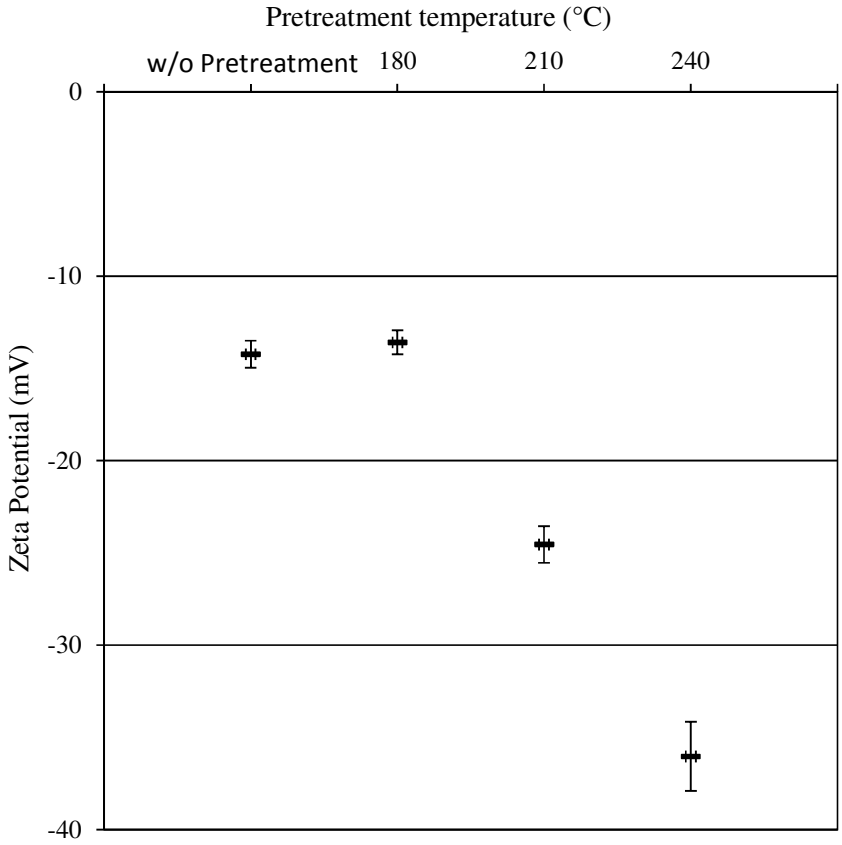

Fig 4.13 Zeta potential analysis of wood particles with HTP

The measurement of the zeta potential of wood particles in a wood water slurry showed that pretreatment enhanced the slurry stability. It showed with a pretreatment temperature of 240°C, resulted in a zeta potential of wood water slurry of about 36mV.

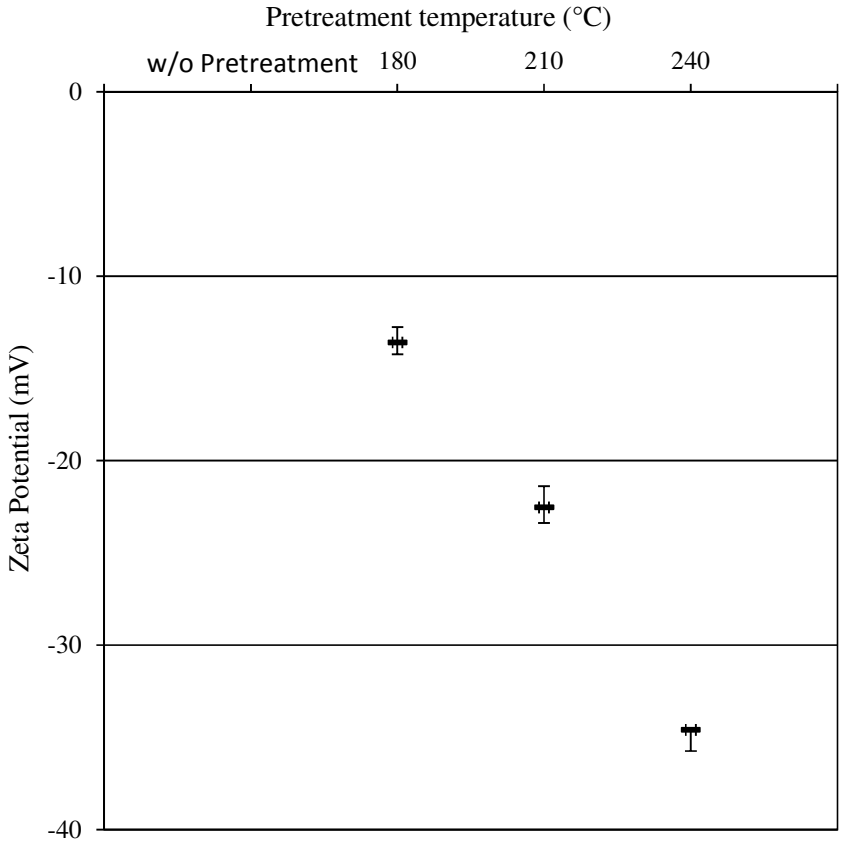

Fig 4.14 Zeta potential analysis of comingled wood and biosolids particles with HTP

Similar trends of zeta potential values were observed for the comingled biomass and bisolids slurry. When compared to the biomass water slurry, the absolute value of the zeta potential value in biomass biosolids slurries was slightly less than that in biomass water slurries. This is due to the present of biosolids in the slurry phase.

A slurry in a colloidal system became stable with a zeta potential of over 40mv, so all slurries produced from HTP were unstable and tended to settle with gravity force.

A dispersant would need to be added if storage of a slurry is long (several hours) after the HTP process.

5 Scale-up of Hydrothermal Pretreatment

In this section, a detailed process scale-up is presented for the Hydrothermal Pretreatment (HTP). This includes a Process Demonstration Unit (PDU) scale and a commercial scale HTP process.

5.1 Process Demonstration Unit Scale Hydrothermal Pretreatment Process

A PDU scale of the HTP process discussed in the previous section was designed and built for the gasification laboratory at CE-CERT. It is part of the demonstration scale of CE-CERT's Steam Hydrogasification process. The capacity of this demonstration scale HTP process is 10lb/hr of dry feedstock. Green city wastes (wood waste) and biosolids discharged from a waste water treatment facility will be comingled and used as the feedstock. The goals are: 1) to prove the viability of the HTP process in a continuous operating environment with a pretreatment capacity of 10lb/hr, 2) to test the consistency of the physiochemical properties of the resultant slurries. This information can be used to provide the initial design for a pilot scale and commercial scale facility.

5.1.1 Design of a Demonstration Scale HTP Process

The demonstration scale HTP contains four parts: gas supply and vent, a constant stirred batch reactor, an internal cooling system and a control system. To this end, the demonstration scale HTP process was configured and built as shown in Figure 5.1. The specific details follow.

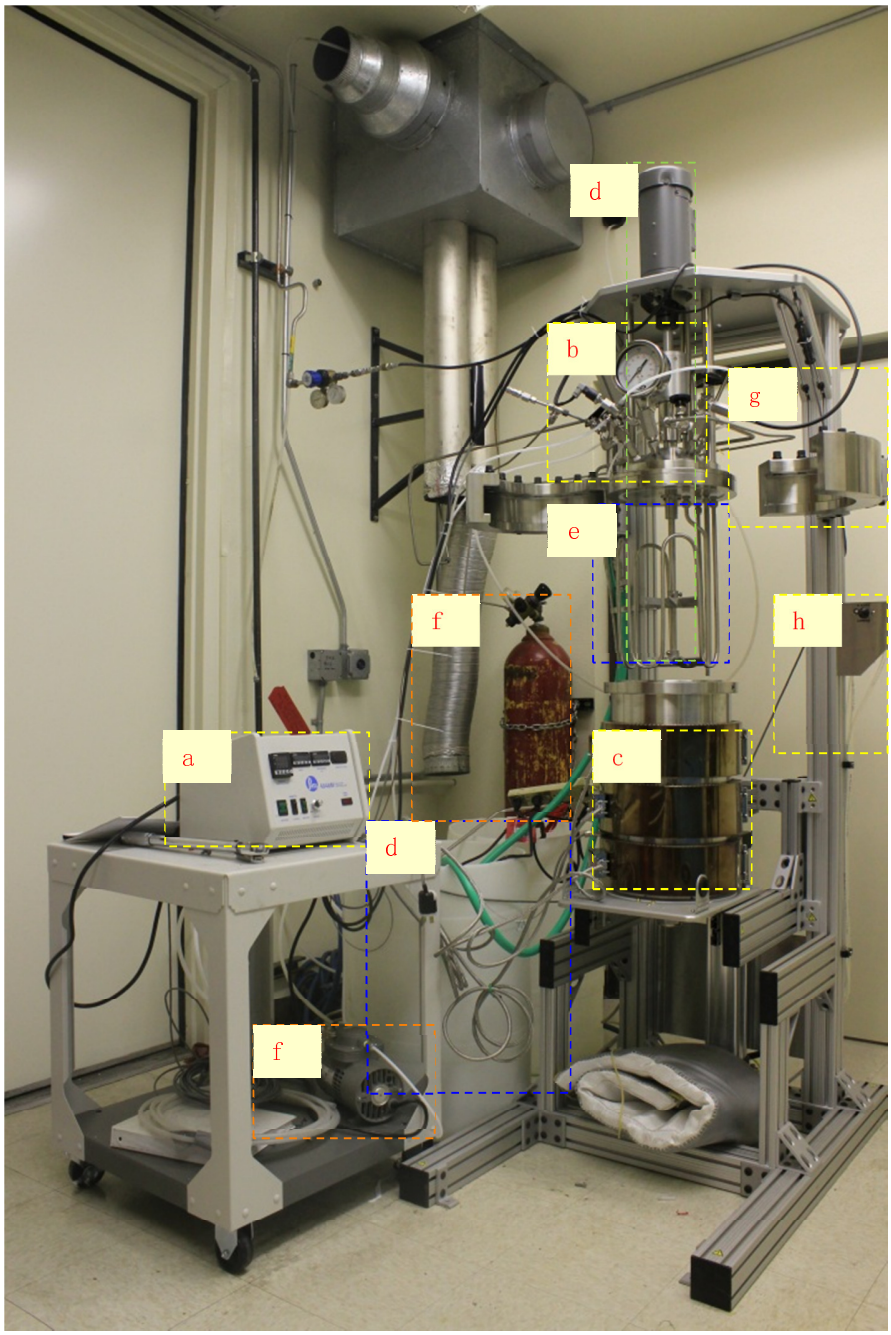

Fig 5.1 Demonstration Scale HTP Process Configuration

Components:

a) Master slave box controller
b) Temperature and pressure sensor
c) Electric heater

d) Magnetic agitator assembly
e) Internal cooling assembly
f) Gas supply and vent
g) Seal and safety rupture disc
h) Pneumatic lift and support

To achieve a pretreatment capacity of 10lb/hr, a minimum of two 5 gallon HTP reactors are needed. In real application, these two batch process would be operated in parallel to maintain a constant stream of slurry product. Figure 5.2 shows a continuous operation of two HTP reactors to maintain constant slurry production.

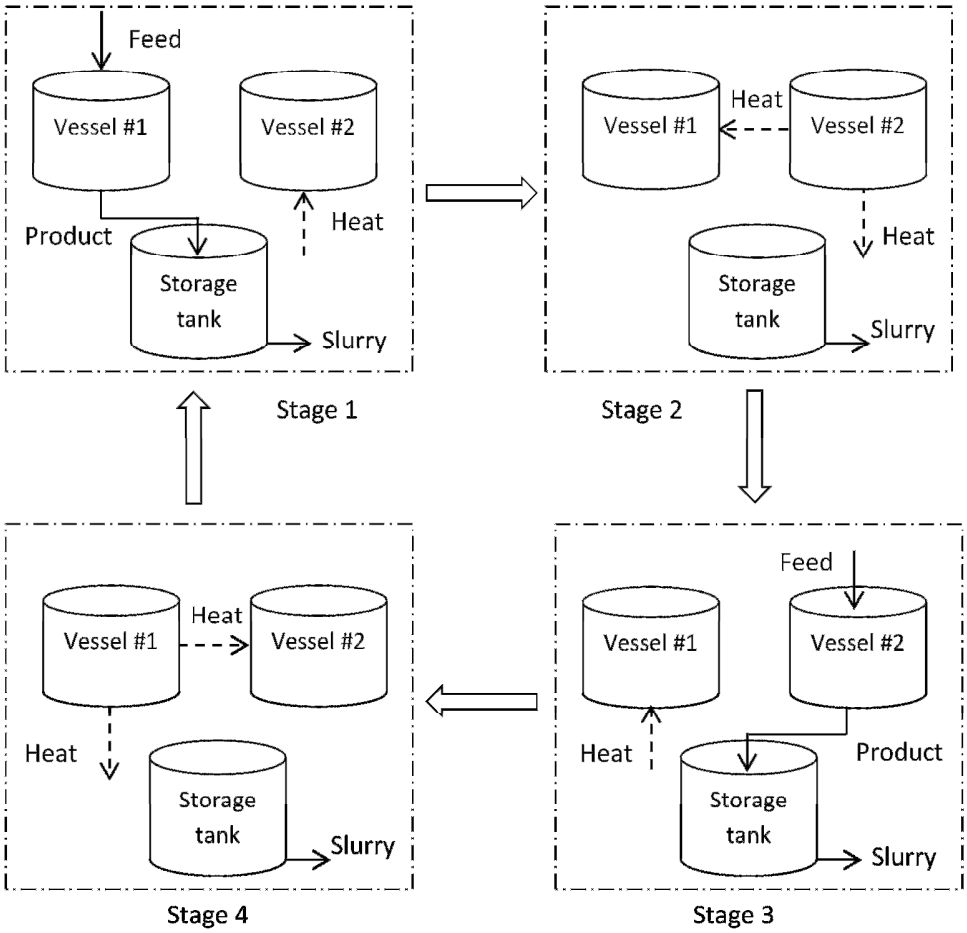

Fig 5.2 Continuous Slurry Production by Parallel Operation of two HTP Reactors

Slurry product from the previous run is collected at stage 1, and the comingled wood and biosolids feedstock is fed into the reactor. The feedstock in vessel #2 is being hydrothermally pretreated. At stage 2, HTP is completed in vessel #2, and it is being quenched to ambient temperature by exchanging heat to vessel #1. Part of the heat is lost. At stage 3, the slurry product is collected from vessel #2 and the fresh comingled

feedstock is fed into the reactor, while feedstock in vessel #1 is being hydrothermally pretreated. At stage 4, the HTP is complete in vessel #1, and it is being quenched to ambient temperature by exchanging heat to vessel #2, and is prepared for the next operation cycle. During the pretreatment, the slurry product is stored in a storage tank before being pumped into the gasifier. Once the continuous fed of the slurry into the gasifier and the slurry product from the HTP is balanced, the continuous operation of gasification is achieved.

Constant Stirred Batch Reactor

A 5 gallon stirred batch reactor was designed in accordance to ASME Boiler and Pressure Vessel Code, Section VIII, Division 1. The design specification of the demonstration scale HTP is listed in Table 5.1.

Table 5.1 Design Specification of Demonstration Scale HTP

Design specs	Comments
Product capacity	10 lb/hr
Heating rate	10~40 °C/min
Cooling rate	20~40 °C/min
Agitator capacity	Capable of stirring 10 Pa·s slurry at a speed of 100 rpm
Reactor ratings	Maximum Allowable Working Pressure (MAWP): 3000 psi Maximum Allowable Working Temperature (MAWT) : 350 °C

The batch vessel was made in a cylindrical shape with a height of 17.40inches and an inner diameter of 9.25inches. The design Maximum Allowable Working Pressure

(MAWP) was 3000psi, and the design Maximum Allowable Working Temperature (MAWT) was 350°C. Material was selected to handle the pressure and temperature based on the following factors:

- Strength
- Corrosion Resistance
- Resistance to Hydrogen Attack
- Fracture Toughness
- Fabricability

Lab scale HTP test results showed that the slurry products after pretreatment were mildly acidic, with a pH of 3 to 4. This is due to the acetic acids produced from the decomposition of wood wastes and biosolids during the HTP. Therefore, the materials of the HTP reactor needed to be corrosion resistant. 316-stainless steel was chosen as the reactor material because it contains high nickel and molybdenum concentration, and has affordable corrosive resistance to sulfuric, phosphoric, and acetic acid. Since the temperature of the HTP was restricted to be less than 300°C, hydrogen dissociation would not happen in the HTP, thus no hydrogen attack was considered. The chemical and mechanical properties of SS-316 are listed in Table 5.2.

Table 5.2 Chemical and Mechanical Properties of SS-316

Properties	Specification
Chemical composition, %	C: <0.08, Mn: <2.0, Si: <1.0, Cr: 16.0~18.0, Ni: 10.0~14.0, Mo: 2.0~3.0
Tensile strength, psi	84,000
Proof Stress (0.2% offset), psi	45,000

The thickness of the cylindrical wall was calculated according to ASME code by:

$$t_p = \frac{P \times R}{S \times E - 0.6 \times P} \qquad \text{(Eq. 5.1)}$$

And the thickness of the flanged and dished head was calculated by:

$$t_p = \frac{1.77 \times P \times L}{2 \times S \times E - 0.2 \times P} \qquad \text{(Eq. 5.2)}$$

Where

t_p= minimum required thickness (in.)

P= Design pressure (psi)

R= Inner radius (in.)

S= Allowable stress (psi)

L= Inner spherical radius (in.)

E= Weld joint efficiency factor, 0.85 for spot.

Vessel components are weakened when nozzles openings exist in the top flange. The vessel was reinforced by increasing the vessel wall thickness on the top flange. Thickness of the vessel was examined by the following equation:

$$A_r < (A_s + A_n) \qquad \text{(Eq. 5.3)}$$

Where

$$A_s = \ larger\ of\ d(T_s - t_s) - 2T_n(T_s - t_s)\ or\ 2(T_s + t_n)(T_s - t_s) - 2t_n(T_s - t_s)$$

$$A_n = \ smaller\ of\ 2[2.5 \times T_s(T_n - t_n)] \text{ or } 2[2.5 \times T_n(T_n - t_n)]$$

T_s= Actual thickness of shell (in.)

t_s= Required thickness of shell (in.)

T_n= Actual thickness of nozzle (in.)

t_n= required thickness of nozzle (in.)

Results of the nozzle positioning in the flanged head is shown in Figure 5.3. Thickness of the flanged and dished head is shown in Figure 5.4.

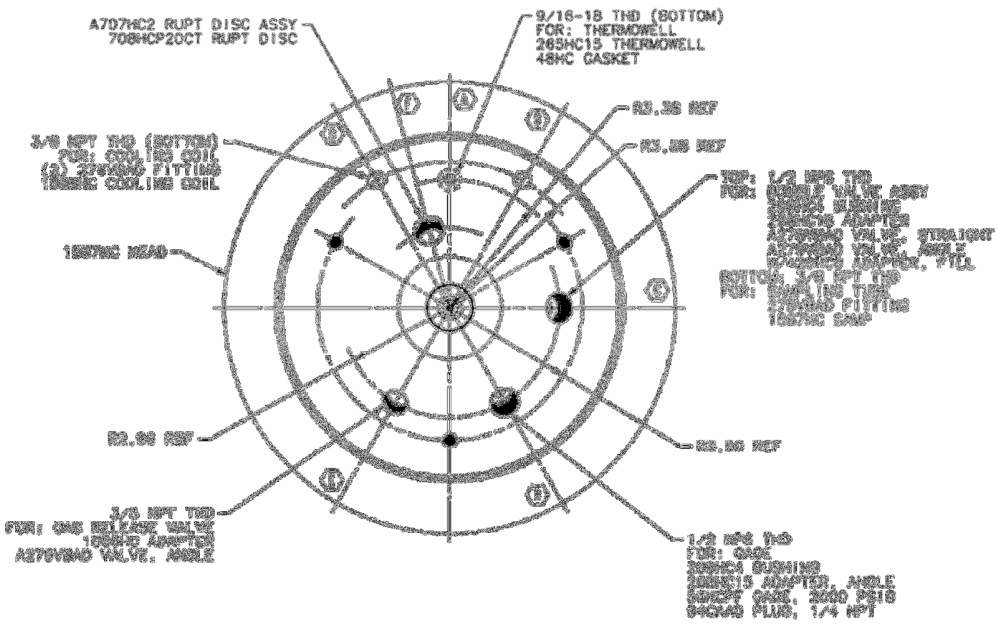

Fig 5.3 Nozzle Positioning in the Flanged Head of HTP Reactor

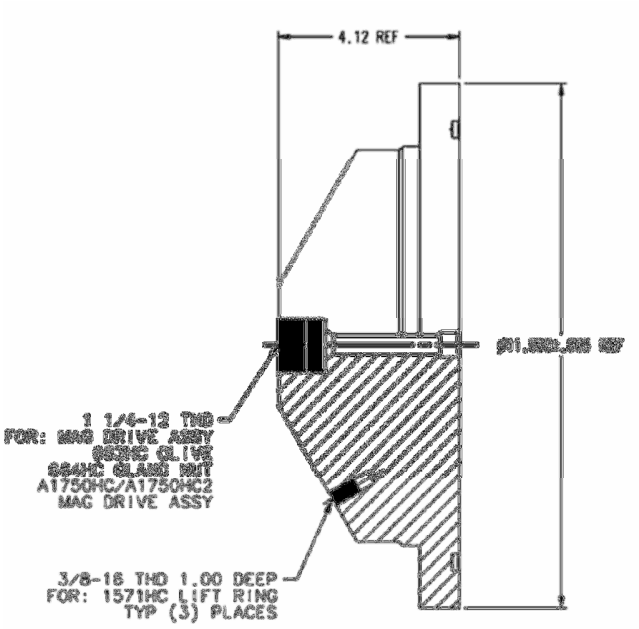

Fig 5.4 Thickness of the Flanged Head of HTP reactor

Heating and Cooling Assembly

The HTP reactor is heated by a three zone electric heater jacket, as shown in Figure 5.5. A serpentine cooling coil with a coolant circulating system was installed to transfer heat out of the hydrothermal reactor when the pretreatment is finished. Ethylene glycol was used for coolant in the cooling system. This is to minimize the fouling effect that may have caused by use of water. A second stage cooling coil was then installed to quench the heat from the ethylene glycol. A flow diagram of the demonstration scale HTP is shown in Figure 5.6.

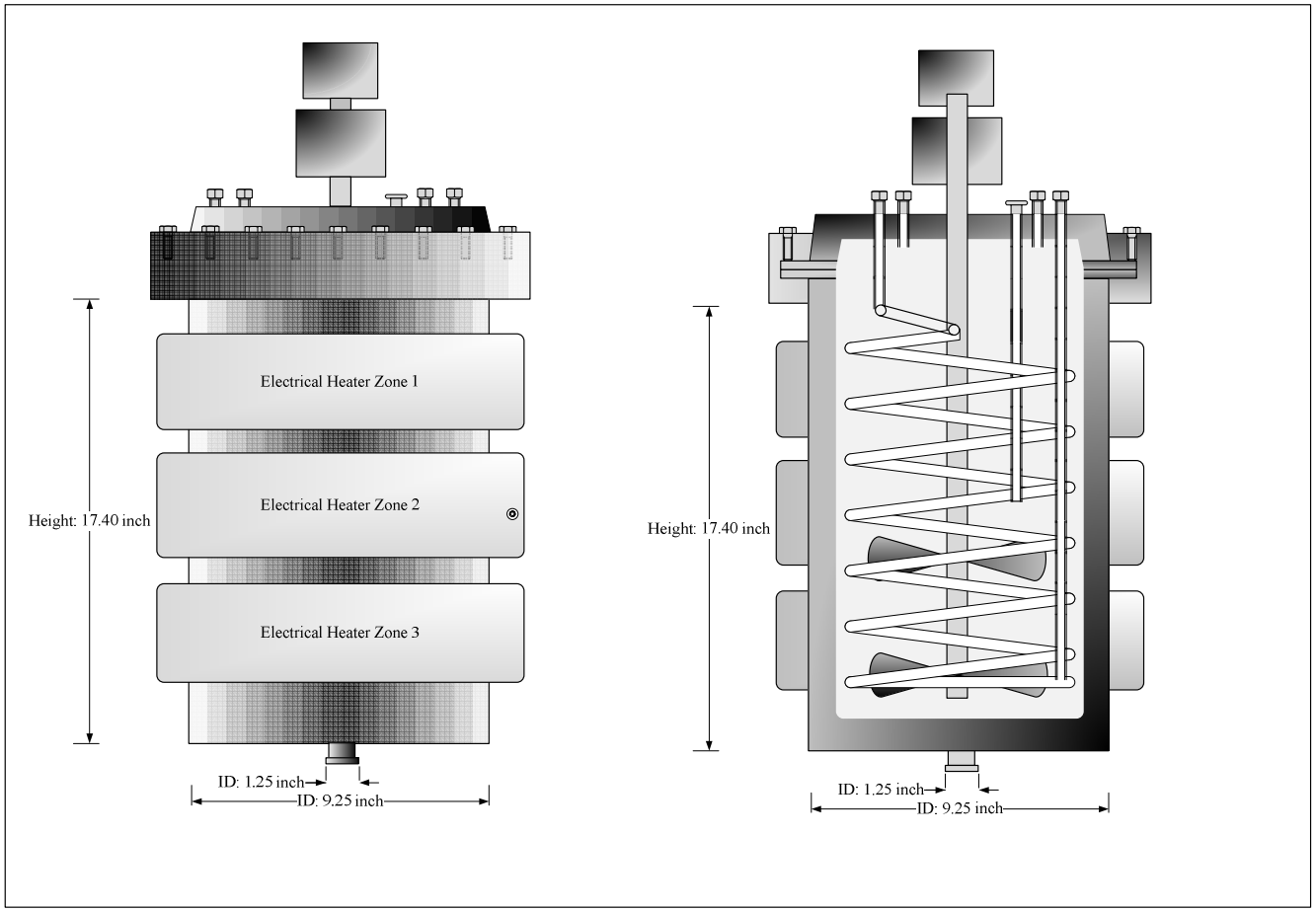

Fig 5.5 HTP Reactor Assemblies

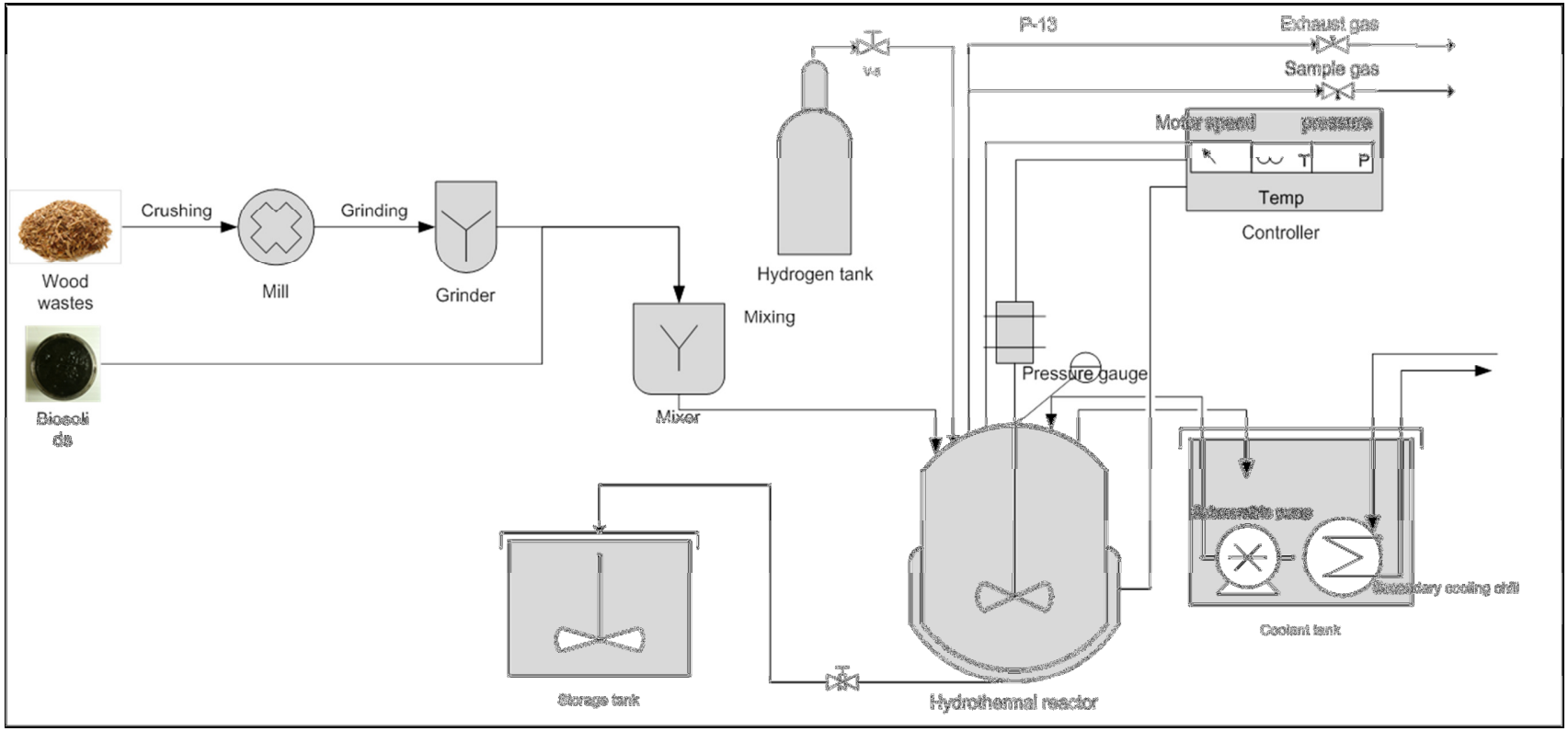

Fig 5.6 Process Flow Diagram of CE-CERT Demonstration Scale HTP

Master Slave Box Controller

A three zone slave control box was designed in conjunction with a Master controller to monitor and control the temperature, pressure and motor speed of the agitator online. The slave box obtains its signal inputs from thermal couples and pressure sensor in the reactor. The slave box has two 25A fuses on the electric heater, which provides a total of 50A electric power to the electric heater. There are four selectable zone switches in the slave box controller, which provides a wide range of heating rates available within a single heater assembly. Wiring of control box was configured as:

- Zone 1 wired with bottom side heater
- Zone 2 wired with middle side heater
- Zone 3 wired with top side heater.

Temperature and Pressure Sensor

Temperature is monitored by thermocouples. Two Type J (iron-constantan, stainless steel sheath, 1/8 inch diameter) thermocouples were installed in the reactor. One was buried in the reactor by a thermo-well penetrating through the head of the reactor. It monitors the real time temperature of inside the reactor. The other is installed in the heater. It controls the power of the heater and protects it from overheating. The total resistance of the thermocouple and the lead wires should not exceed 20Ohms. Higher resistance of the thermocouple circuit would result in reduced sensitivity of the control system, which was not desired and avoided.

A pressure gage, typically a 0-2000psi with a T316 stainless steel Bourdon tube, was mounted on the head. A Pressure Display Module (PDM) with transducer was also

mounted on the head. The transducer was connected to the master slave box which enabled online reading of the pressure inside the reactor.

Electric Heater

A 3-zone heater was installed in the jackets surrounding the hydrothermal reactor. Each heating zone was rated at 230V, 50/60 Hz, 15A. The entire heating assembly was powered by the master slave box controller. Type J temperature sensor was installed at zone #2 to monitor the operating temperature of the heater. This was also programmed to shut the heat off when overheating is inspected.

Magnetic Agitator Assembly

A 60in/lb footless heavy duty magnetic stirrer is mounted in the fixed head support stand. Homogeneity of the feedstock is achieved by using such a design. In the magnetic drive, magnets for the inner rotor to which the stirrer shaft was attached were enclosed in stainless steel housing, permanently sealed by laser welding and supported by graphite-filled, PTFE bushings. Such design avoids leakage problems which can arise with a packed gland stirrer drive, as shown in Figure 5.7. A direct drive was used to power the magnetic impeller. The direct drive has the motor mounted vertically above the reactor with the drive coupler connected to the motor shaft. The direct drive included a motor to provide variable speed of the impeller. Maximum power output of the direct drive was 3/4hp. Speed of the motor ranged from 0 to 400rpm.

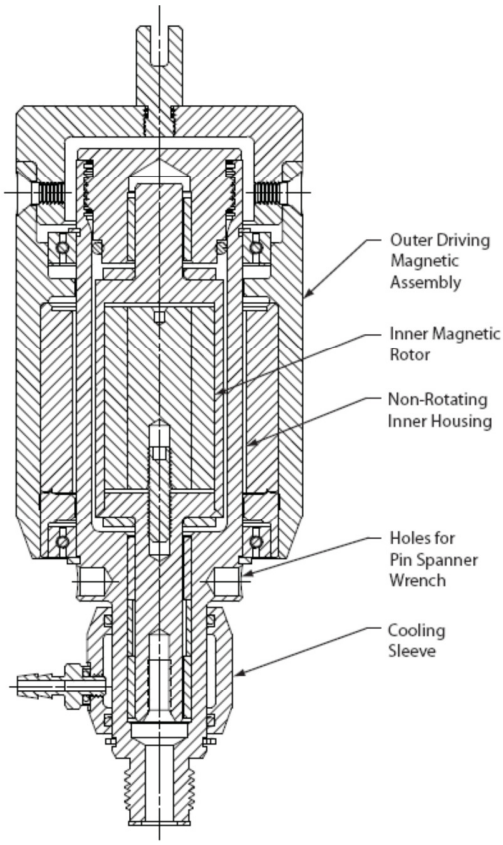

Fig 5.7 Magnetic Drive Assemblies

Internal Cooling Assembly

Three parts of the HTP system require external cooling. They are the hydrothermal reactor, the direct drive motor and the PDM pressure transducer.

A cooling coil (3/8 inch in diameter) with a serpentine configuration runs through the hydrothermal reactor. Two openings on the head of the reactor allow coolant to be introduced and pass through, as shown in Figure 5.8. A coolant tank was designed and positioned next the reactor. Coolant is pumped through the cooling coil pipe by a

submersible pump. The flow rate of coolant is controlled by a Solenoid Valve Module (SVM).

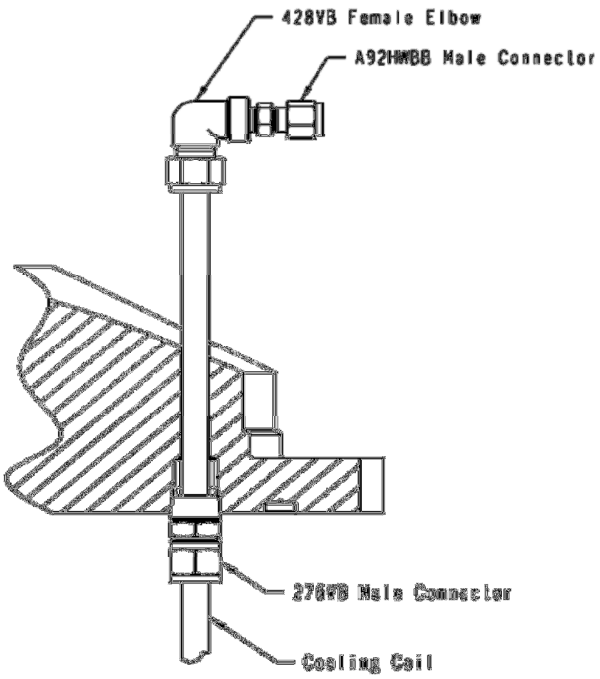

Fig 5.8 Welding of Cooling Coil on Flanged Head of the HTP Reactor

Coolant pipe (1/4 inch diameter) also runs serially through the direct drive motor and the PDM pressure transducer. Its flow rate is controlled by a hydraulic flow meter.

Gas Supply and Vent

Hydrogen is supplied by a size-K hydrogen tank purchased from Praxair. Hydrogen is introduced into the reactor through a dip tube on the head, as shown in Figure 5.9. When pretreatment is completed, gas is released through a releasing needle valve. An extra port is also provided when the exhaust gas needs to be sampled and analyzed. A vacuum pump was installed in the exhaust line which is used to vacuum the

reactor before the HTP and provide head space gas pressurization, and is used after the HTP for ventilation of potentially hazardous exhaust gas.

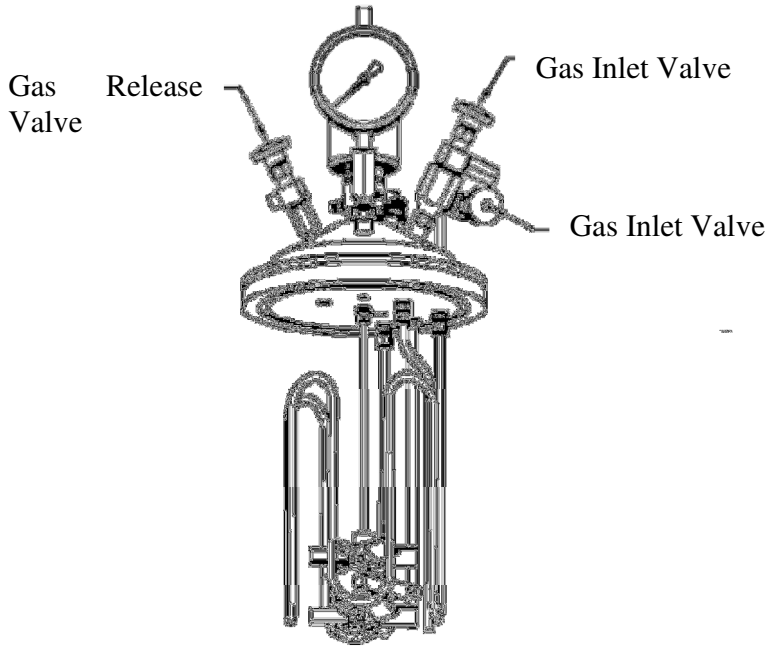

Fig 5.9 Gas Inlet and Release Line

Seal and Safety Rupture Disc

A PTFE flat gasket was installed in a recess in the vessel head and a machine pilot on the cylinder closed the recess to completely contain the gasket. The split ring closure used with this gasket has compression bolts which were tightened to develop loading on the gasket. The closure was designed so that the compression bolts in the split ring sections would contact within a lip on the compression ring and bring the split sections into their proper position.

There is a safety rupture disc attached to the head of the reactor which is intended to rupture and release the pressure before it reaches a dangerous level. The outlet of the rupture disc is connected to a vacuum vent, which ensures safe evacuation of hazardous gas exhaust if maximum operating parameters are exceeded.

5.1.2 Demonstration Scale HTP Test

Experimental Procedure

Pine wood was used as a representative for wood. Dissolved Air Floatation Thickener (DAFT: discharged from Riverside Wastewater Treatment Plant, Riverside, CA) was used as a representative of biosolids. The pine wood is first crushed in a laboratory mill (Thomas – Willey model 4, Arthur H. Thomas Company). The crushed wood particles were then grinded in a coffee grinder (Braun KSM-2W). All wood particles passed through a 35 mesh sieve (<500μm). The particles were then dried in an oven at 105°C to reduce the inherent moisture. The reason for performing the drying procedure is to precisely control the moisture content in the comingled feedstock. After that, the dried wood particles were mixed with biosolids to prepare a comingle wood and biosolids mixture. The mixture was then loaded into the hydrothermal reactor to be hydrothermally pretreated. The head space gas inside the reactor before HTP was controlled by vacuuming and pressurizing with 200psi of hydrogen three times. Then the vessel was heated up to a desired temperature and was thermally treated for 1 hour. The agitator is on during the entire test. After the HTP, the vessel is convectively cooled off by pumping coolant through the cooling coil inside the reactor. The wood particles are mixed with biosolids. The solid content of the comingled wood and biosolids is

controlled by weighting the wood and biosolids before mixing. For example, to obtain a comingled mixture with solid content of 43wt.%, wood and biosolids were mixed by a mass ratio of 1:1.5.

The comingled wood and biosolids mixture is fed into the hydrothermal reactor. The head space in the reactor is pressurized with hydrogen. It is done by vacuuming and pressurizing the reactor with hydrogen at 100psi for three times. Final pressure of the head space gas was controlled by setting up the pressure supply in the hydrogen tank. When HTP is completed, the reactor is quenched to ambient temperature by opening the cooling system. When the temperature of the hydrothermal reactor deceases to room temperature, the exhaust gas in the head space is either vented or sampled. The reactor is vacuumed before being opened. Slurry product is collected from a 1.5 inch drainage hole on the bottom of the reactor. After the slurry is collected, the reactor is cleaned for the next operation.

Results and Discussion

Leak Tests

The stirred batch hydrothermal reactor is rated at a Maximum Allowable Water Temperature (MAWT) of 350˚C and a Maximum Allowable Water Pressure (MAWP) of 3000 psi. The approximate operation temperature and pressure of the HTP, based on a lab scale batch test, are 240~270˚C and 1200~1400psi, respectively. The operation temperature and pressure were simulated by heating 3 liters (equally 5.7lb) of water to 300˚C. Head space in the reactor was kept at 200psi by pressurizing nitrogen before it was heated. When the temperature in the reactor reached 300˚C, it was kept constant for

over an hour, such that the pressure in the reactor was also kept constant at 1245psi. Experimental result of the leak test is shown in Figure 5.10.

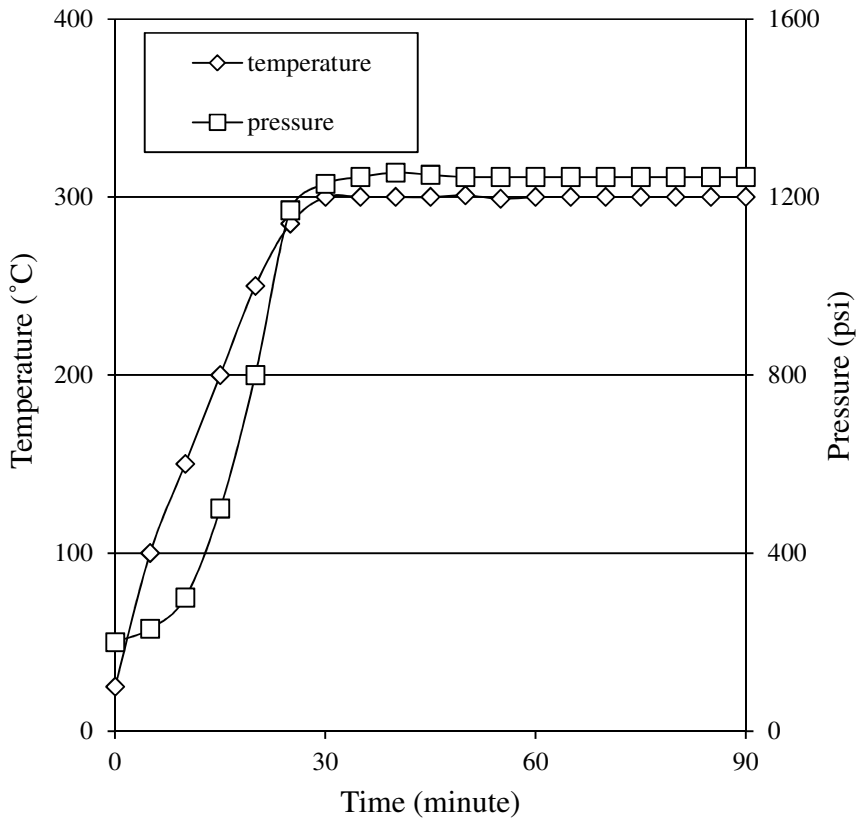

Fig 5.10 Leak Test Results of Demonstration Scale HTP Reactor

The leak test results showed that reactor was sealed during the entire process, and the pressure was well kept constant at 1425psi with a constant temperature of 300˚C.

Heating and Cooling Rate

It is essential to examine the heating and cooling rates of the stirred batch hydrothermal reactor. There are two reasons for this: 1) the operation time of the

pretreatment process is important for continuous feeding in the downstream Steam Hydrogasfication Reaction (SHR); 2) energy consumption of the pretreatment process depends on its heating rate. The heating and cooling rate of the HTP reactor was measured by heating water and wood wastes mixture in the HTP reactor. The heating and cooling ramp were then calculated and results are plotted in Figure 5.11.

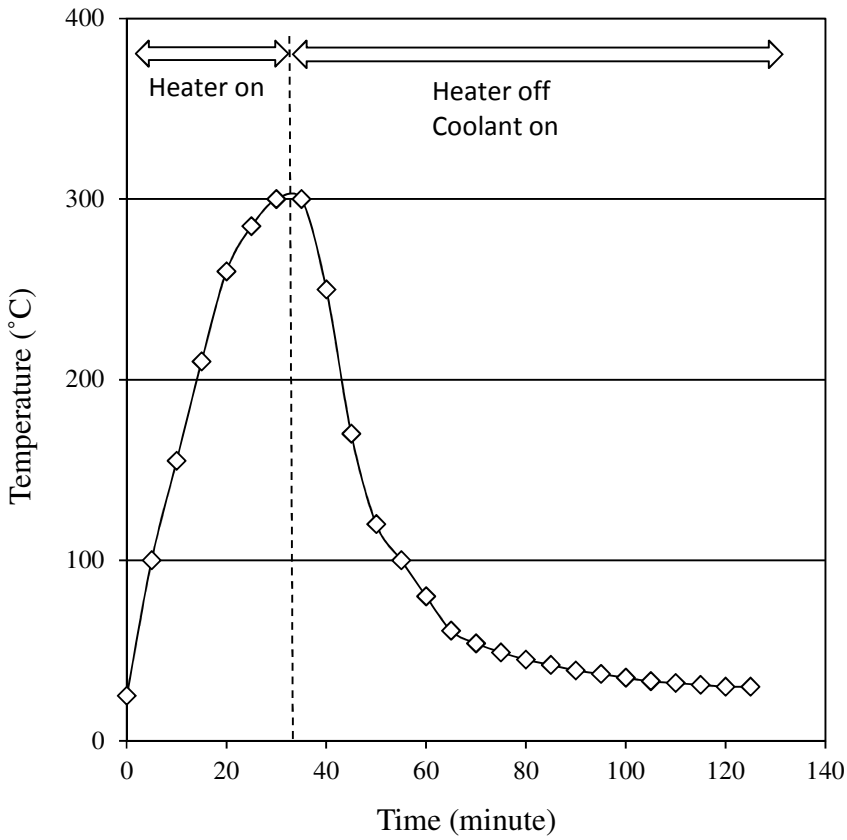

Fig 5.11 Heating and Cooling Rate of Demonstration Scale HTP

It is shown in Figure 5.11 that heating of the stirred batch reactor from room temperature to 300˚C took about 30minutes. Cooling of the stirred batch reactor from

300˚C to 30˚C took about 1.5hrs. If hydrothermal pretreatment was set to be 2hours, the entire HTP process would take about 4 hours to complete.

Agitator test results

A stirring test was performed with a total of 6.0 lb water and 0.66kg wood. Such a slurry had a viscosity value of 1.3Pa·s. The purpose of the agitator test was to examine agitator speed and motor capacity when the feedstock was pretreated. A 60in/lb footless heavy duty magnetic stirrer was used to power the agitator. The magnetic stirrer coupled with the agitator had been tested to be capable of stirring a paste with viscosity value of 10pa·s by vendor. The agitator test result is shown in Figure 5.12. Result shows that within a test time of 5min, motor speed was kept constant around at 100rpm.

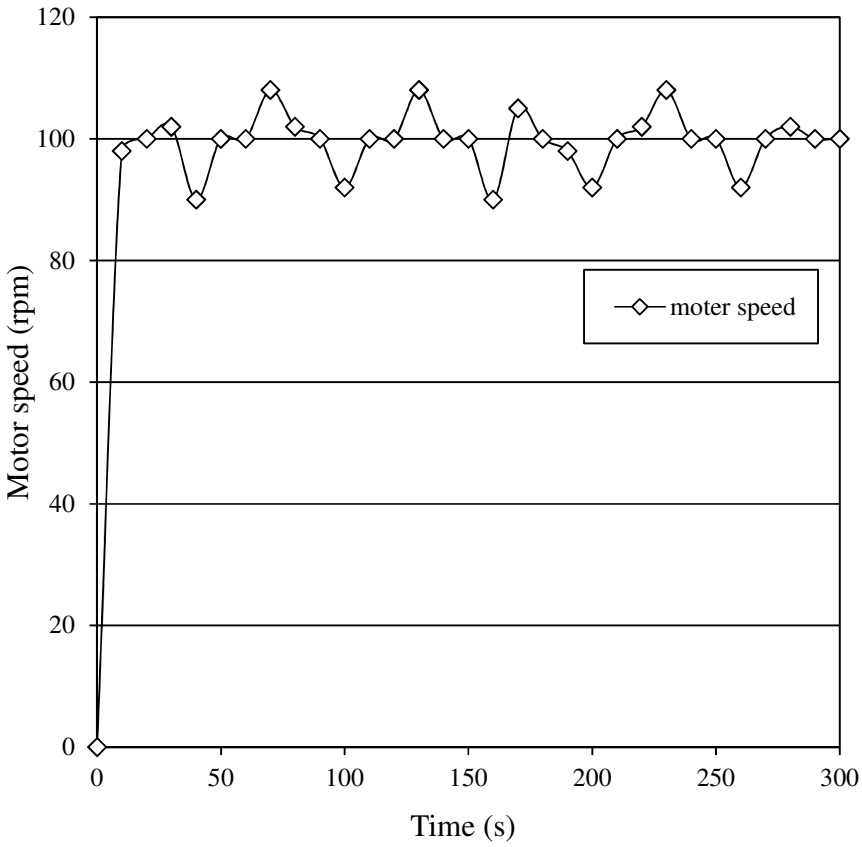

Fig 5.12 Agitator Test Results of Demonstration Scale HTP

Optimum Operation Conditions of Demonstration Scale HTP of Comingled Wood and Biosolids were found in this study. A total of 13 tests of HTP of comingled wood wastes and biosolids were carried out, as listed in Table 5.3.

Table 5.3 Test plan in the 5 gallon stirred batch pretreatment vessel

	1	2	3	4	5	6	7	8	9	10	11	12	13
Total load (kg)	4.8	4.8	4.8	3.6	3.6	3.6	3	3	3	3	3	3	3
Biosolids load (kg)	3.6	3.6	3.6	2.4	2.4	2.4	1.8	1.8	1.8	1.8	1.8	1.8	1.8
Wood waste load (kg)	1.2	1.2	1.2	1.2	1.2	1.2	1.2	1.2	1.2	1.2	1.2	1.2	1.2
Biosolids to wood waste ratio	3:1	3:1	3:1	2:1	2:1	2:1	1.5:1	1.5:1	1.5:1	1.5:1	1.5:1	1.5:1	1.5:1
Initial solid load (wt.%)	28.8	28.8	28.8	36.7	36.7	36.7	43.0	43.0	43.0	43.0	43.0	43.0	43.0
Initial headspace gas and pressure	H_2@200 psi	H_2@200 psi	H_2@200 psi	H_2@200 psi	H_2@200 psi	H_2@200 psi	H_2@200 psi	H_2@200 psi	H_2@200 psi	H_2@100 psi	H_2@400 psi	H_2@200 psi	H_2@200 psi
Pretreatment time (hr)	2	2	2	2	2	2	2	2	2	2	2	1	1.5
Pretreatment Temperature (˚C)	210±10	240±10	270±10	210±10	240±10	270±10	210±10	240±10	270±10	270±10	270±10	270±10	270±10

The influence of the operating conditions described above on the product properties were determined, these include the initial total solid loadings, initial wood to biosolids ratios, initial head space gas composition and operation time. Results of optimum operation condition tests of HTP of comingled wood and biosolids are given below.

Table 5.4 Results of optimum operation conditions tests of HTP of comingled wood waste and biosolids

Test number	Slurry form (yes/no)
1	Y
2	Y
3	Y
4	N
5	Y
6	Y
7	N
8	N
9	Y
10	N
11	Y
12	N
13	N

Slurry formation described in Table 1 was determined by visualizing the free water in the resultant mixtures after HTP. A flowable slurry was defined qualitatively in that there was noticeable amount of free water in the resultant mixture when the mixture was tilted in a transparent glass beaker. And, a non-flowable mixture had no or

unnoticeable free water. Figure 5.13 shows the comparison of a flowable and unflowable mixtures after HTP.

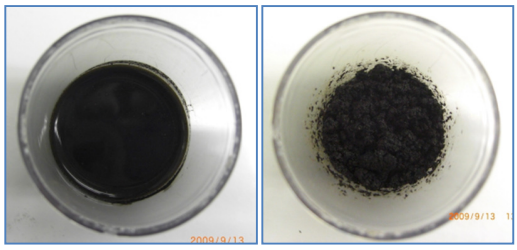

Fig 5.13 Comparison of Flowable and Non-flowable Product after HTP:

a) biosoilds and biomass mass ratio of 1.5:1, pretreatment temperature of 240 °C;
b) biosolids and biomass mass ratio of 2:1, pretreatment temperature of 240 °C.

It is important to point out that the flowable slurry is different from pumpable slurry which is defined as slurry with a viscosity value of less than 1.5pa·s. Optimum operation conditions were defined as when the highest initial solid loading was achieved to produce a flowable slurry, and is listed in Table 5.5.

Table 5.5 Optimum Operation Condition of Demonstration Scale HTP

Parameters	Operation conditions
Initial wood wastes to biosolids ratio	1:1.5
Initial solid loading	43wt.%
Temperature	270˚C
Initial head space pressure	200psi
Operation time	2 hrs

The initial solid loading had a major impact on the product slurry formation. Results show that with an initial wood to biosoilds ratio of 1:3 (initial solid loading of

28.8wt.%), slurry can be produced when the comingled feedstock was hydrothermally pretreated with a temperature at 210˚C. With an initial wood to biosoilds ratio of 1:2 (initial solid loading of 36.7wt.%), a slurry can be produced when the comingled feedstock was hydrothermally treated with a temperature at 240˚C. And with an initial wood to biosoilds ratio of 1:1.5 (initial solid loading of 43wt.%), slurry can be produced when the comingled feedstock was hydrothermally treated with a temperature at 270˚C. So it was concluded that in order to produce comingled wood wastes and biosolids slurry with an initial solid loading of over 40wt.%, the required temperature of HTP should be set above 270˚C. At 270˚C, the initial pressure of hydrogen in the head space gas needed was over 200psi. Operation time was also an important, not only because it affected the product formation, but it affected the continuous feedstock production rate as well. It was found that with an operation time of 2hours, slurry form of product was successfully produced, and the total feedstock production rate was able to meet the requirement of a continuous running of the downstream fluidized bed SHR Process.

Rheology Analysis of Comingled Wood Waste and Biosolids Slurry from Demonstration Scale HTP

The rheology properties of comingled wood and biosolids slurry with initial solid loading of 43.wt% are plotted in Figure 5.14. This slurry was pretreated at the optimum operation conditions, the pretreatment temperature was 270˚C, initial head space gas was 200psi of hydrogen and pretreatment time was 2 hours.

The rheometer was calibrated with standard oil before the rheology tests. And the rheology tests results show that at the optimum operation conditions, the resultant slurry

has a viscosity of less than 1.0Pa·s when shear rate was greater than 80s^{-1}. According to other research, the shear rates of the pump during slurry mixing, pipe flow and injection are 10-1000s^{-1}, 1-1000s^{-1} and 1000-10000s^{-1}, respectively. So it is concluded that the comingled wood and biosolids slurry produced after HTP at the optimum operation condition is pumpable. This is one of the most important successful goal of this research.

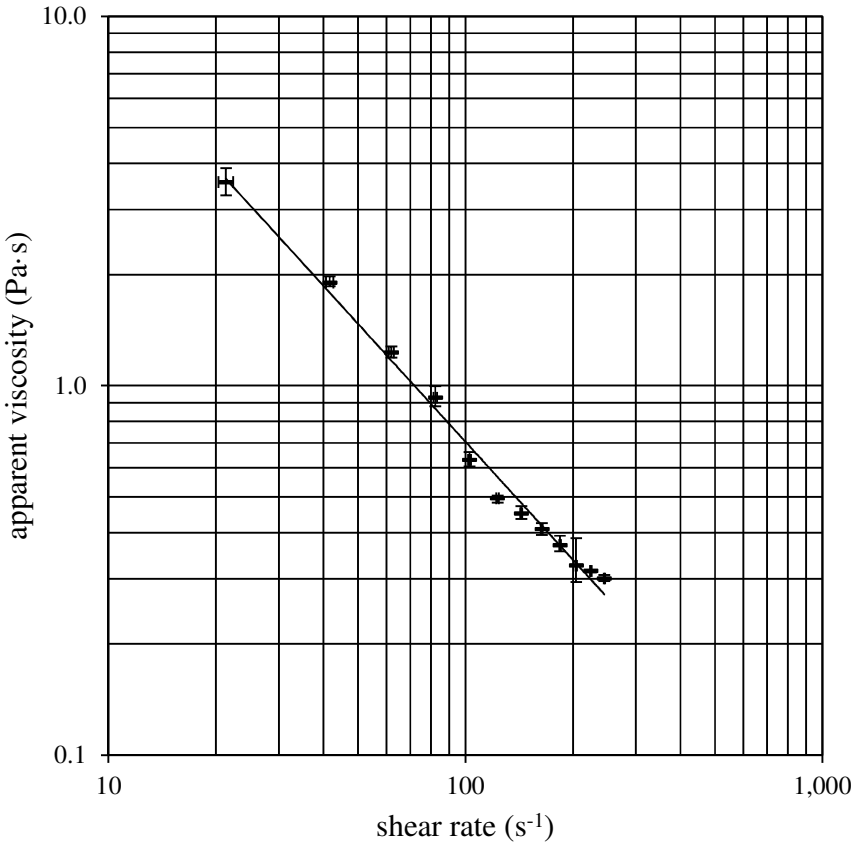

Fig 5.14 Rheology Properties of Comingled Wood Waste and Biosolids Slurry from Demonstration Scale HTP

5.2 Commercial Scale HTP Simulation

Presently, the Steam Hydrogasification Reaction (SHR) process with a Hydrothermal Pretreatment (HTP) unit has been built in CE-CERT at both a laboratory scale and a process demonstration scale. A commercial scale process is still not available for several reasons. Thus a technological and economical assessment of a commercialized SHR- HTP system cannot be based on any real world experience. Such evaluations, however, are required to effectively transfer this technology to the end-user. We did perform several modeling exercises and it is felt this modeling work can assist in material selection and energy utilization for a commercial scale HTP process.

In this section, an ASPEN Plus process simulator developed by ASPEN Tech, Inc.was used to model a 400 tons of feedstocks per day (dry basis) HTP process.

ASPEN uses a process flow-sheet simulator, which consists of a built-in model library. By choosing close-to-reality reactor types and use the thermodynamic relationships in the package, ASPEN can simulate chemical processes with reasonable detail. ASPEN Plus, compared with other chemical process simulator, such as ChemCad and Pro/II, included a user's definition method of non-conventional feedstocks, which makes it suitable for simulation of solid feedstocks, such as coal and biomass.

Thermodynamic properties

Near-realistic estimation of the HTP operation, with a capability of predicting optimum operational condition, is the goal of this simulation, so it is important to incorporate both material stream and energy stream constrains into the simulation. ASPEN Plus will then routinely calculate the required computations as long as the

chemical species are completely defined and characterized. In this study, pure chemicals in the reactions, such as oxygen, hydrogen, water, carbon monoxide, carbon dioxide, hydrocarbons, dissolved inorganic carbohydrates and dissolved sugars in liquid phase were defined in ASPEN Plus build-in database. Methods of computing their thermodynamic properties were provided by ASPEN Plus. Other non-conventional chemicals in the solid phase, such as biomass and biosolids, required manual definition. This is due to the fact that those feedstocks are mixtures of numerous chemical constituents, thus they have no defined atomic compositions. A non-conventional solids definition module provided by ASPEN Plus was utilized to alleviate this shortage. Complete energy computation and thermodynamic properties of these nonconventional solids need to be defined in such a way that allows ASPEN Plus to perform necessary calculations. The PENG-ROB property retaining method was applied to calculate the thermodynamic properties of all chemical constituents. The PENG-ROB method calculates all thermodynamic properties based on a cubic equation of state except the liquid molar volume. It is a recommended standard method by ASPEN Plus when high temperature/pressure hydrocarbon gas processing is involved. Table 5.6 summarizes the chemical compositions and property methods used in this simulation hydrocarbon gas processing is involved.

Table 5.6 Universal property methods applied in ASPEN Plus simulation

Chemical compositions	Conventional	H_2, water (H_2O), CO, CO, C_xH_y, CO_3^{2-} and $C_5H_{10}O_5$
	Nonconventional	Org, Ash, Porg
Properties methods		PENG-ROB

Non-conventional solids, as mentioned above, require manual definition. Wood contains an enormous number of individual constituents. By nature, it contains inherent moisture; its polymeric structure consists of cellulose, hemicellulose and lignin. Ash components remain when wood is combusted, which mainly consist of silicone oxides and metal oxides. Even the polymeric hydrocarbon species in wood cannot be atomically described due to the variation of their chain length. Biosolids are more complex than wood, in which more metal and hydrocarbon species exist. It is beyond the scope of thesis to deal with a complex characterization process of biomass and biosolids in detail. However to allow for meaningful simulations the Universal property methods (see Table 5.7) applied in ASPEN Plus simulation can provide basic conceptual assumption of the physical/chemical properties of biomass and biosolids.

The admixed feedstocks within the HTP can be assumed to be composed of an organic component, an ash component and moisture or water. The organic and ash component in these feedstocks can be treated as nonconventional solids. The organic component in the comingled feedstock was assigned as Org, and the organic component in the product was assigned as Porg. Org and Porg are assumed to be pseudo-chemicals

with consistent chemical composition. Org decomposes in the HTP to produce Porg, hydrocarbon, carbon oxide, organic solids and sugar.

To define Org, Porg and ash in ASPEN Plus, Huffman analysis was done. Enthalpy of Org and Porg was then calculated by the Dulong Correlation as given below:

$$H_c = 33.8x_c + 143.9 \times \left(x_H - \frac{x_0}{8}\right) + 9.4 \times x_s \qquad \text{(Eq. 5.4)}$$

Where the x's are weight fractions of C, H, O and S and the enthalpy is given in unit of MJ/kg.

The heat capacities of all nonconventional components are calculated by the Kirov correlation, which uses the proximate analysis of a component to compute the heat capacity at certain temperature. The function is given below:

$$C_p = x_m(4180) + x_f(690 + 2.85T_c - 0.00176T_c^2) + x_{vp}(1650 + 3.39T_c) + x_{vs}(2970 + 3.39T_c) + x_a(753 + 0.589T_c) \qquad \text{(Eq. 5.5.)}$$

Where the heat capacity is given in $J \cdot kg^{-1}K^{-1}$, x_a is the moisture weight fraction, x_f is fixed carbon weight fraction, x_{vp} is the primary volatile matter, x_{vs} is the secondary volatile matter weight fraction, x_a is the ash weight fraction and T_c is the temperature in Celsius. The primary volatile matter is defined as volatile matter in excess of 10% of the component on a dry, ash-free basis and secondary volatile matter is equal to the volatile matter content up to 10%. In this study, only Primary volatile matter was measured.

Ash components were considered unchanged in the HTP, even though in reality, they could be modified, but such change would not strongly influence the overall material and energy balance due to its low concentration, and so it was not considered.

HTP pseudo-chemistry

A critical simulation step in this study is to simulate the decomposition of biomass in the HTP. A decomposition reaction was assumed. Products were calculated from the experimental results. Chemical compositions of Org were defined by Huffman elemental tests, and chemical compositions of Porg were then calculated by balancing the overall stoichiometry of the reaction. Results of Org and Porg chemical compositions are listed in Table 5.7.

Table 5.7 Chemical compositions of feedstocks and product solid fractions

	biomass		biosolids		Org	Porg				
						pretreatment temperature				
						180°C	210°C	240°C		
						Initial biosolids to wood ratio				
						3:1			2:1	1.5:1
	wt.%	atom/C	wt.%	atom/C	atom/C	atom/C				
C	47.56	1.00	40.80	1.00	1.00	1.00	1.00	1.00	1.00	1.00
H	6.31	1.59	6.22	1.83	1.62	1.72	1.68	1.66	1.70	1.75
O	45.81	0.72	23.14	0.43	0.68	0.65	0.63	0.63	0.61	0.63

The overall chemical reaction in HTP was defined as follow:

$$Org \rightarrow \alpha\, Porg + \beta\, CH_4 + \gamma\, CO + \delta\, CO_2 + \varepsilon\, C_5H_{10}O_5 \qquad \text{(Eq. 5.6)}$$

Concluded from our experimental results, methane was the major hydrocarbon component, and so hydrocarbons were approximated by methane in this study. Inorganic composition in the liquid phase was detected at a low level, and so it was not considered. Xylose ($C_5H_{10}O_5$) is the precursor of hemicellulose, which is the major solvolyzed sugar

in the liquid phase after HTP. Other minor species, such as N, S and Cl are at low levels in the feedstock, and so they were omitted for simplification. The stoichiometry of the pseudo-chemistry was then obtained. The results are shown in Table 5.8.

Table 5.8 Reaction stoichiometry of biomass HTP

	Porg				
	pretreatment temperature				
	180°C	210°C	240°C		
	Initial biosolids to wood ratio				
	3:1			2:1	1.5:1
α	0.93	0.94	0.95	0.93	0.91
β	4.3E-06	1.4E-05	7.1E-05	7.0E-05	1.1E-03
γ	0.05	0.01	0.00	0.01	0.02
δ	0.01	0.03	0.03	0.04	0.05
ε	0.002	0.004	0.004	0.004	0.004

Process Simulation of HTP

The process flow diagram of HTP is shown in Figure 5.15. Pinewood was first pulverized to reduce its particle size to 75μm-90μm. Then it was mixed with biosolids at a fixed ratio. The mixture was then pressurized by hydrogen to 100psi and was preheated by exchanging heat from the hot slurry product. The preheated mixture was then pretreated in the HTP reactor. After HTP, the hot slurry product was cooled down by exchanging heat to cold feedstocks, and then was cooled down to room temperature

before it was flashed to separate the gas components. Lastly, the slurry product was pumped into a gasifier at 450psi by a centrifugal pump.

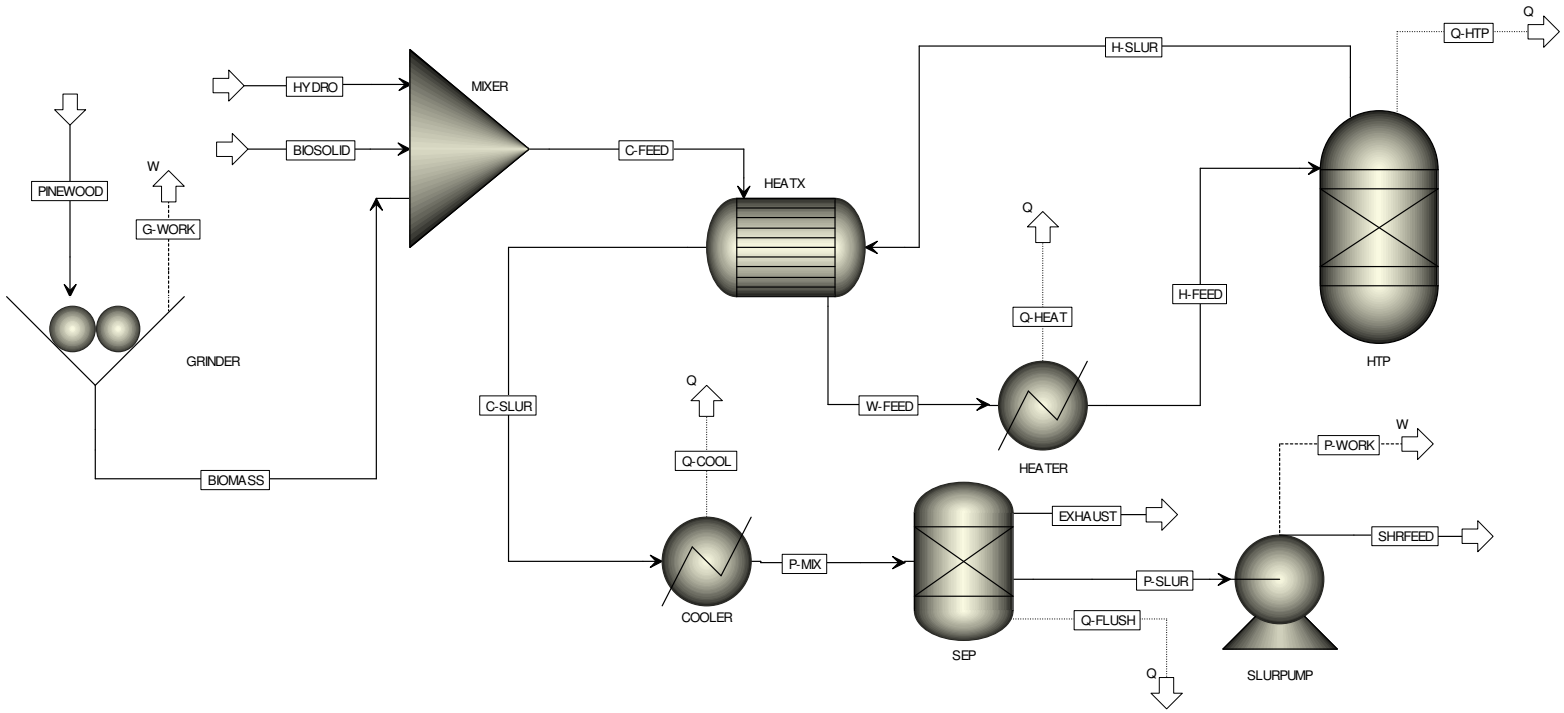

Fig 5.15 Simulation flow diagram of HTP

The unit modular used in this simulation was summarized in Table 5.9.

Table 5.9 Modular and its specification in HTP simulation

Unit	Model	Specification
Grinder	Jaw Crusher	homogeneous wood grinder, heat produced by the breaking process uncounted
HeatX	Heat Exchanger	contercurrent shell&tube type with constant overall heat transfer coefficient
HTP	R-Yield	Product yield is obtained from PDU experimental data
SHRPump	pump	fixed output pressure

Simulation Results

Material balance of the 400tons/day commercial scale HTP are listed in Appendix A. Based on an initial biosolids to wood ratio, 36.8 to 56.2tons/hr slurry can be produced by the simulated HTP plant, and approximately 1.46 to 2.2tons/hr exhaust gas is also generated during this process. The exhaust gas contains 400 to 800kg/hr CO_2, 150 to 320kg/hr of CO and around 30kg/hr H_2, with a heating value of 4 to 8MMBtu/hr The exhaust gas is pressurized to 220 -250psi, and can be compressed and injected into the SHR as blow gas.

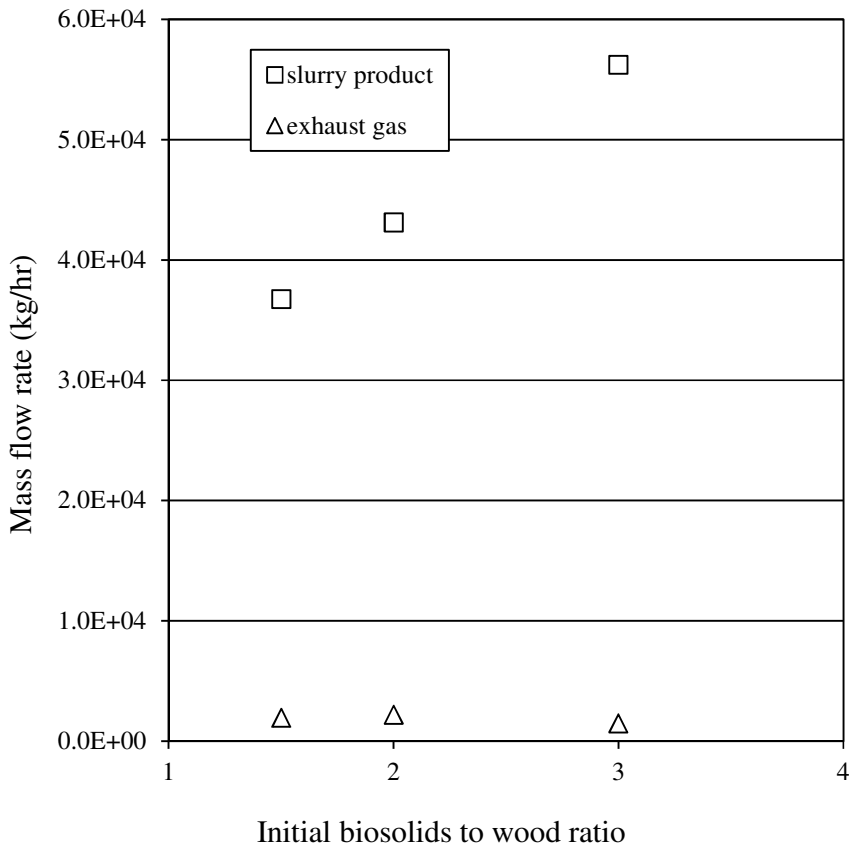

Fig 5.16 Material flow of 400 tons/day HTP plant regarding initial biosolids to wood ratio

The slurry product contains a solid loading ranging from 27% to 41% depending on the initial biosolids to wood loading.

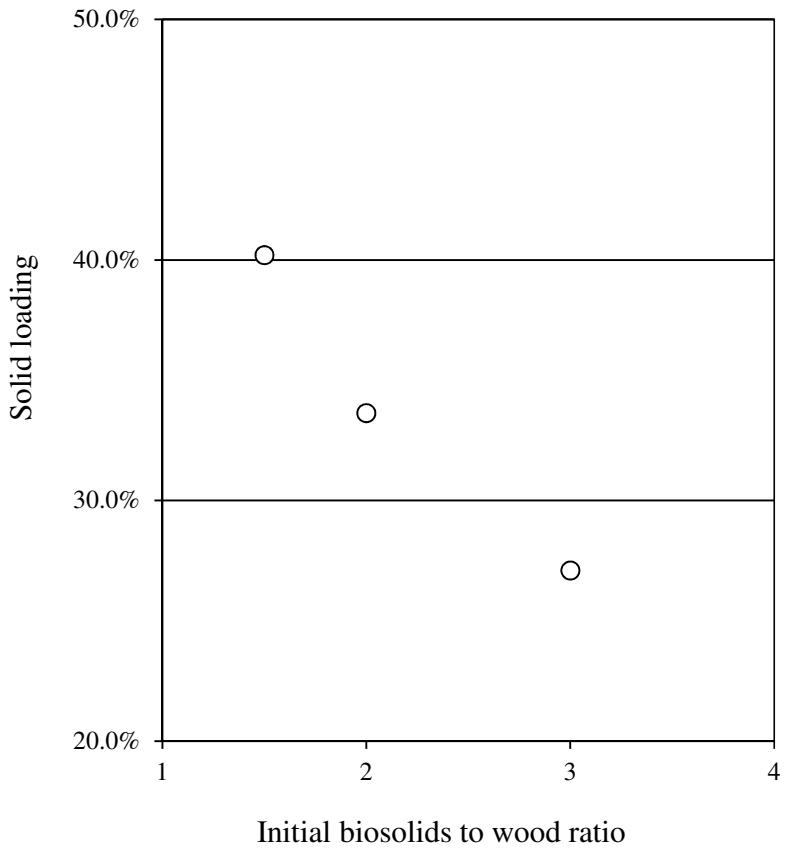

Fig 5.17 Solid loading of slurry product in 400 tons/day HTP plant regarding initial biosolids to wood ratio

Energy calculations of the commercial HTP plant were done for varying pretreatment temperature and initial biosolids to wood ratio. Results are presented below for each step of the process.

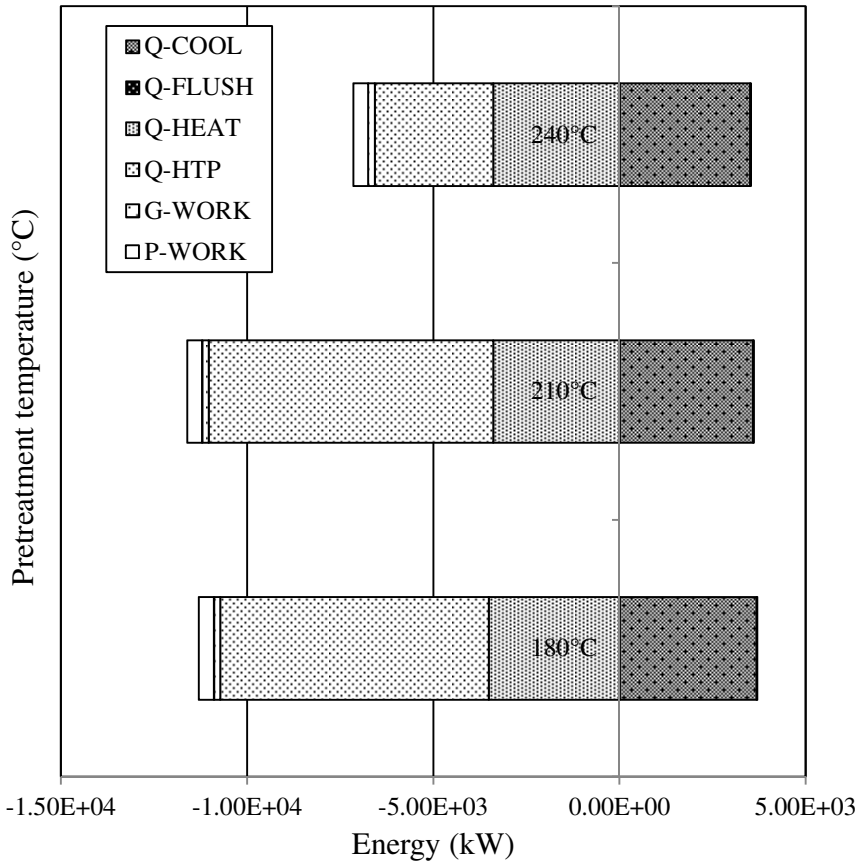

Fig 5.18 Stage-wise energy consumption in a 400 tons/day HTP plant regarding pretreatment temperature

Negative values in Figure 5.18 represent energy consumption, and positive numbers represents energy lost in the process. The results indicate that the total energy consumption of the HTP plant reached the lowest point when the pretreatment temperature was set at 240°C. This is due to the fact that it is more efficient to preheat the feedstocks in contact with hot slurry with higher temperature. Therefore, the heat duty required to heat the feedstocks to pretreatment temperature is less at higher pretreatment

temperature. Energy was majorly consumed in the HTP reactor, at a rate from 3.2MW to 7.2MW. This included the energy consumed to decompose the polysaccharides in the feedstocks, and the heat to maintain the temperature of the reactor. The second main energy consumption was to heat the feedstocks to the pretreatment temperature, at a rate from 3.4MW to 3.5MW. The energy consumed in grinding of the wood and pumping the final product into gasifier totaled at around 0.25MW. A large portion of the input energy was lost during the cooling process of the slurry product. Efficient heat exchanger would compensate such energy loss by transferring most of the heat into the incoming feedstocks. Sensitive analyses of the energy consumption with respect to some processing parameters, such as grinding of the feedstocks, heat duty of the heat exchanger and the pumping of feedstocks with varying viscosity were performed.

Energy consumption of grinding stage is determined by both particle size of wood in the feedstock and the grindability of feedstocks. Before the HTP, the particle size of the wood was usually reduced to 50-200μm. The energy consumption of grinding wood particles to a size range of 50-200μm was then calculated. Biomass is hard to grind compared with coal. This is due to the nature of its structure and strong fiber strength. ASPEN Plus uses Hardgrove Grindability Index (HGI) to represents how difficult the material can be grinded. It is an empirical test result and depends heavily on the mechanical strength of the material being tested. A study has been performed to investigate the HGI of different biomass, and Table 5.10 summarizes HGI of coal and biomass by categories.

Table 5.10 HGI of coal and biomass

Materials	HGI	Reference
Coal	>40	[249, 250]
Agricultural residual	<1	[172]
Hardwood	<30	[251]
Softwood	<10	-

The energy consumption of grinding stage of 400tons/day HTP plant was calculated by varying the wood particle size and its grindability. As shown in Figure 5.19, grinding fine wood particles required more energy consumption. More than twice the energy was needed to reduce the wood particle size from 75μm to 50μm, and this significantly increased the total energy consumption. Therefore, in the real practice, it is reasonable to set the wood particle size to be larger than 75μm. As grindability of the feedstock decreased to less than 30, significant energy is required to grind the feedstocks. Which means for the agricultural residuals and most soft wood, large particle size would be used to reduce the energy consumed in the grinding process. But as was proven by previous experiments, HTP also reduced solid particle size, so it is possible to obtain desired particle size without fine grinding in front of the HTP. It is important to point out that, in this simulation, jaw grinder was used to simulate the grinding process, whereas in real application, knife mill will be more suitable for biomass particle size reduction. Unfortunately, such alternation of grinding equipment is not available in aspen package, and the general purpose jaw grinder was used in the simulation. In other study of biomass

torrefaction has shown that HTP upgraded the grindability of biomass feedstocks, so it would also be rational to install the grinding process after HTP to obtain fine particles. Since desired particle size in the slurry has to be determined by design of the fluidized bed gasifier, it is out of the scope of this study to quantify the optimum particle size in the slurry.

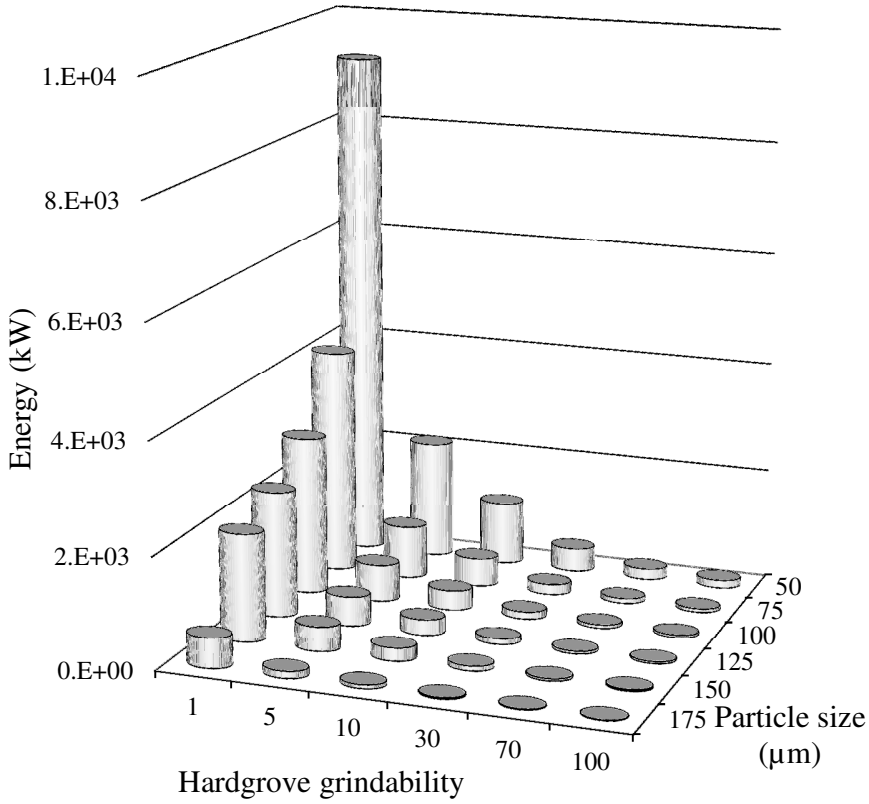

Fig 5.19 Grinding energy consumption and total energy consumption regarding wood particle size

As the stage total energy consumption graph showed, a large portion of the energy consumption was provided to heat the cold feedstocks to the pretreatment temperature. And so the energy consumption difference with varying heat exchanger duty was compared and results are shown in Figure 5.20.

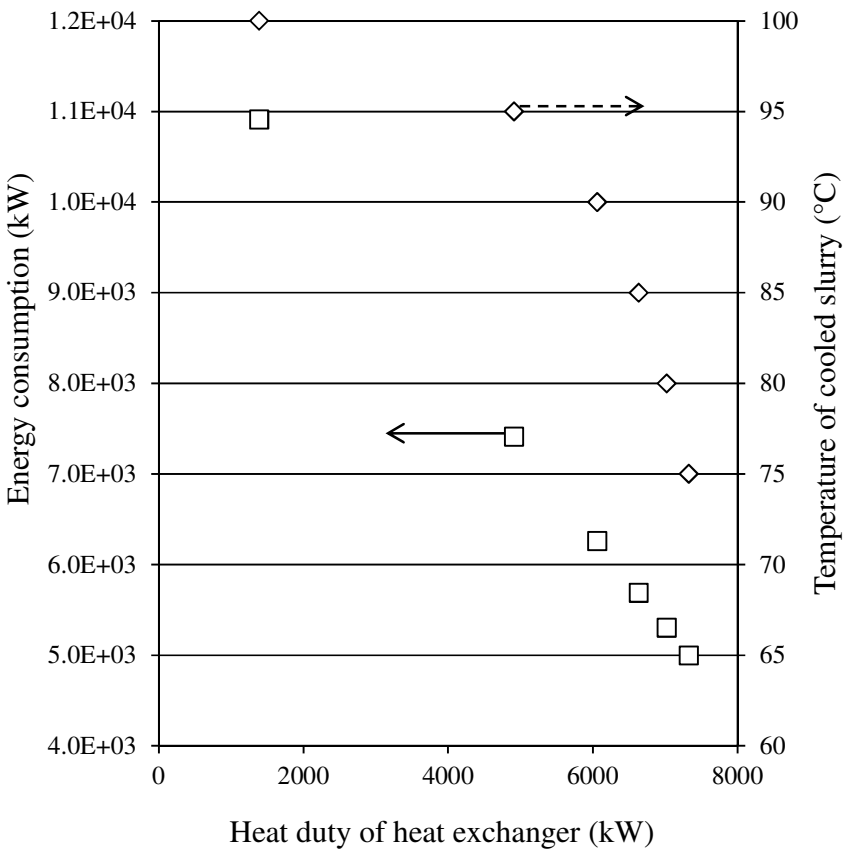

Fig 5.20 Total energy consumption of 400 tons/day HTP plant regarding the heat duty of heat exchanger and the respective temperature of cooled slurry.

As the heat duty of heat exchanger approached 7.4MW, the temperature of the cooled slurry was reduced to less than 80°C, which in practice, is a temperature that

further heat exchange would be inefficient. The total energy consumption would double when the temperature of the cooled slurry increased from 75°C to 100°C, but the heat duty of the heat exchanger would be reduced from 7.4MW to 1.1MW. With larger exchanger heat duty, more exchanger contacting area is required, which means high capital cost for the heat exchanger. So it would be practical to consider its economic impact. However, such economic analysis was not performed in this study, and should be considered in the future.

Viscosity of the slurry product would have an impact on the slurry pump efficiency and change the energy consumed in pumping the slurry into a pressurized gasifier. So the pump efficiency would be corrected by the viscosity value of the slurry. A correction method was studied and proposed by the Hydraulic Institute (HI) on Rotodynamic Slurry Pumps [252, 253]. To obtain the correction factor of pump efficiency, parameter, B, was calculated by following function:

$$B = \frac{16.5 \times v^{0.5} \times H^{0.0625}}{N^{0.25} \times Q^{0.375}} \qquad \text{(Eq. 5.7)}$$

Where

v is the kinematic viscosity in cP;

Q is the volumetric flow rate of materials in m3/hr;

H is the water head in m;

N is the rotating speed of the pump in rpm.

In this study, kinematic viscosity of the product slurry varied from 700cP to 1000cP at a shear rate of $102s^{-1}$. Slurry pump working condition was 1000rpm with water head gain of 95m, total volumetric flow rate of the slurry was $30.6m^3$/hr. The value of B

was then obtained, by which correction factor of pump efficiency was obtained from graph given by HI:

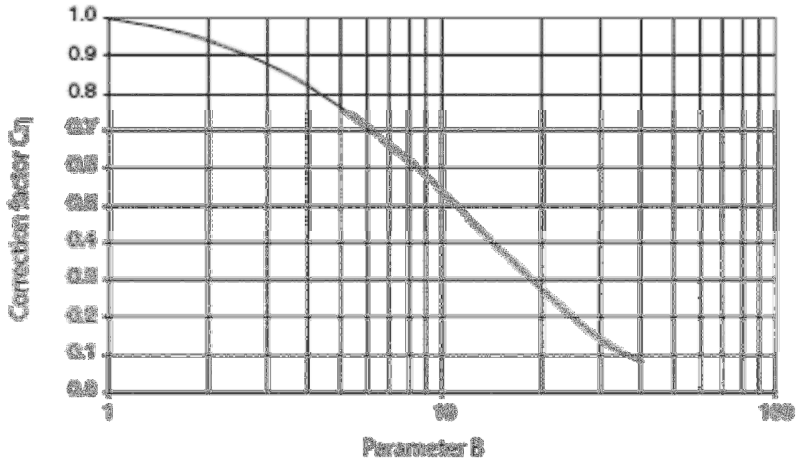

Fig 5.21 Slurry pump efficiency correction factors

Table 5.11 Correction factor for slurry pump in 400tons/day HTP plant regarding slurry kinematic viscosity

Viscosity (cP)	B factor	Correction factor
1	0.960956	1
100	9.609557	0.55
400	13.58997	0.4
700	25.4245	0.2
1000	30.38809	0.09

It is important to point out that slurries with a viscosity value of over 1000cP could be efficiently pumped in practice but such viscosity range was not considered in the

study above. The energy consumption of slurry pump was then obtained by applying these correction factors for the 400tons/day HTP plant, and the results are shown below:

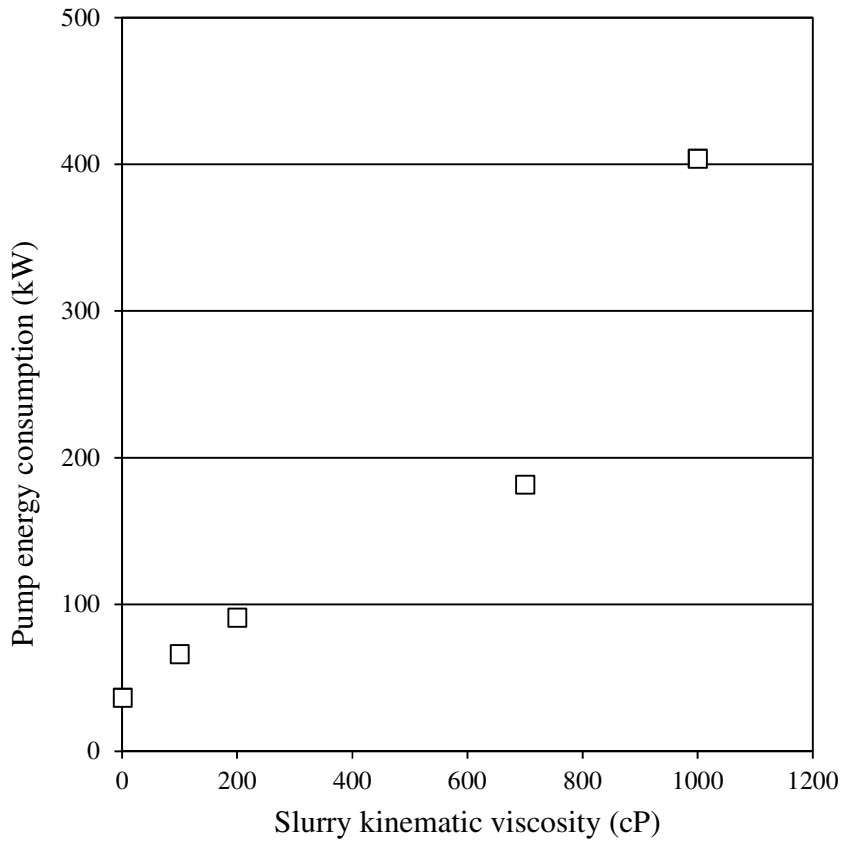

Fig 5.22 Pump Energy Consumption as a Function of Slurry Kinematic Viscosity

Results of the pump correction showed that the change of energy consumption is up to 0.4MW and it is insignificant compared with the total energy consumption of the HTP plant, which is above 7MW.

Conclusion

An innovative and cost effective Hydrothermal Pretreatment (HTP) method for biomass and other carbonaceous material was developed in this thesis. The HTP process prepares a pumpable high solid biomass slurry for gasification technologies. A lab scale and Process Demonstration Unit (PDU) scale HTP process were designed, built and evaluated using several feedstocks. The optimum operational conditions to yield a pumpable biomass slurry with an acceptable carbon to water ratio for the CE-CERT Steam Hydrogasification technology have been determined. In addition, a 400ton/day commercial scale HTP plant was simulated using ASPEN Plus. The energy and material balance were calculated based on experimental data developed as part of the thesis research. Three sub tasks were completed with the following conclusions:

1. A series of experiments have been performed to determine the optimum operation conditions of Hydrothermal Pretreatment (HTP) to yield desired viscosity and carbon content of the several carbonaceous slurries. In this sub task, the following results were obtained:
    1) A pumpable comingled wood-coal water slurry was produced with a solid content of over 50wt.% after it was hydrothermally treated for over 30min at a pretreatment temperature of 240°C. The slurry had an apparent viscosity of less than 1.0Pa·s, and the water to carbon ratio, by weight, was lower than 3:1. The slurry has a water to carbon ratio that favors Steam Hydrogasification, and thus could be gasified in an efficient manner;

2) A significant decrease of the apparent viscosity of biosolids was observed when biosolids was hydrothermally treated at a temperature of above 180°C, but the further increase of pretreatment temperature has no obvious impact on the apparent viscosity of biosolids;
3) A comingled wood-biosolds slurry was produced with a solid content of over 43wt.% after being hydrothermally treated for over 30min at a pretreatment temperature of 240°C. The apparent viscosity of this slurry was less than 1.0pa·s, and the water to carbon ratio, by weight, was lower than 3:1. This slurry contains a water to carbon ratio that favors Steam Hydrogasification, and thus could be gasified in an efficient manner;
4) Slurries settled faster after hydrothermal treatment than before the pretreatment. The presence of biosolids in the slurry elongated the settlement time and enhanced the stability of slurries.

2. The influence of operation conditions of HTP on the carbon redistribution were investigated by varying the pretreatment temperature, initial solid loading, initial wood particle size and pretreatment time. In this sub task, the following results were concluded:
    1) Increased levels of hydrocarbons were in the gas phase with increased pretreatment temperature. Carbon monoxide was the major carbon component in the gas when pretreatment was carried out at 180°C, but when pretreatment temperature increased to 240°C, carbon monoxide was converted to carbon dioxide. Total carbon oxide (carbon monoxide and

carbon dioxide) concentration in the gas increased with an increase of pretreatment temperature;

2) Hydrocarbon components with higher carbon number were the major carbon species in the gas phase when the initial wood to biosolids ratio is 1:1.5, while hydrocarbon components with lower carbon number were the major carbon species in the gas phase when initial wood to biosolids ratio is 1:3. Both carbon monoxide and carbon dioxide concentration in the gas decreased with decreased wood to biosolids ratio. As more carbon species were available in the slurry, with an increased wood to biosolids ratio the concentrations of hydrocarbons and carbon oxides increased;
3) The initial wood particle size has an insignificant impact on carbon compositions in the gas phase;
4) The carbon compositions in the gas increased when pretreatment time was elongated from 30min to 1hour, but no significant change has been observed if the pretreatment time was over 1hour. This suggests a thermodynamic equilibrium of carbon between the gas and slurry phases was reached with pretreatment time of over 1hour;
5) HTP resulted in organic carbon components release from the biosolids into its liquid phase, but did not have obvious impact on the inorganic carbon concentration in the liquid phase;

6) Higher TOC was detected in the liquid phase with higher pretreatment temperature of wood and biosolids mixtures, no significant increase of IC concentration in the liquid phase was observed;
7) TOC in the liquid phase increased with an increased wood to biosolids weight ratio, as more carbon species were available in the wood and biosolids mixture with higher wood to biosolids weight ratio;
8) Pretreatment resulted in less volatile carbon and more fixed carbon in the solid phase of products, which favors gasification process as less tar would be produced;
9) The carbon compositions presented in the liquid and gas phase after hydrothermal pretreatment was lower than 1.2wt.% of the initial carbon in the feedstocks. Most carbon is conserved in the solid phase which favors gasification processes.

3. To investigate the mechanism of how HTP promoted slurry formation of wood and biosolids mixture: (1) the free liquid in the bulk phase of wood biosolids mixture was measured, (2) the particle size of the solid in the slurry was measured, (3) surface electrokinetics of the solid particle was measured and (4) the micro structure of solid particles was photographed by a SEM. In this sub task, the following results were concluded:
    1) The Scanning Electron Microscope photos showed that the microstructure of biosolids was disrupted by HTP. Wood cells were disrupted by HTP as well, and with increased temperature of HTP, an obvious open structure

could be visualized in the wood cells. Wood lumps were broken into smaller pieces due to the HTP. Inherent moisture of the feedstock was release into the bulk phase by breaking cell walls of the wood;

2) The mean particle size of the wood particles reduced from 216µm to 140µm, 120µm and 75µm after being pretreated at a temperature of 180°C, 210°C and 240°C, respectively. The reduction of wood cell size resulted in release of inherent moisture of in the wood cells, thus increased the free liquid in the bulk phase;
3) More free liquid was available in the bulk phase after the pretreatment, and it increased with increase of pretreatment temperature. The available free liquid was the fluid agent in the slurry which enhanced the slurribility of the wood and biosolids mixtures;
4) The Zeta potential of biosolids increased after HTP and decreased with increase of pretreatment temperature. Zeta potential of wood particles decreased after HTP and increased with increase of pretreatment temperature. The addition of biosolids increased the zeta potential of particles in the mixtures. Results indicated increased stability of wood particles in the slurry.

4. A 400ton/day commercial scale HTP process was simulated by using ASPEN Plus. The process included grinding of wood chips, heat exchange between the influent and effluent mixture, and a slurry pump to elevate pretreated slurry into

gasifier with a pressure of 450psi. In this sub task, the following results were concluded:

1) A pseudo-chemical reaction scheme was derived by using the experimental data obtained from lab scale and PDU scale HTP tests.
2) In the 400ton/day commercial scale HTP plant, 36.8 to 56.2tons/hr slurry can be produced with about 1.46 to 2.2tons/hr exhaust gas generated. The exhaust gas contains 400 to 800kg/hr CO_2, 150 to 320kg/hr of CO and around 30kg/hr H_2, with a heating value of 4 to 8MMBtu/hr;
3) The slurry product contains a solid loading ranging from 27% to 41% depending on the initial biosolids to wood loading;
4) Total energy consumption of the HTP plant was lowest when pretreatment temperature was set at 240°C. This is due to the fact that it is more efficient to preheat the feedstocks in contact with hot slurry with higher temperature. Energy was consumed in the HTP reactor at a rate from 3.2MW to 7.2MW. The second main energy requirement was to heat the feedstocks to the pretreatment temperature, at a rate from 3.4MW to 3.5MW. The energy consumed in grinding of the wood and pumping the final product into the gasifier totaled at around 0.25MW;
5) Grinding to very fine wood particle size required more energy consumption. More than twice the energy was needed to reduce the wood particle size from 75µm to 50µm, and thus significantly increased the total energy consumption. Therefore, in real practice, it is reasonable to set the

wood particle size to be larger than 75μm. Significant energy is required to grind the feedstocks as the grindability of the feedstock decreased to less than 30;

6) The temperature of a cooled slurry reduced to less than 80°C as the heat duty of the heat exchanger approached 7.4MW, which in practice, is the temperature that further heat exchange would be inefficient. The total energy consumption would double when the temperature of the cooled slurry increased from 75°C to 100°C, but the heat duty of the heat exchanger would be reduced from 7.4MW to 1.1MW;
7) Results of the pump correction showed that the change of energy consumption is up to 0.4MW and it is insignificant compared with the total energy consumption of the HTP plant, which is above 7MW.

Future work

A lab scale and Process demonstration scale Hydrothermal Pretreatment (HTP) was developed and tested with the completion of this thesis. A 400ton/day commercial scale HTP plant was simulated with the assistance of ASPEN Plus. Rheology analysis and carbon balance of the products of HTP of biomass (wood waste and biosolids) were experimentally investigated. The follow tasks will need to be performed to further investigate the overall pretreatment performance on preparing suitable slurry for gasification technologies:

1. Design and test the flow performance of pretreated biomass slurry in a centrifugal pump and a membrane pump, its flow in pipelines and at the injection nozzles of the gasifier;
2. Gasification of pretreated biomass slurry, compare the carbon conversion rate and Cold Gas Efficiency of slurry feedstock in comparison with those of untreated biomass feedstocks;
3. Evaluation of the fuel properties of the pretreated biomass slurry feedstocks in a gasification environment, which may include the energy density, ash softening behavior, etc.;
4. HTP of other renewable feedstocks, such as animal manure, solid sludge waste, food waste, etc. The slurry product pumpability and carbon concentration will need to be investigated.

Reference

1. Scragg, A., *Biofuels: production, application and development*. Cabi Series. 2009 Cambridge, UK: CABI, 2009.
2. Twidell, J. and A.D. Weir, *Renewable energy resources*. 2006: Taylor & Francis.
3. Hoogwijk, M., et al., *Exploration of the ranges of the global potential of biomass for energy.* Biomass and Bioenergy, 2003. **25**(2): p. 119-133.
4. Rojstaczer, S., S.M. Sterling, and N.J. Moore, *Human Appropriation of Photosynthesis Products.* Science, 2001. **294**(5551): p. 2549-2552.
5. Ragauskas, A.J., et al., *The Path Forward for Biofuels and Biomaterials.* Science, 2006. **311**(5760): p. 484-489.
6. Hall, D.O., K.K. Rao, and B. Institute of, *Photosynthesis*. 1999: Cambridge University Press.
7. Silverstein, A., et al., *Photosynthesis*. 2007: Lerner Publishing Group.
8. Ke, B., *Photosynthesis: photobiochemistry and photobiophysics*. 2001: Kluwer Academic Publishers.
9. Tiwari, G.N. and M.K. Ghosal, *Renewable energy resources: basic principles and applications*. 2005: Alpha Science International.
10. Niele, F., *Energy: engine of evolution*. 2005: Elsevier.
11. National Research Council . Committee on America's Energy Future. Panel on Alternative Liquid Transportation, F., *Liquid transportation fuels from coal and biomass: technological status, costs, and environmental impacts*. 2009: National Academies Press.
12. Dewulf, J. and H.V. Langenhove, *Renewables-based technology: sustainability assessment*. 2006: Wiley.
13. European Conference of Ministers of, T., *Cutting transport CO2 emissions: what progress?* 2007: European Conference of Ministers of Transport.
14. Tissot, B.P. and D.H. Welte, *Petroleum formation and occurrence: a new approach to oil and gas exploration*. 1978. Medium: X; Size: Pages: 554.
15. Liu, P.I., *Energy, technology, and the environment*. 2005: ASME Press.
16. Publishing, B.E. and R. Curley, *Fossil Fuels*. 2011: Encyclopaedia Britannica.
17. Shafiee, S. and E. Topal, *When will fossil fuel reserves be diminished?* Energy Policy, 2009. **37**(1): p. 181-189.
18. Lindzen, R., *Some coolness concerning global warming.* Bulletin of the American Meteorological Society, 1990. **71**: p. 288.
19. Broecker, W.S., et al., *Fate of Fossil Fuel Carbon Dioxide and the Global Carbon Budget.* Science, 1979. **206**(4417): p. 409-418.
20. Hoel, M. and S. Kverndokk, *Depletion of fossil fuels and the impacts of global warming.* Resource and Energy Economics, 1996. **18**(2): p. 115-136.
21. Dorian, J.P., H.T. Franssen, and D.R. Simbeck, *Global challenges in energy.* Energy Policy, 2006. **34**(15): p. 1984-1991.

22. Armaroli, et al., *The future of energy supply : Challenges and opportunities*. Vol. 46. 2007, Weinheim, ALLEMAGNE: Wiley-VCH. 15.
23. Toman, M.A., *International oil security: problems and policies.* The Brookings review, 2002. **20**(2): p. 20.
24. Adelman, M.A., *Mineral Depletion, with Special Reference to Petroleum.* The Review of Economics and Statistics, 1990. **72**(1).
25. Campbell, C.J., A.G. Dore, and R. Sinding-Larsen, *World oil: reserves, production, politics and prices*, in *Norwegian Petroleum Society Special Publications*. 1996, Elsevier. p. 1-20.
26. IHT. *56% of Proven Oil Reserves Are in the Middle East 2007*. 2007 [cited 2011 07/18]; Available from: http://colli239.fts.educ.msu.edu/2007/06/03/oil-reserves-2007/.
27. EIA, *Annual Energy Outlook 2004: With Projections to 2025*. 2004: Energy Information Administration.
28. EIA, *Natural Gas Annual 2001*. 2001: DIANE Publishing.
29. EIA, *EIA Annual Coal Report, 2001*. 2001: DIANE Publishing.
30. USCongress, *Energy Independence and Security Act of 2007*, U.S. Congress, Editor. 2007: Washington, DC.
31. EIA, *Annual Energy Review, 2008*. 2009: United States Dept. of Energy.
32. Adams, F.G. and Y. Shachmurove, *Modeling and forecasting energy consumption in China: Implications for Chinese energy demand and imports in 2020.* Energy Economics, 2008. **30**(3): p. 1263-1278.
33. Umbach, F., *Global energy security and the implications for the EU.* Energy Policy, 2010. **38**(3): p. 1229-1240.
34. Salameh, M.G., *The new frontiers for the United States energy security in the 21st century.* Applied Energy, 2003. **76**(1-3): p. 135-144.
35. Bloomberg. *Energy & oil price: natural gas, electrisity and oil*. 2011 [cited 2011 07/18/2011]; Available from: http://www.bloomberg.com/energy/.
36. Yahaba, N., *How Does A Decrease In Oil Production Affect The World Economy?* 2010, Australia-Japan Research Centre, Crawford School, Australian National University.
37. Drapcho, C.M., *Biofuels Engineering Process Technology*. 2008, New York: McGraw-Hill.
38. EIA, *International Energy Outlook 2009*. 2009: Bernan Assoc.
39. Huang, R.D., R.W. Masulis, and H.R. Stoll, *Energy Shocks and Financial Markets.* Journal of Futures Markets, Vol. 16, No. 1, pp. 1-27, 1996, 1996.
40. Myers, N., *Consumption: Challenge to Sustainable Development ?* Science, 1997. **276**(5309): p. 53-55.
41. Delworth, T.L. and T.R. Knutson, *Simulation of Early 20th Century Global Warming.* Science, 2000. **287**(5461): p. 2246-2250.
42. Kerr, R.A., *How Urgent Is Climate Change?* Science, 2007. **318**(5854): p. 1230-1231.
43. Kerr, R.A., *Global Warming Is Changing the World.* Science, 2007. **316**(5822): p. 188-190.

44. Hoegh-Guldberg, O., et al., *Coral Reefs Under Rapid Climate Change and Ocean Acidification.* Science, 2007. **318**(5857): p. 1737-1742.
45. Hughes, T.P., et al., *Climate Change, Human Impacts, and the Resilience of Coral Reefs.* Science, 2003. **301**(5635): p. 929-933.
46. Meehl, G.A., et al., *How Much More Global Warming and Sea Level Rise?* Science, 2005. **307**(5716): p. 1769-1772.
47. Oerlemans, J., *Quantifying Global Warming from the Retreat of Glaciers.* Science, 1994. **264**(5156): p. 243-245.
48. Baer, H.A., *Toward a Critical Anthropology on the Impact of Global Warming on Health and Human Societies.* Medical Anthropology, 2008. **27**(1): p. 2-8.
49. Trostle, J., *Anthropology Is Missing: On the World Development Report 2010: Development and Climate Change.* Medical Anthropology, 2010. **29**(3): p. 217-225.
50. Massink, R., et al., *The Climate Value of Cycling.* Natural Resources Forum, 2011. **35**(2): p. 100-111.
51. Oppenheimer, M. and R. Alley, *Ice sheets, global warming, and article 2 of the UNFCCC.* Climatic Change, 2005. **68**(3): p. 257-267.
52. Jotzo, F., *Comparing the Copenhagen Emissions Targets.* SSRN eLibrary, 2011.
53. Olsson, L. and B.K. Ahring, *Biofuels*. 2007: Springer.
54. Gosselink, J.W., *Pathways to a more sustainable production of energy: sustainable hydrogen--a research objective for Shell.* International Journal of Hydrogen Energy, 2002. **27**(11-12): p. 1125-1129.
55. Parikka, M., *Global biomass fuel resources.* Biomass and Bioenergy, 2004. **27**(6): p. 613-620.
56. Romm, J.J. and A.B. Lovins, *Fueling a competitive economy.* Journal Name: Foreign Affairs; (United States), 1992.
57. Turner, J.A., *A Realizable Renewable Energy Future.* Science, 1999. **285**(5428): p. 687-689.
58. Maczulak, A., *Renewable Energy: Sources and Methods*. 2009: Facts On File.
59. Hall, J. and R. Kerr, *Innovation dynamics and environmental technologies: the emergence of fuel cell technology.* Journal of Cleaner Production, 2003. **11**(4): p. 459-471.
60. Dresselhaus, M.S. and I.L. Thomas, *Alternative energy technologies.* Nature, 2001. **414**(6861): p. 332-337.
61. Van Mierlo, J., G. Maggetto, and P. Lataire, *Which energy source for road transport in the future? A comparison of battery, hybrid and fuel cell vehicles.* Energy Conversion and Management, 2006. **47**(17): p. 2748-2760.
62. Ross, D.K., *Hydrogen storage: The major technological barrier to the development of hydrogen fuel cell cars.* Vacuum, 2006. **80**(10): p. 1084-1089.
63. Houghton, R.A., *Aboveground Forest Biomass and the Global Carbon Balance.* Global Change Biology, 2005. **11**(6): p. 945-958.
64. Montagnini, F. and P.K.R. Nair, *Carbon sequestration: An underexploited environmental benefit of agroforestry systems.* Agroforestry Systems, 2004. **61-62**(1): p. 281-295.

65. Fargione, J., et al., *Land Clearing and the Biofuel Carbon Debt.* Science, 2008. **319**(5867): p. 1235-1238.
66. Lal, R., *Carbon sequestration.* Philosophical Transactions of the Royal Society B: Biological Sciences, 2008. **363**(1492): p. 815-830.
67. Bhojvaid, P.P., Energy, and I. Resources, *Biofuels: towards a greener and secure energy future*. 2006: TERI Press.
68. McKendry, P., *Energy production from biomass (part 1): overview of biomass.* Bioresource Technology, 2002. **83**(1): p. 37-46.
69. Bajpai, D. and V.K. Tyagi, *Biodiesel: Source, Production, Composition, Properties and Its Benefits.* Journal of Oleo Science, 2006. **55**(10): p. 487-502.
70. MacFarlane, D.W., *Potential availability of urban wood biomass in Michigan: Implications for energy production, carbon sequestration and sustainable forest management in the U.S.A.* Biomass and Bioenergy, 2009. **33**(4): p. 628-634.
71. Hess, J.R., et al., *Roadmap for Agriculture Biomass Feedstock Supply in the United States*. 2003. p. Medium: ED.
72. Tafdrup, S., *Viable energy production and waste recycling from anaerobic digestion of manure and other biomass materials.* Biomass and Bioenergy, 1995. **9**(1-5): p. 303-314.
73. Socolow, R.H., *Industrial ecology and global change*. 1996: Cambridge University Press.
74. Lin, Y. and S. Tanaka, *Ethanol fermentation from biomass resources: current state and prospects.* Applied Microbiology and Biotechnology, 2006. **69**(6): p. 627-642.
75. Lynd, L.R., et al., *Fuel Ethanol from Cellulosic Biomass.* Science, 1991. **251**(4999): p. 1318-1323.
76. Worldwatch, I., *Biofuels for transport: global potential and implications for sustainable energy and agriculture*. 2007: Earthscan.
77. Demirbas, A., *Biofuels sources, biofuel policy, biofuel economy and global biofuel projections.* Energy Conversion and Management, 2008. **49**(8): p. 2106-2116.
78. Petrus, L. and M.A. Noordermeer, *Biomass to biofuels, a chemical perspective.* Green Chemistry, 2006. **8**(10): p. 861-867.
79. Alam, et al., *Combustion and emissions performance of low sulfur, ultra low sulfur and biodiesel blends in a DI diesel engine*. 2004, New York, NY, ETATS-UNIS: Society of Automotive Engineers. 12.
80. Demirbas, A., *Progress and recent trends in biofuels.* Progress in Energy and Combustion Science, 2007. **33**(1): p. 1-18.
81. Farrell, A.E. and D. Sperling, *A Low-Carbon Fuel Standard for California, Part 1: Technical Analysis*. 2007, Institute of Transportation Studies, UC Davis.
82. Hertel, T.W., et al., *Effects of US Maize Ethanol on Global Land Use and Greenhouse Gas Emissions: Estimating Market-Mediated Responses.* BioScience, 2010. **60**(3): p. 223-231.
83. Sperling, D. and S. Yeh, *Low Carbon Fuel Standards*. 2009, Institute of Transportation Studies, UC Davis.

84. Pahl, G., *Biodiesel: growing a new energy economy*. 2008: Chelsea Green Pub. Co.
85. Naik, S.N., et al., *Production of first and second generation biofuels: A comprehensive review.* Renewable and Sustainable Energy Reviews, 2010. **14**(2): p. 578-597.
86. Fatih Demirbas, M., *Biorefineries for biofuel upgrading: A critical review.* Applied Energy, 2009. **86**(Supplement 1): p. S151-S161.
87. Havlik, P., et al., *Global land-use implications of first and second generation biofuel targets.* Energy Policy, 2010. **In Press, Corrected Proof**.
88. Escobar, J.C., et al., *Biofuels: Environment, technology and food security.* Renewable and Sustainable Energy Reviews, 2009. **13**(6-7): p. 1275-1287.
89. Anselm, E., *Sustainable Production of Second-Generation Biofuels: Potential and Perspectives in Major Economies and Developing Countries*. 2010, OECD Publishing.
90. Sims, R.E.H., et al., *An overview of second generation biofuel technologies.* Bioresource Technology, 2010. **101**(6): p. 1570-1580.
91. Kumar, R., S. Singh, and O. Singh, *Bioconversion of lignocellulosic biomass: biochemical and molecular perspectives.* Journal of Industrial Microbiology & Biotechnology, 2008. **35**(5): p. 377-391.
92. Wyman, C.E., *Ethanol from lignocellulosic biomass: Technology, economics, and opportunities.* Bioresource Technology, 1994. **50**(1): p. 3-15.
93. Bayraktar, H., *Experimental and theoretical investigation of using gasoline-ethanol blends in spark-ignition engines.* Renewable Energy, 2005. **30**(11): p. 1733-1747.
94. Yusel, F. and B. Yusel, *The use of ethanol-gasoline blend as a fuel in an SI engine.* Renewable Energy, 2004. **29**(7): p. 1181-1191.
95. Alvira, P., et al., *Pretreatment technologies for an efficient bioethanol production process based on enzymatic hydrolysis: A review.* Bioresource Technology, 2010. **101**(13): p. 4851-4861.
96. Wen, F., N.U. Nair, and H. Zhao, *Protein engineering in designing tailored enzymes and microorganisms for biofuels production.* Current Opinion in Biotechnology, 2009. **20**(4): p. 412-419.
97. Wyman, C.E., *What is (and is not) vital to advancing cellulosic ethanol.* Trends in Biotechnology, 2007. **25**(4): p. 153-157.
98. Sohel, M.I. and M. Jack, *Efficiency improvements by geothermal heat integration in a lignocellulosic biorefinery.* Bioresource Technology, 2010. **101**(23): p. 9342-9347.
99. Mu, D., et al., *Comparative Life Cycle Assessment of Lignocellulosic Ethanol Production: Biochemical Versus Thermochemical Conversion.* Environmental Management, 2010. **46**(4): p. 565-578.
100. Higman, C. and M. Burgt, *Gasification*. 2003: Elsevier/Gulf Professional Pub.
101. Rezaiyan, J. and N.P. Cheremisinoff, *Gasification technologies: a primer for engineers and scientists*. 2005: Taylor & Francis.

102. McKendry, P., *Energy production from biomass (part 3): gasification technologies.* Bioresource Technology, 2002. **83**(1): p. 55-63.
103. Quaak, P., H. Knoef, and H.E. Stassen, *Energy from biomass: a review of combustion and gasification technologies*. 1999: World Bank.
104. Crocker, M., *Thermochemical Conversion of Biomass to Liquid Fuels and Chemicals*. 2010: Royal Society of Chemistry.
105. Bridgwater, A., *Thermal biomass conversion and utilization: biomass information system*. 1996: Office for Official Publications of the European Communities.
106. Comolli, A.G., et al., *The Shenhua coal direct liquefaction plant.* Fuel Processing Technology, 1999. **59**(2-3): p. 207-215.
107. Nolan, P., A. Shipman, and H. Rui, *Coal Liquefaction, Shenhua Group, and China's Energy Security.* European Management Journal, 2004. **22**(2): p. 150-164.
108. Liu, Z., S. Shi, and Y. Li, *Coal liquefaction technologies--Development in China and challenges in chemical reaction engineering.* Chemical Engineering Science, 2010. **65**(1): p. 12-17.
109. Bouvier, J.M., M. Gelus, and S. Maugendre, *Wood liquefaction--An overview.* Applied Energy, 1988. **30**(2): p. 85-98.
110. Elliott, D.C., et al., *Developments in direct thermochemical liquefaction of biomass: 1983-1990.* Energy & Fuels, 1991. **5**(3): p. 399-410.
111. Smoot, L.D. and P.J. Smith, *Coal combustion and gasification*. 1985: Plenum Press.
112. Figueiredo, J.L., J.A. Moulijn, and D. North Atlantic Treaty Organization. Scientific Affairs, *Carbon and coal gasification: science and technology*. 1986: Martinus Nijhoff.
113. Bell, D.A. and B.F. Towler, *Coal Gasification and Its Applications*. 2010: Elsevier Science Ltd.
114. Overend, R., M. Canada. Energy, and C. Resources, *Gasification: an overview*. 1980: Energy, Mines and Resources Canada.
115. Perry, R.H. and D.W. Green, *Perry's chemical engineers' handbook*. 2008: McGraw-Hill.
116. Knoef, H. and J. Ahrenfeldt, *Handbook biomass gasification*. 2005: BTG Biomass Technology Group.
117. Surhone, L.M., M.T. Timpledon, and S.F. Marseken, *Partial Oxidation*. 2010: VDM Verlag Dr. Mueller AG & Co. Kg.
118. Chmielniak, T. and M. Sciazko, *Co-gasification of biomass and coal for methanol synthesis.* Applied Energy. **74**(3-4): p. 393-403.
119. Baker, E.G., L.K. Mudge, and M.D. Brown, *Methanol and ammonia from biomass.* Journal Name: Chem. Eng. Prog.; (United States); Journal Volume: 80:12, 1984: p. Medium: X; Size: Pages: 43-46.
120. Balat, M., *Gasification of Biomass to Produce Gaseous Products.* Energy Sources, Part A: Recovery, Utilization, and Environmental Effects, 2009. **31**(6): p. 516-526.
121. Smith, A.R. and J. Klosek, *A review of air separation technologies and their integration with energy conversion processes.* Fuel Processing Technology, 2001. **70**(2): p. 115-134.

122. Leppaahti, J., P. Simell, and E. Kurkela, *Catalytic conversion of nitrogen compounds in gasification gas.* Fuel Processing Technology, 1991. **29**(1-2): p. 43-56.
123. Kanniche, M. and C. Bouallou, *CO2 capture study in advanced integrated gasification combined cycle.* Applied Thermal Engineering, 2007. **27**(16): p. 2693-2702.
124. Shoko, E., et al., *Hydrogen from coal: Production and utilisation technologies.* International Journal of Coal Geology, 2006. **65**(3-4): p. 213-222.
125. Mueller-Langer, F., et al., *Techno-economic assessment of hydrogen production processes for the hydrogen economy for the short and medium term.* International Journal of Hydrogen Energy, 2007. **32**(16): p. 3797-3810.
126. Mulen, H.-J., K.H. van Heek, and H. Jutgen, *Kinetic studies of steam gasification of char in the presence of H2, CO2 and CO.* Fuel, 1985. **64**(7): p. 944-949.
127. Fushimi, C., et al., *Effect of Heating Rate on Steam Gasification of Biomass. 1. Reactivity of Char.* Industrial & Engineering Chemistry Research, 2003. **42**(17): p. 3922-3928.
128. Pfeifer, C., S. Koppatz, and H. Hofbauer, *Steam gasification of various feedstocks at a dual fluidised bed gasifier: Impacts of operation conditions and bed materials.* Biomass Conversion and Biorefinery, 2011. **1**(1): p. 39-53.
129. Nagel, F.P., et al., *Biomass integrated gasification fuel cell systems-Concept development and experimental results.* Biomass and Bioenergy, 2011. **35**(1): p. 354-362.
130. Allen, S.G., et al., *Biomass Gasification in Supercritical Water 鈥?AU - Antal,, Michael Jerry.* Industrial & Engineering Chemistry Research, 2000. **39**(11): p. 4040-4053.
131. Kruse, A., *Supercritical water gasification.* Biofuels, Bioproducts and Biorefining, 2008. **2**(5): p. 415-437.
132. Schmieder, H., et al., *Hydrothermal gasification of biomass and organic wastes.* The Journal of Supercritical Fluids, 2000. **17**(2): p. 145-153.
133. Waldner, M.H. and F. Vogel, *Renewable Production of Methane from Woody Biomass by Catalytic Hydrothermal Gasification.* Industrial & Engineering Chemistry Research, 2005. **44**(13): p. 4543-4551.
134. Lu, Y.J., et al., *Hydrogen production by biomass gasification in supercritical water: A parametric study.* International Journal of Hydrogen Energy, 2006. **31**(7): p. 822-831.
135. Resende, F.L.P. and M. University of, *Supercritical water gasification of biomass*. 2009: University of Michigan.
136. Garg, M., et al., *The hydrogasification of wood.* Industrial & Engineering Chemistry Research, 1988. **27**(2): p. 256-264.
137. Tomeczek, J. and S. Gil, *The kinetics of coal chars hydrogasification.* Fuel Processing Technology, 2010. **91**(11): p. 1564-1568.
138. Gardner, N., E. Samuels, and K. Wilks, *Catalyzed Hydrogasification of Coal Chars*, in *Coal Gasification*. 1974, AMERICAN CHEMICAL SOCIETY. p. 217-236.

139. Suzuki, T., et al., *Catalytic activities of ion-exchanged nickel and iron in low temperature hydrogasification of raw and modified birch chars.* Fuel, 1994. **73**(12): p. 1836-1841.
140. Raju, A.S.K., C.S. Park, and J.M. Norbeck, *Synthesis gas production using steam hydrogasification and steam reforming.* Fuel Processing Technology, 2009. **90**(2): p. 330-336.
141. Reed, T.E., *Biomass gasification: principles and technology*. Related Information: Energy Technology Review No. 67. 1981. Medium: X; Size: Pages: 401.
142. Prins, M.J., K.J. Ptasinski, and F.J.J.G. Janssen, *From coal to biomass gasification: Comparison of thermodynamic efficiency.* Energy, 2007. **32**(7): p. 1248-1259.
143. Han, J. and H. Kim, *The reduction and control technology of tar during biomass gasification/pyrolysis: An overview.* Renewable and Sustainable Energy Reviews, 2008. **12**(2): p. 397-416.
144. Baker, M.D., *Gasification: Chemistry, Processes and Applications*. 2011: Nova Science Pub Inc.
145. Dry, M.E., *The fischer-tropsch process - commercial aspects.* Catalysis Today, 1990. **6**(3): p. 183-206.
146. van Dyk, J.C., M.J. Keyser, and M. Coertzen, *Syngas production from South African coal sources using Sasol-Lurgi gasifiers.* International Journal of Coal Geology, 2006. **65**(3-4): p. 243-253.
147. Meyers, R.A., *Handbook of synfuels technology*. 1984. Medium: X; Size: Pages: 928.
148. Anthony, R.G., J.J. McKetta, and W.A. Cunningham, *Encyclopedia of chemical processing and design*. 1987: Dekker.
149. Bunt, J.R., J.P. Joubert, and F.B. Waanders, *Coal char temperature profile estimation using optical reflectance for a commercial-scale Sasol-Lurgi FBDB gasifier.* Fuel, 2008. **87**(13-14): p. 2849-2855.
150. Dry, M.E. and H.B.W. Erasmus, *Update of the Sasol Synfuels Process.* Annual Review of Energy, 1987. **12**(1): p. 1-46.
151. Warnecke, R., *Gasification of biomass: comparison of fixed bed and fluidized bed gasifier.* Biomass and Bioenergy, 2000. **18**(6): p. 489-497.
152. Devi, L., K.J. Ptasinski, and F.J.J.G. Janssen, *A review of the primary measures for tar elimination in biomass gasification processes.* Biomass and Bioenergy, 2003. **24**(2): p. 125-140.
153. Corella, J., J.M. Toledo, and R. Padilla, *Catalytic Hot Gas Cleaning with Monoliths in Biomass Gasification in Fluidized Beds. 1. Their Effectiveness for Tar Elimination.* Industrial & Engineering Chemistry Research, 2004. **43**(10): p. 2433-2445.
154. Basu, P., *Combustion and gasification in fluidized beds*. 2006: CRC/Taylor & Francis.
155. Howard, J.R., *Fluidized bed technology: principles and applications*. 1989: A. Hilger.

156. Brown, A.L., et al., *Design and Characterization of an Entrained Flow Reactor for the Study of Biomass Pyrolysis Chemistry at High Heating Rates.* Energy & Fuels, 2001. **15**(5): p. 1276-1285.
157. Freihaut, J.D., W.M. Proscia, and D.J. Seery, *Chemical characteristics of tars produced in a novel low-severity, entrained-flow reactor.* Energy & Fuels, 1989. **3**(6): p. 692-703.
158. Jeon, S.K., et al., *Characteristics of steam hydrogasification of wood using a micro-batch reactor.* Fuel, 2007. **86**(17-18): p. 2817-2823.
159. Arun SK Raju, C.S.P., Joseph M Norbeck, *Steam hydrogasification of coal-wood mixtures in a batch reactor*, in *International Pittsburgh Coal Conference 2008*. 2008: Pittsburgh, PA, USA.
160. David Gray, C.W., etc, *Increasing Security and Reducing Carbon Emissions of the U.S. Transportation Sector: A Transformational Role for Coal with Biomass*. 2007, National Energy Technology Laboratory.
161. Scurlock, J., *Bioenergy feedstock characteristics*. 2001, Oak Ridge National Laboratory, Bioenergy Feedstock Development Programs.
162. Huang, Y., et al., *Biomass co-firing in a pressurized fluidized bed combustion (PFBC) combined cycle power plant: A techno-environmental assessment based on computational simulations.* Fuel Processing Technology, 2006. **87**(10): p. 927-934.
163. Li, K., R. Zhang, and J. Bi, *Experimental study on syngas production by co-gasification of coal and biomass in a fluidized bed.* International Journal of Hydrogen Energy, 2010. **35**(7): p. 2722-2726.
164. Jenkins, B.M., L.L. Baxter, and T.R. Miles, *Combustion properties of biomass.* Fuel Processing Technology, 1998. **54**(1-3): p. 17-46.
165. Levine, J.S., *Biomass Burning and Global Change: Remote sensing, modeling and inventory development, and biomass burning in Africa*. 1996: MIT Press.
166. Di Blasi, C., *Influences of physical properties on biomass devolatilization characteristics.* Fuel, 1997. **76**(10): p. 957-964.
167. Raveendran, K., A. Ganesh, and K.C. Khilar, *Pyrolysis characteristics of biomass and biomass components.* Fuel, 1996. **75**(8): p. 987-998.
168. De Bari, I., et al., *Air Gasification of Biomass in a Downdraft Fixed Bed:鈦?A Comparative Study of the Inorganic and Organic Products Distribution.* Energy & Fuels, 2000. **14**(4): p. 889-898.
169. Chen, W.-H. and P.-C. Kuo, *A study on torrefaction of various biomass materials and its impact on lignocellulosic structure simulated by a thermogravimetry.* Energy, 2010. **35**(6): p. 2580-2586.
170. Park, C.S. and J.M. Norbeck, *Rheological Study of Comingled Biomass and Coal Slurries with Hydrothermal Pretreatment 鈦?AU - He, Wei.* Energy & Fuels, 2009. **23**(10): p. 4763-4767.
171. Dowgiallo, A., *Cutting force of fibrous materials.* Journal of Food Engineering, 2005. **66**(1): p. 57-61.
172. Loo, S.V. and J. Koppejan, *The handbook of biomass combustion and co-firing*. 2008: Earthscan.

173. Mani, S., L.G. Tabil, and S. Sokhansanj, *Grinding performance and physical properties of wheat and barley straws, corn stover and switchgrass.* Biomass and Bioenergy, 2004. **27**(4): p. 339-352.
174. Raveendran, K., A. Ganesh, and K.C. Khilar, *Influence of mineral matter on biomass pyrolysis characteristics.* Fuel, 1995. **74**(12): p. 1812-1822.
175. Seggiani, M., *Empirical correlations of the ash fusion temperatures and temperature of critical viscosity for coal and biomass ashes.* Fuel, 1999. **78**(9): p. 1121-1125.
176. Zhou, J., et al., *Release of Fuel-Bound Nitrogen during Biomass Gasification.* Industrial & Engineering Chemistry Research, 2000. **39**(3): p. 626-634.
177. Zevenhoven-Onderwater, M., et al., *The ash chemistry in fluidised bed gasification of biomass fuels. Part I: predicting the chemistry of melting ashes and ash-bed material interaction.* Fuel, 2001. **80**(10): p. 1489-1502.
178. Sutton, D., B. Kelleher, and J.R.H. Ross, *Review of literature on catalysts for biomass gasification.* Fuel Processing Technology, 2001. **73**(3): p. 155-173.
179. Bornemann, G.A. and D.G. Sundstrom, *Commercialization of the Dow gasification process*. 1986. Medium: X; Size: Pages: 270-273.
180. Cummer, K.R. and R.C. Brown, *Ancillary equipment for biomass gasification.* Biomass and Bioenergy, 2002. **23**(2): p. 113-128.
181. Svoboda, K., et al., *Pretreatment and feeding of biomass for pressurized entrained flow gasification.* Fuel Processing Technology, 2009. **90**(5): p. 629-635.
182. Guo, X., et al., *Performance of an entrained-flow gasification technology of pulverized coal in pilot-scale plant.* Fuel Processing Technology, 2007. **88**(5): p. 451-459.
183. Schell, D., *High pressure solids feeding using a lockhopper system: Design and operating experience.* Applied Biochemistry and Biotechnology, 1988. **17**(1): p. 73-87.
184. Michael, L.S., A.M. Mark, and D.S. Darren, *FEED SYSTEM INNOVATION FOR GASIFICATION OF LOCALLY ECONOMICAL ALTERNATIVE FUELS (FIGLEAF)*, in *Other Information: PBD: 1 Nov 2001*. 2001. p. Medium: ED; Size: 59 pages.
185. Maniatis, K., *Progress in Biomass Gasification: An Overview*, in *Progress in Thermochemical Biomass Conversion*. 2008, Blackwell Science Ltd. p. 1-31.
186. Morel, W.C., *Economic comparison of coal feeding systems in coal gasification - lock hopper vs slurry.* Journal Name: Prepr. Pap. - Am. Chem. Soc., Div. Fuel Chem.; (United States); Journal Volume: 22:7, 1977: p. Medium: X; Size: Pages: 155-164.
187. Zheng, L. and E. Furinsky, *Comparison of Shell, Texaco, BGL and KRW gasifiers as part of IGCC plant computer simulations.* Energy Conversion and Management, 2005. **46**(11-12): p. 1767-1779.
188. Hotchkiss, R., *Coal gasification technologies.* Proceedings of the Institution of Mechanical Engineers, Part A: Journal of Power and Energy, 2003. **217**(1): p. 27-33.

189. Macosko, C.W., *Rheology: principles, measurements, and applications*. 1994: Wiley-VCH.
190. Tanner, R.I., *Engineering rheology*. 2000: Oxford University Press.
191. Atesok, G., et al., *The effect of coal properties on the viscosity of coal-water slurries.* Fuel, 2002. **81**(14): p. 1855-1858.
192. Boylu, F., H. Diner, and G. Atesok, *Effect of coal particle size distribution, volume fraction and rank on the rheology of coal-water slurries.* Fuel Processing Technology, 2004. **85**(4): p. 241-250.
193. Kawatra, S.K., A.K. Bakshi, and T.E. Miller, *Rheological characterization of mineral suspensions using a vibrating sphere and a rotational viscometer.* International Journal of Mineral Processing, 1996. **44-45**: p. 155-165.
194. Turian, R.M., et al., *Characterization, settling, and rheology of concentrated fine particulate mineral slurries.* Powder Technology, 1997. **93**(3): p. 219-233.
195. Lu, P. and M. Zhang, *Rheology of coal-water paste.* Powder Technology, 2005. **150**(3): p. 189-195.
196. Roh, N.-S., et al., *Rheological behaviour of coal-water mixtures. 1. Effects of coal type, loading and particle size.* Fuel, 1995. **74**(8): p. 1220-1225.
197. Roh, N.-S., et al., *Rheological behaviour of coal-water mixtures. 2. Effect of surfactants and temperature.* Fuel, 1995. **74**(9): p. 1313-1318.
198. Nam-Sun, R.O.H., et al., *Rheological behaviour of coal-water mixtures*. Vol. 74. 1995, Kidlington, ROYAUME-UNI: Elsevier.
199. Natarajan, V.P. and G.J. Suppes, *Rheological studies on a slurry biofuel to aid in evaluating its suitability as a fuel.* Fuel. **76**(14-15): p. 1527-1535.
200. Shimojo, M.I., Kazunobu. etc., *METHOD OF REFORMING BIOMASS AND REFORMING APPARATUS*. 2006.
201. McMahon, M.A.S., R. M. McKeon, R. J. Brent, A., *Partial oxidation of sewage sludge*. 1991: US.
202. Pimenova, N. and T. Hanley, *Measurement of rheological properties of corn stover suspensions.* Applied Biochemistry and Biotechnology, 2003. **106**(1): p. 383-392.
203. Seyssiecq, I., J.-H. Ferrasse, and N. Roche, *State-of-the-art: rheological characterisation of wastewater treatment sludge.* Biochemical Engineering Journal, 2003. **16**(1): p. 41-56.
204. McKetta, J.J., *Piping design handbook*. 1992: M. Dekker.
205. McKetta, J.J., *Encyclopedia of Chemical Processing and Design: Slurry Systems, Instrumentation to Solid-Liquid Separation*. 1995: M. Dekker.
206. Calle, F.R., *The biomass assessment handbook: bioenergy for a sustainable environment*. 2007: Earthscan.
207. Vassilev, S.V., et al., *An overview of the chemical composition of biomass.* Fuel, 2010. **89**(5): p. 913-933.
208. Parikh, J., S.A. Channiwala, and G.K. Ghosal, *A correlation for calculating elemental composition from proximate analysis of biomass materials.* Fuel, 2007. **86**(12-13): p. 1710-1719.

209. Shen, J., et al., *The prediction of elemental composition of biomass based on proximate analysis.* Energy Conversion and Management, 2010. **51**(5): p. 983-987.
210. Wu, J., et al., *Effect of fiber pretreatment condition on the interfacial strength and mechanical properties of wood fiber/PP composites.* Journal of Applied Polymer Science, 2000. **76**(7): p. 1000-1010.
211. Homan W, T.B., Beckers E., Jorissen A., *Structural and other properties of modified wood*, in *Proc World Conference on Timber Engineering 2000*. 2000: Whistler, Canada.
212. P. Rezayati Charani, J.M.R., B. Mohebby, O. Ramezani (2007) *Influence of hydrothermal treatment on the dimensional stability of beech wood.* **Volume**, 125-131
213. Jingshen, W., et al., *Effect of fiber pretreatment condition on the interfacial strength and mechanical properties of wood fiber/PP composites.* Journal of Applied Polymer Science, 2000. **76**(7): p. 1000-1010.
214. Garrote, G., H. Domínguez, and J.C. Parajó, *Hydrothermal processing of lignocellulosic materials.* European Journal of Wood and Wood Products, 1999. **57**(3): p. 191-202.
215. Manya, J.J., E. Velo, and L. Puigjaner, *Kinetics of Biomass Pyrolysis: 鈦?a Reformulated Three-Parallel-Reactions Model.* Industrial & Engineering Chemistry Research, 2002. **42**(3): p. 434-441.
216. Rao, T.R. and A. Sharma, *Pyrolysis rates of biomass materials.* Energy, 1998. **23**(11): p. 973-978.
217. Ranzi, E., et al., *Chemical Kinetics of Biomass Pyrolysis.* Energy & Fuels, 2008. **22**(6): p. 4292-4300.
218. Ramiah, M.V., *Thermogravimetric and differential thermal analysis of cellulose, hemicellulose, and lignin.* Journal of Applied Polymer Science, 1970. **14**(5): p. 1323-1337.
219. Hosoya, T., H. Kawamoto, and S. Saka, *Cellulose-hemicellulose and cellulose-lignin interactions in wood pyrolysis at gasification temperature.* Journal of Analytical and Applied Pyrolysis, 2007. **80**(1): p. 118-125.
220. Antal, M.J., Jr. and G. Varhegyi, *Cellulose Pyrolysis Kinetics: The Current State of Knowledge.* Industrial & Engineering Chemistry Research, 1995. **34**(3): p. 703-717.
221. Yang, H., et al., *In-Depth Investigation of Biomass Pyrolysis Based on Three Major Components: 鈦?Hemicellulose, Cellulose and Lignin.* Energy & Fuels, 2005. **20**(1): p. 388-393.
222. Yang, H., et al., *Characteristics of hemicellulose, cellulose and lignin pyrolysis.* Fuel, 2007. **86**(12-13): p. 1781-1788.
223. Mosier, N., et al., *Features of promising technologies for pretreatment of lignocellulosic biomass.* Bioresource Technology, 2005. **96**(6): p. 673-686.
224. Wyman, C.E., et al., *Coordinated development of leading biomass pretreatment technologies.* Bioresource Technology, 2005. **96**(18): p. 1959-1966.

225. Bonn, G., R. Concin, and O. Bobleter, *Hydrothermolysis — a new process for the utilization of Biomass.* Wood Science and Technology, 1983. **17**(3): p. 195-202.
226. Brownell, H.H., E.K.C. Yu, and J.N. Saddler, *Steam-explosion pretreatment of wood: Effect of chip size, acid, moisture content and pressure drop.* Biotechnology and Bioengineering, 1986. **28**(6): p. 792-801.
227. Datar, R., et al., *Hydrogen production from the fermentation of corn stover biomass pretreated with a steam-explosion process.* International Journal of Hydrogen Energy, 2007. **32**(8): p. 932-939.
228. Yamashiki, T., et al., *Characterisation of cellulose treated by the steam explosion method. Part 1: Influence of cellulose resources on changes in morphology, degree of polymerisation, solubility and solid structure.* British Polymer Journal, 1990. **22**(1): p. 73-83.
229. Suzuki, S., et al., *Preparation of Binderless Boards from Steam Exploded Pulps of Oil Palm (Elaeis guneensis Jaxq.) Fronds and Structural Characteristics of Lignin and Wall Polysaccharides in Steam Exploded Pulps to be Discussed for Self-Bindings.* Holzforschung, 1998. **52**(4): p. 417-426.
230. Zwart, R.W.R., H. Boerrigter, and A. van der Drift, *The Impact of Biomass Pretreatment on the Feasibility of Overseas Biomass Conversion to Fischer-Tropsch Products.* Energy & Fuels, 2006. **20**(5): p. 2192-2197.
231. Bergman, P.C.A., *Combined torrefaction and pelletisation: the TOP process.* 2005: Netherlands Energy Research Foundation.
232. Pentananunt, R., A.N.M.M. Rahman, and S.C. Bhattacharya, *Upgrading of biomass by means of torrefaction.* Energy, 1990. **15**(12): p. 1175-1179.
233. Felfli, F.F., et al., *Wood briquette torrefaction.* Energy for Sustainable Development, 2005. **9**(3): p. 19-22.
234. Arias, B., et al., *Influence of torrefaction on the grindability and reactivity of woody biomass.* Fuel Processing Technology, 2008. **89**(2): p. 169-175.
235. Prins, M.J., K.J. Ptasinski, and F.J.J.G. Janssen, *Torrefaction of wood: Part 1. Weight loss kinetics.* Journal of Analytical and Applied Pyrolysis, 2006. **77**(1): p. 28-34.
236. Prins, M.J., K.J. Ptasinski, and F.J.J.G. Janssen, *Torrefaction of wood: Part 2. Analysis of products.* Journal of Analytical and Applied Pyrolysis, 2006. **77**(1): p. 35-40.
237. Deng, J., et al., *Pretreatment of agricultural residues for co-gasification via torrefaction.* Journal of Analytical and Applied Pyrolysis, 2009. **86**(2): p. 331-337.
238. Repellin, V., et al., *Energy requirement for fine grinding of torrefied wood.* Biomass and Bioenergy, 2010. **34**(7): p. 923-930.
239. Badger, P.C. and P. Fransham, *Use of mobile fast pyrolysis plants to densify biomass and reduce biomass handling costs--A preliminary assessment.* Biomass and Bioenergy, 2006. **30**(4): p. 321-325.
240. Luo, Z., et al., *Research on biomass fast pyrolysis for liquid fuel.* Biomass and Bioenergy, 2004. **26**(5): p. 455-462.
241. MASAO., N.M.H.T.K.R.S.K.T.F.T., *Production of Bio-Coal Fuel from Low Rank Coal and Woody Biomass Mixture by Using a Bench-Scale Continuous*

Hydrothermal Equipment. Journal of the Mining and Materials Processing Institute of Japan, 2006. **122**(10/11): p. 522-527.
242. Mikio Shimojo, K.I., Masao Tsurui, Yoshinori Suto, Tsutomu Katagiri, Koji Tamura, Fujio Tsuchiya, Katsuaki Osato, *Process For Reforming Biomass And Apparatus For Reforming Biomass*. 2005, JGC CORPORATION.
243. YOSHINORI, K.K.S., *Thermal Decomposition and Combustion Behavior of Woody-Biomass Slurry Fuel*. Transactions of the Japan Society of Mechanical Engineers. B, 2004. **70**(699): p. 2899-2906.
244. Falls, M.A.M.W., *Coal Beneficiation*. 1980, Texaco Inc.: US.
245. John D. Winter, J.E.M., William R. Deever, *Process for treating oily sludge*. 1992, Texaco Inc.: US.
246. EnerTech Environmental, I. *The SlurryCarb™ Process*. 2008 [cited; Available from: http://www.enertech.com/downloads/SlurryCarbOverview.pdf.
247. Malkin, A.I.A., A.Y. Malkin, and A.I. Isayev, *Rheology: concepts, methods & applications*. 2006: ChemTec Pub.
248. Abulnaga, B.E., *Slurry systems handbook*. 2002: McGraw-Hill.
249. Speight, J.G., *Handbook of coal analysis*. 2005: Wiley-Interscience.
250. Kalkreuth, W., et al., *Exploring the possibilities of using Brazilian subbituminous coals for blast furnace pulverized fuel injection*. Fuel, 2005. **84**(6): p. 763-772.
251. Bridgeman, T.G., J.M. Jones, and A. Williams, *Overview of Solid Fuels, Characteristics and Origin*, in *Handbook of Combustion*. 2010, Wiley-VCH Verlag GmbH & Co. KGaA.
252. Hydraulic, I. and I. American National Standards, *Rotodynamic (Centrifugal) Slurry Pumps: Ansi/hi 12. 1-12. 6*. 2005: Hydraulic Institute, Incorporated.
253. Wilson, K.C., *Slurry transport using centrifugal pumps*. 2006: Springer.

Appendices A

Material Balance of Aspen Simulation

	PINEWOOD	HYDRO	WATER	EXHAUST	SHRFEED
Mole Flow	lbmol/hr				
H_2	0.0	47.5	0.0	40.5	0.0
H_2O	0.0	0.0	2900.3	2870.3	0.0
CO	0.0	0.0	0.0	28.2	0.0
CO_2	0.0	0.0	0.0	44.9	0.0
CH_4	0.0	0.0	0.0	1.4	0.0
$C_5H_{10}O_5$	0.0	0.0	0.0	2.2	0.0
Total Flow	0.0	47.5	2900.3	2987.5	0.0
Mass Flow	lb/hr				
ORG	3.95E+04	0.0	0.0	0.0	0.0
PORG	0.0	0.0	0.0	0.0	3.66E+04
ASH	1.04E+02	0.0	0.0	0.0	1.04E+02
Total Flow	3.96E+04	0.0	0.0	0.0	3.67E+04
Temperature F	30	30	86	86	86
Pressure psia	100	100	100	100	450